New Tools for Nanotechnology: From Single Molecule Chemistry to Surface Patterning

Tommaso Auletta

2003

Ph.D. thesis
University of Twente

Twente University **Press**

Also available in print:
http://www.tup.utwente.nl/

NEW TOOLS FOR NANOTECHNOLOGY: FROM SINGLE MOLECULE CHEMISTRY TO SURFACE PATTERNING

This research has been financially supported by the Council for Chemical Sciences of the Netherlands Organization for Scientific Research (CW-NWO), grant number 97041. The research was carried out at the Supramolecular Chemistry and Technology group (SMCT), MESA$^+$ Research Institute, University of Twente.

Twente University **Press**

Publisher:
Twente University Press, P.O. Box 217, 7500 AE Enschede, the Netherlands,
www.tup.utwente.nl

Print: Océ Facility Services, Enschede

ISBN 9036518962

NEW TOOLS FOR NANOTECHNOLOGY: FROM SINGLE MOLECULE CHEMISTRY TO SURFACE PATTERNING

PROEFSCHRIFT

ter verkrijging van
de graad van doctor aan de Universiteit Twente,
op gezag van de rector magnificus,
prof. dr. F.A. van Vught,
volgens besluit van het College voor Promoties
in het openbaar te verdedigen
op vrijdag 29 augustus 2003 te 15.00 uur

door

Tommaso Auletta

geboren op 24 oktober 1972
te Palermo, Italië

Dit proefschrift is goedgekeurd door:

Promotor: Prof. dr. ir. D. N. Reinhoudt

Assistent-promotor: Dr. ir. J. Huskens

Learn from yesterday, live for today, hope for tomorrow.
The important thing is to not stop questioning.
--Albert Einstein--

TABLE OF CONTENTS

CHAPTER 6

FORCE SPECTROSCOPY OF β-CYCLODEXTRIN HOST-GUEST COMPLEXES PROBED UNDER THERMODYNAMIC EQUILIBRIUM

CHAPTER 7

HOST-GUEST COMPLEXES ON β-CYCLODEXTRIN SELF-ASSEMBLED MONOLAYERS: SURFACE PATTERNING VIA MULTIPLE NON-COVALENT INTERACTIONS

Chapter 1

General Introduction

Nanotechnology aims to manipulate and control matter at the nanometer level. The possibility to create structures in the 10-100 nm range is a requirement for applications in the fields of, for example, future electronic devices,[1] high-density data storage,[2] and analytical chemistry.[3]

Current developments to pursue miniaturization of devices rely on top-down techniques, which have been developed in the past decades. Patterns with dimensions down to 0.1 μm have been fabricated, pushing photolithography to its physical and economic limits,[4] and nowadays alternative routes have been opened by unconventional techniques[5] such as microcontact printing,[6] microwriting,[7] micromachining,[8] and dip-pen nanolithography.[9] In parallel, the "bottom-up" approach, which consists of the controlled assembly of complex structures of nanometer dimensions starting from the molecular level, is becoming an increasingly realistic tool for nanofabrication.[10]

The combination of top-down and bottom-up approaches allows the creation of nanosized patterns with high lateral resolution. The majority of soft lithographic techniques exploits self-assembled monolayers (SAMs) of organic molecules on a variety of substrates, which can, for example, act as resist layers in chemical etching procedures.

SAMs are monomolecular thin films which form spontaneously based on the interactions taking place between the anchoring moiety of the adsorbate and the surface. The stability of a SAM also relies on Van der Waals forces between the alkyl chains of adjacent molecules.[11] Sulfur-containing molecules such as alkanethiols and dialkyldisulfides have extensively been exploited to modify metal surfaces (especially gold) via self-assembly.[12]

Developments in surface analysis have allowed this trend to miniaturization to happen and new tools have been developed and improved in order to characterize and modify nanosize structures. The invention of Scanning Probe Microscopy (SPM), such as Scanning Tunneling Microscopy (STM) in the early 1980s by Binnig and Rohrer,[13] followed by the Atomic Force Microscope (AFM) in 1986 by Binnig, Quate, and Gerber[14] represented a breakthrough for analytical techniques at the nanometer scale.[15] Sensitivity, limit of detection, and speed, have improved to such an extent that a sample can now be monitored in its “natural” environment, with the least possible perturbation from the probe. SPM represents also one of the most promising techniques to manipulate

and modify surfaces, owing to the reduced dimensions of the tip and to the accurate positioning of the probe.[9,16,17,18,19,20]

The research described in this thesis has focused on methods to exploit SAMs on gold surfaces as platforms for supramolecular interactions, and two main topics can be outlined. The first is the use of SAMs of alkanethiols as platforms in which single receptor molecules are immobilized via an insertion process. These receptors can be addressed subsequently, in a so-called expression stage, by performing coordination chemistry reactions, which can be monitored via AFM at the single molecule level. The second part deals with the development of a *molecular printboard* for supramolecular interactions. Suitably chosen guest molecules can be adsorbed selectively onto these surfaces, by incorporation of appropriate host-guest motifs. Combinations of top-down and bottom-up techniques have been exploited extensively in this work to achieve surface patterning.

Chapter 2 presents an overview of current non-photolithographic patterning techniques, mostly microcontact printing (μCP) and SPM-related techniques, and in the end a short introduction on single molecule detection is given.

Results related to the use of surface-confined dendritic architectures with multiple reactive sites as molecular platforms to perform coordination chemistry are presented in Chapter 3. AFM imaging of the layers before and after the reaction step allows characterization of the system at the single molecule level.

Chapter 4 expands on the same type of chemistry, which, in this case, has been developed to achieve surface confinement of monolayer-protected gold nanoparticles. Control over the position of the anchoring moieties in the SAMs has been achieved using microcontact printed substrates.

Chapter 5 deals with the electrochemistry of mixed SAMs of ferrocenylalkanethiols co-adsorbed with ω-hydroxyalkanethiols. Cyclic voltammetry has been employed to determine the amount of electroactive compound adsorbed on the gold surface and to investigate phase segregation phenomena. The aim of this work has been the development of SAMs containing single and isolated ferrocene moieties embedded into the hydroxyl-terminated thiols.

In Chapter 6, the substrates described in Chapter 5 have been employed in AFM force spectroscopy experiments to determine the host-guest rupture force between the ferrocenyl moieties adsorbed on an AFM tip and a heptathioether β-cyclodextrin (β-CD) SAM. Special focus has been devoted to the chain length effect of the ferrocenyl spacer and to the unloading rate effect on the force value. This approach has been extended to several different guests, and force quanta have been determined. A theoretical model has

been developed to correlate the force quanta to the thermodynamics of the host-guest complexation.

In Chapter 7, the β-CD SAMs have been further characterized and employed as a molecular printboard, on which guest molecules are selectively immobilized. Multiple host-guest interactions, investigated by surface plasmon resonance spectroscopy, between the β-CD SAMs and molecules adsorbed from solution are studied. These inclusion complexes are stable enough to employ such a system in surface patterning, and transfer of guest molecules onto the β-CD SAM has been obtained by *supramolecular* microcontact printing and dip pen nanolithography, achieving submicrometer resolution.

References and notes

[1] a) Gittins, D. I.; Bethell, D.; Schiffrin, D. J.; Nichols, R. J. *Nature* **2000**, *408*, 67–69. b) Collier, C. P.; Mattersteig, G.; Wong, E. W.; Luo, Y.; Beverly, K.; Sampaio, J.; Raymo, F. M.; Stoddart, J. F.; Heath, J. R. *Science* **2000**, *289*, 1172–1175. c) Chen, J.; Reed, M. A.; Rawlett, A. M.; Tour, J. M. *Science* **1999**, *286*, 1550–1552.

[2] a) Lutwyche, M. I.; Despont, M.; Drechsler, U.; Dürig, U.; Häberle, W.; Rothuizen, H.; Stutz, R.; Widmer, R.; Binnig, G. K.; Vettiger, P. *Appl. Phys. Lett.* **2000**, *77*, 3299–3301. b) Mizutani, W.; Ishida, T.; Tokumoto, H. *Langmuir* **1998**, *14*, 7197–7202.

[3] a) Service, R. E. *Science* **1995**, *268*, 26-27. b) Manz, A. *Chimia* **1996**, *59*, 140-145. c) Craston, D.; Cowen, S. *Chem. Br.* **1996**, 31-33. d) Day, P. *Chem. Br.* **1996**, 29-31.

[4] a) Ito, T.; Okazaki, S. *Nature* **2000**, *406*, 1027-1031. b) Walraff, G. M.; Hinsberg, W. D. *Chem. Rev.* **1999**, *99*, 1801-1821. c) Okazaki, S. *J. Vac. Sci. Technol. B* **1991**, *9*, 2829-2833. d) Jeong, H. J.; Markle, D. A.; Owen, G.; Pease, F.; Grenville, A.; von Bünau, R. *Solid State Technol.* **1994**, *37*, 39-47. e) Levenson, M. D. *Solid State Technol*. **1995**, *38*, 57-66. f) Geppert, L. *IEEE Spectrum* **1996**, *33*(4), 33-38.

[5] Xia, Y.; Rogers, J. A.; Paul, K. E.; Whitesides, G. M. *Chem. Rev.* **1999**, *99*, 1823-1848.

[6] a) Xia, Y.; Whitesides, G. M. *Angew. Chem. Int. Ed.* **1998**, *37*, 550-575. b) Biebuyck, H. A.; Larsen, N. B.; Delamarche, E.; Michel, B. *IBM J. Res. Dev.* **1997**, *41*, 159-170.

[7] a) Kumar, A.; Abbott, N. L.; Kim, E.; Biebuyck, H. A.; Whitesides, G. M. *Acc. Chem. Res.* **1995**, *28*, 219-226. b) Kumar, A.; Biebuyck, H. A.; Abbott, N. L.; Whitesides, G. M. *J. Am. Chem. Soc.* **1992**, *114*, 9188-9189.

[8] a) Abbott, N. L.; Kumar, A.; Whitesides, G. M. *Chem. Mater.* **1994**, *6*, 596-602. b) Abbott, N. L.; Folkers, J. P.; Whitesides, G. M. *Science* **1992**, *257*, 1380-1382.

[9] a) Piner, R. D.; Zhu, J.; Xu, F.; Hong, S.; Mirkin, C. A. *Science* **1999**, *283*, 661-663. b) Mirkin, C. A.; Hong, S.; Levine, R. D. *ChemPhysChem* **2001**, *2*, 37-39.

[10] Gimzewski, J. K.; Joachim, C. *Science* **1999**, *283*, 1683–1688.

[11] a) Ulman, A. *An Introduction to Ultrathin Organic Films from Langmuir-Blodgett to Self-Assembly*, Academic Press: San Diego, CA, 1991. b) Ulman, A. *Chem. Rev*. **1996**, *96*, 1533-1554.

[12] a) Dubois, L. H.; Nuzzo, R. G. *Ann. Rev. Phys. Chem.* **1992**, *43*, 437-463. b) Allara, D. L. *Biosens. Bioelectron.* **1995**, *10*, 771-783.

[13] Binnig, G.; Rohrer, H. *Helv. Phys. Acta* **1982**, *55*, 726-735.

[14] Binnig, G.; Quate, C. F.; Gerber, C. *Phys. Rev. Lett.* **1986**, *56*, 930-933.

[15] For a review on Scanning Force Microscopy see: Takano, H.; Kenseth, J. R.; Wong, S.-S.; O'Brien, J. C.; Porter, M. O. *Chem Rev.* **1999**, *99*, 2845-2890.

[16] a) Xu, S.; Liu, G.-Y. *Langmuir* **1997**, *13*, 127-129. b) Xu, S.; Laibinis, P. E.; Liu, G.-Y. *J. Am. Chem. Soc.* **1998**, *120*, 9356-9361. c) Xu, S.; Laibinis, P. E.; Liu, G.-Y. *Langmuir*, **1999**, *15*, 7244-7251.

[17] Müller, W. T.; Klein, D. L.; Lee, T.; Clarke, J.; McEuen, P. L.; Schultz, P. G. *Science* **1994**, *268*, 272-273.

[18] a) Wilder, K.; Soh, H. T.; Atalar, A.; Quate, C. F.; *J. Vac. Sci. Technol. B* **1997**, *15*, 1811-1817. b) Marrian, C. R. K.; Colton, R. J. *Appl. Phys. Lett.* **1990**, *56*, 755-757. c) Day, H. C.; Allee, D. R.; George, R.; Burrows, W. A. *Appl. Phys. Lett.* **1993**, *62*, 1629-1631. d) Albrecht, T. R.; Dovek, M. M.; Lang, C. A.; Grütter, P.; Quate, C. F.; Kuan, S. W. J.; Frank, C. W.; Pease, R. F. W. *J. Appl. Phys*. **1998**, *64*, 1178-1184.

[19] Tully, D. C.; Wilder, K.; Frechet, J. M. J.; Trimble, A. R.; Quate, C. F. *Adv. Mater.* **1999**, *11*, 314-318.

[20] a) Eigler, D. M.; Schweizer, E. K. *Nature*, **1990**, *344*, 524-526. b) Crommie, M. F.; Lutz, C. P.; Eigler, D. M. *Science* **1993**, *262*, 218-220. c) Hong, S.; Jin, Z.; Mirkin, C. A. *Science* **1999**, *286*, 523-525. d) Hong, S.; Mirkin, C. A. *Science* **2000**, *288*, 1808-1811. e) Lee, K.-B.; Park, S.-J.; Mirkin, C. A.; Smith, J. C.; Mrksich, M. *Science* **2002**, *295*, 1702-1705. f) Demers, L. M.; Ginger, D. S.; Park, S.-J.; Li, Z.; Chung, S.-W.; Mirkin, C. A. *Science* **2002**, *296*, 1836-1838. g) Noy, A.; Miller, A. E.; Klare, J. E.; Weeks, B. L.; Woods, B. W.; DeYoreo, J. J. *Nano Lett.* **2002**, *2*, 109-112. h) McKendry, R.; Huck, W. T. S.; Weeks, B.; Fiorini, M.; Abell, C.; Rayment, T. *Nano Lett.* **2002**, *2*, 713-716. i) Agarwal, G.; Sowards, L. A.; Naik, R. R.; Stone M. O. *J. Am. Chem. Soc.* **2003**, *125*, 580-583.

Chapter 2

Unconventional Approaches to Nanotechnology: Soft Lithography and Top-down/Bottom-up Combinations

The aim of this chapter is to give an overview on general nanotechnology issues related to unconventional nanofabrication methodologies that are relevant for the subject of this thesis. Soft lithographic techniques like microcontact printing and combinations of bottom-up/top-down approaches, such as dip-pen nanolithography are reviewed. The potential of controlling matter at a single atom/molecule level is intimately related to nanotechnological applications and miniaturization of devices. Therefore, a brief overview on single molecule detection techniques is given.

2.1 Introduction to nanotechnology

"There is plenty of room at the bottom" is the paradigm of nanoscience and nanotechnology expressed by Richard Feynman[1] already in 1959, and it summarizes the potential to control the position and properties of matter with nanometer accuracy.[2] The first and most direct applications relate to the development of electronic devices to increase both storage capacity and computational power.[3] However, it must be realized that benefits from miniaturization could arise in fields related to medicine, life sciences, and chemistry, as well.[4,5,6,7,8] Interest in nanoscience is also linked to the properties that matter exhibits at the nanoscale level, which are determined by quantum effects.[9]

The most widely explored approach to achieve miniaturization of devices is by so-called top-down techniques, which mainly rely on the reproduction of a master via photolithography.[10] Moore's law, predicting an exponential decrease in size and increase in performance in the microelectronics industry, has been fulfilled for over 40 years.[11]

Traditional top-down techniques mostly make use of a protective resist layer that can be patterned selectively by exposure to light, allowing transfer of the master features onto the substrate. The size of the features that can be produced by photolithography has in first approximation the same order of magnitude as the wavelength of the radiation employed. This implies that the quest for decrease in feature size requires light sources with progressively shorter wavelengths.[10e] In order to produce patterns in the 100 nm

range, deep UV lithography[10f] is required and beyond this threshold photolithography reaches its physical limits, mainly due to diffraction effects.

Production of masters with nanosized features can be accomplished by using highly sophisticated techniques, such as electron beam lithography.[12] However, such techniques cannot easily be exploited as mass production tools, due to the extremely high production costs connected to the low manufacturing speed and to the serial production process. Moreover, other issues such as material homogeneity become crucial at the nanoscale level.[13] At present, non-photolithographic top-down methods[14] such as soft-lithography,[15] imprint lithography,[16] and dip-pen nanolithography,[17] are investigated as complements or alternatives to photolithographic nanofabrication.

While top-down techniques are based on making existing patterns smaller and smaller, the alternative and very promising bottom-up approach relies on spontaneous formation, or self-assembly,[18] of nanosized structures via weak interactions, starting from smaller components[19] such as molecules or even atoms. The ultimate target is the ability to control and manipulate matter at the single atom or molecular level and to build single molecule devices.[20] Nature itself shows a variety of outstanding examples on how to build complex functional aggregates starting from molecular components, which are held together by multiple, non-covalent weak interactions.[21] Single molecule research began with biomolecules, like DNA, not only because they are the "building blocks of life", but also because of their large size, which facilitates their visualization.[22] The first imaging attempts, using scanning tunneling microscopy, date back to 1983.[23] In recent years, the development of optical tweezers has made the manipulation of single biomolecules possible,[24] and techniques such as near-field scanning optical microscopy (NSOM) and atomic force microscopy (AFM) are used to study the physical,[25] dynamic,[26] and mechanical[27,136] properties of single molecules.

After a brief introduction on self-assembled monolayers (SAMs), non-conventional nanofabrication techniques are presented, with special focus on microcontact printing, probe manipulation techniques, and dip pen nanolithography. In addition single molecule detection methods are reviewed.

2.2 Self-assembled monolayers

Nuzzo and Allara reported the first study of self-assembled monolayers in 1983.[28] Since then, this field has expanded rapidly, especially *n*-alkanethiol monolayers on gold adsorbed either from solution or the gas phase.[29] Interest in SAMs arises from the possibility to form homogeneous monomolecular films with well-defined surface properties. In order to characterize these structures, several surface analytical techniques

have been developed.[26a,30] Among sulfur-containing molecules, both alkanethiols and dialkyldisulfides assembled on metal surfaces (especially gold) have been the most studied classes of compounds,[31] while thioether monolayers have been studied less extensively.[28,32]

There are two main contributions that lead to the formation of a stable SAM of an alkanethiol on gold (Scheme 2.1): the binding force between the anchoring sulfur group and gold (S-Au bond energy of 45 kcal mol^{-1})[31b] and the interchain interactions (Van der Waals attractions on the order of a few kcal mol^{-1} per CH_2).[33]

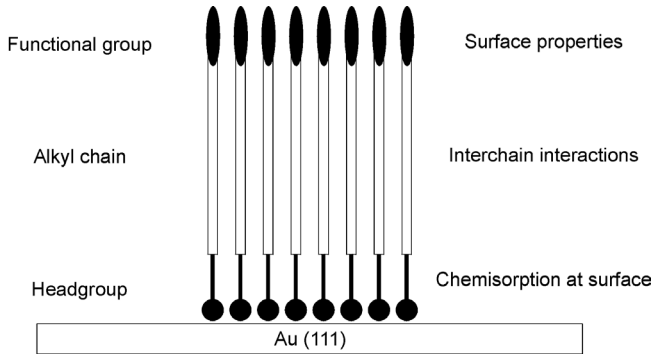

Scheme 2.1 Schematic representation of interactions in SAMs (tilting of the alkyl chains has been omitted for clarity) (adapted from ref 29c).

The stability of SAMs is an important issue in order to develop nanodevices. Thermal stability studies have shown that initial heating of the monolayer improves its quality, while longer exposures and higher temperatures result in desorption.[34] It has been proven that monolayers are in equilibrium with the solution with which they are in contact.[35] Exchange[36] or desorption[35] processes are possible upon exposure of the SAM to a solution of a different thiol or to a pure solvent (see *e.g.* Chapters 3 and 4).

2.3 Microcontact printing

2.3.1 Introduction

Features with dimensions below 100 nm pose fundamental limits on photolithographic techniques, and such limitations have pushed research towards alternative nanofabrication techniques. One such new class of techniques that gives access to micrometer patterns and yet requires very limited technological resources is soft lithography. This class of techniques relies on the use of a polymeric stamp or mold to

transfer patterns onto a substrate, and on the use of organic molecules or soft materials. Most of these approaches have been developed in the group of Whitesides and currently under investigation are approaches such as replica molding (REM),[15d] microtransfer molding (μTM),[15e] micromolding in capillaries (MIMIC),[15f] and solvent-assisted micro-molding (SAMIM).[15g] Soft lithography generates micropatterns of self-assembled monolayers[29] by contact printing, and also forms microstructures in materials by embossing and replica molding.[37] This section focuses on microcontact printing (μCP).

2.3.2 The microcontact printing process

Microcontact printing was introduced by Whitesides *et al.* to pattern gold surfaces with alkanethiols.[38] The different steps are depicted schematically in Scheme 2.2. Central to the process is the conformal contact between the substrate and a flexible elastomeric stamp, usually poly(dimethylsiloxane) (PDMS),[39] prepared by replica molding of a master, which is used to transfer the molecular ink onto the surface. The PDMS stamp is then cured, peeled off from the master (Scheme 2.2b), and inked with the thiol solution (Scheme 2.2c), allowing the ink to diffuse into the stamp. Upon contacting a clean gold surface it is possible to transfer selectively the ink to form a self-assembled monolayer exclusively in the contact areas between stamp and substrate (Scheme 2.2d-e). The patterned SAM can act as a resist in a subsequent wet-etching step, shielding the underlying metal layer from the etchant (Scheme 2.2f). Scheme 2.2g shows that exposing the patterned SAM substrate to a solution of another adsorbate allows the uncovered regions to be filled in with another molecule, leading to patterned SAMs with different chemical functionalities. Stamps can be reused, often even without reinking, and the smallest features produced to date with this printing technique are 35 nm lines spaced by 350 nm.[15b]

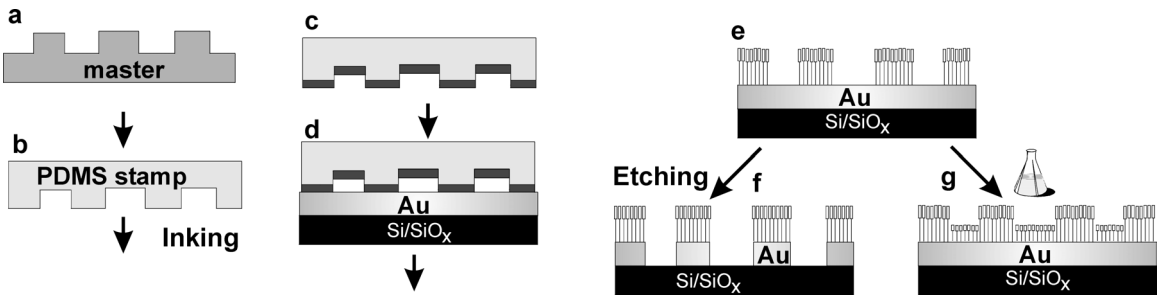

Scheme 2.2 Schematic representation of μCP of thiols on gold.

The edge sharpness of printed features can partly be attributed to autophobic pinning as shown for printing of alkanethiols on gold.[40] Ink diffusion both through the gas phase and laterally across the surface poses a problem for edge resolution. Gas phase deposition from a stamp has been observed even at 1 mm distance between stamp and surface for dodecanethiol.[41] A partial solution to this problem is the application of inking stamps via an "ink pad", a flat piece of PDMS which is inked via normal wet inking, which prevents inking of the recessed areas of the stamp.[42]

Another approach to improve the edge resolution of the printed structures is through the use of high molecular weight inks. Delamarche *et al.* demonstrated that printing monolayers of eicosanethiol on gold provides the best practical compromise between self-assembly of the resist and its transport along the stamp and substrate interfaces as well as through the gas phase, showing the feasibility of fabricating 100 nm features on gold.[43] In our group, molecules such as calix[4]arene and cavitand tetrakis(thioether)s have been employed. These inks yield monolayers with qualities comparable to thiol SAMs, and good resolution of the gold structures is obtained after etching, while their molecular weight is about 5 times that of eicosanethiol.[44]

The mechanical properties of the stamp are crucial to achieve good pattern transfer and a number of drawbacks related to stamp deformation still exist. The elastomeric stamps employed are in fact characterized by small Young's moduli (1–10 MPa) and large thermal expansion coefficients (c.a. 10^{-3} K^{-1}). These properties render them prone to distortions both at the microscopic[45] and at the macroscopic scale[46] with a consequent loss of quality and reproducibility of the pattern transfer. A general approach to reduce long-range stamp deformation is to bond them to a stiff backplane.[46b,47] It has been shown that the use of ultrathin stamps down to 1 μm thickness on a rigid support provides good mechanical stability, and it is suitable for high quality and high-resolution microcontact printing down to 50-100 nm over large areas.[46b,48] Furthermore, ultrathin stamps on a rigid backplane allow accurate alignment, demonstrating the viability of multilevel fabrication schemes.

If the ink is of a polar nature it does not spontaneously wet a PDMS stamp, and uptake of polar substances from the ink onto or into the stamp is unlikely. Surface hydrophilization of PDMS stamps is needed for microcontact printing of polar inks.[49] A simple treatment consists of a brief exposure of the stamp to an oxygen plasma to oxidize the outer surface of the stamp.[50] Although simple and efficient, this method produces a thin, glassy silicate layer on the stamp, which is brittle and quickly loses its hydrophilic character unless the stamp is kept in water.[51] Delamarche *et al.*[52] proposed a method to derivatize covalently

the PDMS stamp by use of self-assembled monolayers, rendering the surface polar. The covalent linking allows retention of the hydrophilic character of the stamp up to 20 days.

μCP is a very flexible technique that allows patterning of surfaces by self-assembled monolayers with submicron resolution.[53] It is possible to pattern different types of materials employing appropriate ink molecules and quasi-three-dimensional structures have been realized by combination with other techniques.[54]

The patterned surfaces generated by μCP can be analyzed by several techniques.[55] In an example from Whitesides *et al.*[56a] microcontact printing was performed using hexadecanethiol (HDT) as the ink and the remaining regions were subsequently filled with $HS(CH_2)_{15}COOH$. AFM in friction mode was employed to visualize the areas patterned with the two different thiols. Relatively high friction forces between the probe and the substrate were detected in areas covered with the COOH-terminated SAM, and relatively low forces for the areas covered with the CH_3-terminated SAM.[56]

A systematic scanning tunneling microscopy (STM) study of the monolayer properties carried out by Larsen *et al.* showed that printing with 10 mM dodecanethiol in ethanol and applying the stamp with a contact time of at least 0.3 s, produces highly ordered SAMs on Au(111) that are indistinguishable from those formed by adsorption from solution.[41]

2.3.3 Applications of patterned SAMs in surface engineering

SAMs are monomolecular thin films, with a thickness generally of 1-2 nm. They do not fulfill requirements to be employed as etch masks in conventional reactive ion etching processes.[57] However, they proved to be resistant to a number of wet etching processes, protecting the underlying metal substrate.[53,58] The combination of μCP and selective chemical etching (Scheme 2.2f) allows for the fabrication of structures with a high degree of complexity.

μCP was successfully employed in the preparation of gold or silver patterns as secondary masks in the etching of underlying substrates such as SiO_2, silicon, and GaAs.[59] Etched structures were generated on layered $Ag/Si/SiO_2$ substrates by μCP of hexadecanethiol and selective wet etching of the unprotected silver layer (50 nm thick) in an aqueous ferro/ferricyanide etchant.[60] The patterned silver layer was used as a secondary mask in the anisotropic wet etching of Si(100) in an aqueous solution containing KOH and 2-propanol, and the profile of the relief structures etched in the Si(100) wafer could be controlled precisely by changing the etching conditions such as temperature and etching time.

Although a recent study showed that the density of defects in SAMs is still too high to be useful for fabricating high-resolution microelectronic devices,[61] the patterned microstructures fabricated using μCP are acceptable for applications in many other areas, including MEMS,[4] microanalytical systems,[5] sensors,[7] solar cells,[62] and optical components.[59b,63] Patterned SAMs have also been used as supports to control both azimuthal and polar orientations of nematic liquid crystals.[64]

2.3.4 Patterned SAMs as passivating layers in selective deposition

Self-assembly of organic compounds onto a surface provides a straightforward way to modify surface properties. The use of adsorbates with different end groups in microcontact printing allows the patterning of solid substrates with areas characterized by different surface properties such as wetting, dewetting,[65] nucleation, or deposition of other materials, with a lateral resolution in the micrometer range. Microcontact printing in combination with selective dewetting has been applied to direct the deposition of different materials, such as aqueous solutions,[59a,66] hydrophobic liquids,[67] polymers[68] and biological materials.[69]

Whitesides *et al.* demonstrated the validity of this approach for the selective adsorption of inorganic materials onto patterned substrates.[70] Selective wetting of both self-assembled monolayers (SAMs) of alkanethiols on gold and alkylsilanes on Si/SiO_2 formed by microcontact printing restricted the deposition of iron oxides to the hydrophilic areas of the surface. The iron oxides were deposited either as magnetite particles from colloidal solution, by precipitation of the oxide from previously deposited drops of water containing an iron(III) salt, or by ferrite plating. The size of the metal oxide patterns was only limited by the resolution obtainable by μCP. The magnetic properties of the deposited iron oxides were characterized by magnetic force microscopy (MFM) and by measurement of the magnetization.

Nuzzo *et al.* demonstrated selective chemical vapor deposition (CVD)[71] on Si/SiO_2 with printed SAMs of silanes as templates.[72] The technique combines the microcontact printing of octadecyltrichlorosilane (OTS) (Scheme 2.3a-b), nonselective copper CVD (Scheme 2.3c), and mild mechanical polishing to fabricate thin film microstructures (Scheme 2.3d).

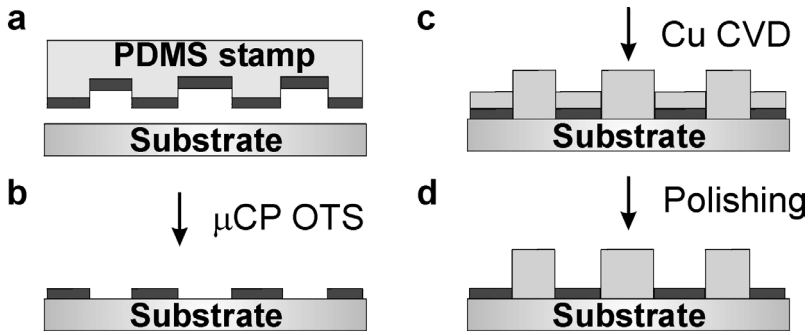

Scheme 2.3 Schematic representation of the procedure used to pattern copper thin films on planar substrates (adapted from ref. 72c).

This technique has been used successfully to deposit copper features with sizes ranging from 5 to 250 μm on a variety of substrates including indium tin oxide (ITO), titanium nitride (TiN), thermal and plasma grown SiO_2, Al_2O_3, and glass. Patterning is obtained via adhesive failure in regions modified by μCP. Nucleation and growth are inhibited in these regions and the copper grains which eventually form on top of the OTS monolayer remain only loosely adhered and thus are easily removed mechanically.

Interesting results in the field of life sciences have been obtained by the use of patterned SAMs as templates to define and control the adsorption of proteins and consequently the attachment of cells.[73] In an example from the group of Whitesides, μCP has been used to place cells in predetermined locations in arrays with defined shapes, sizes, and distances of separation.[74] Evaporation of a thin film of gold on a patterned polyurethane substrate provided an optically transparent substrate, on which SAMs of functionalized alkanethiols were formed. Patterned substrates were obtained by contact printing a hexadecanethiol SAM on the protruding features of the substrate with a flat stamp and passivating the bare gold present in the grooves by subsequently immersing the substrate in a solution of an alkanethiol terminated with a tri(ethylene glycol) group ($HS(CH_2)_{11}(OCH_2CH_2)_3OH$, EG_3OH). Immersion of such a substrate in a solution of fibronectin showed that protein adsorption occurred only on the methyl-terminated area/ridges of the substrate, while the areas functionalized with the tri(ethylene glycol) resisted protein adsorption. A complementary procedure confined protein adsorption and cell attachment to the grooves of the substrate.

Using simple patterning procedures, it is possible to dictate the shape assumed by a cell that attaches to a surface and thus to control certain aspects of cell growth and protein secretion.[75]

2.3.5 Microcontact printing on other materials

Printing on materials other than gold has been achieved as well. Other coinage metals such as copper[76] and silver have been tested by printing alkanethiols. Silver proved to be more convenient to etch and the level of defects in SAMs appeared to be lower than on gold.[77] Furthermore, silver is attractive because it is an excellent electrical and thermal conductor.[78]

The formation of monolayers of organosilanes (*e.g.* octadecyltrichlorosilane, OTS) on oxidic surfaces like glass, Al_2O_3, SiO_2, and ITO has been investigated extensively, but due to their extreme sensitivity to the methods of preparation used, their structure remains less well understood. In general, OTS chains can pack with densities approaching those found in bulk hydrocarbon crystals but even the "highest quality" phases lack the long-range translational order found for thiol SAMs on Au and Ag. It is generally believed that the adsorption of alkyltrichlorosilanes and other alkylsilanes with hydrolyzable bonds proceeds on hydrated surfaces via the formation of silanols as intermediates, which then react with surface OH groups to form a network polymer which is to some degree covalently bound to the surface.[29c,79] Although SAMs of alkyltrichlorosilanes on hydroxyl-terminated surfaces are less ordered than those of alkanethiols on gold, μCP has nonetheless been used to produce patterned SAMs of alkylsiloxanes on Si/SiO_2, Al_2O_3, and TiO_2.[80,81] Characterization of printed layers by Nuzzo *et al.* provided information on the layer properties related to parameters such as the OTS ink concentration and printing time.[82]

Protein microarrays have potential applications in the development of biosensors, clinical immunological assays, mapping the proteome and to examine protein-protein interactions. Microcontact printing has been employed to prepare such platforms either by printing proteins on a preexisting SAM,[83] or by direct printing of biological materials. A multiprotein immunoarray containing three different proteins has been developed by Reifenberger and tested as a detection system for specific antibodies.[84] The substrates were prepared by orthogonal printing of two antigens, mouse IgG (Ag1) and human IgG (Ag2), and the regions between the IgG printed areas were blocked with BSA. The developed immunoassays, performed using the protein microarrays, were characterized by fluorescence microscopy and scanning probe microscopy, revealing a high degree of selectivity for the targeted antigen-antibody interactions.

Microcontact printing has also been applied to a number of inorganic inks such as palladium colloids, [85] and metal complexes.[86]

2.4 Probe lithography

2.4.1 Introduction

μCP can be used to create patterns onto surfaces using an elastomeric stamp and can be applied to different materials. Limitations affecting the lateral resolution are factors such as ink diffusion, conformal contact, and stamp deformation. Probe lithography, relying on nanosized tips for surface modification, allows local manipulation of matter at a much smaller scale and provides complementary approaches to top-down parallel nano-fabrication techniques.

The very sharp tips employed in scanning probe techniques such as STM and AFM can be either used to release materials onto a surface or to rearrange preexisting material on a surface.

Pioneering work in 1990 at IBM-Zürich by Eigler *et al.* employed an STM tip to manipulate single xenon atoms by changing the applied voltage. The IBM logo name was produced using 36 atoms on a nickel surface.[87] In 1993 another remarkable example of atomic manipulation was reported by the same group in which 48 iron atoms were positioned to form a circular structure.[88]

Nanostructures down to a few nm have been reported by the so-called nanoshaving process, using an AFM setup, in combination with self-assembly (Scheme 2.4).[89] In this approach an AFM tip is scanned over a surface and employed to remove locally a preformed monolayer. If the process is carried out in the presence of an adsorbate that can self-assemble in the exposed area, surface patterning with nm lateral resolution and an edge resolution better than 2 nm can be obtained routinely (Scheme 2.4b-c). In addition, the fabricated nanostructures can be modified quickly and characterized *in situ* and employed to direct successive adsorption processes of, *e.g.* proteins, which retain their biological activity after adsorption.[90]

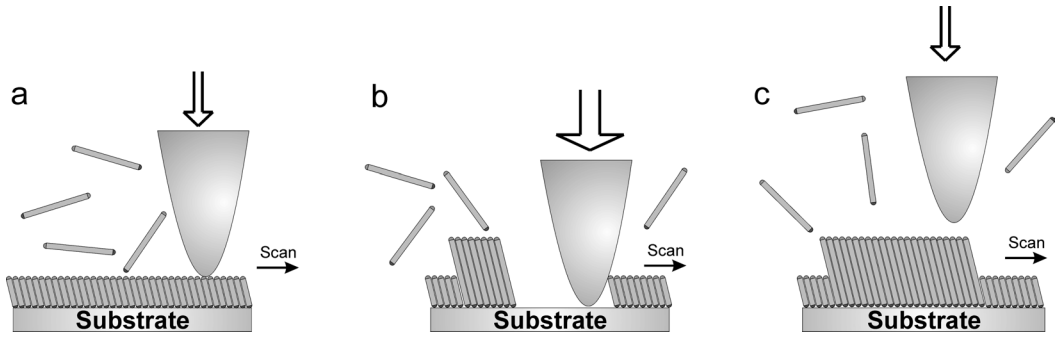

Scheme 2.4 The nanoshaving process in combination with self-assembly (adapted from ref. 89a).

In another approach a current sensing atomic force microscope (CS-AFM) was used to remove locally the alkanethiol molecules in a SAM by applying a sufficient bias at a constant force in an inert solvent. By combination of the features of AFM and STM, the force and bias can be controlled independently to influence the patterning.[91]

Like μCP, dip pen nanolithography (DPN) is a maskless lithographic technique, with a resolution in the nanometer regime. It relies on the transfer of an adsorbate onto a suitable surface by means of an atomic force microscopy tip. Since the first example from the group of Mirkin,[17] this has proven to be a viable and versatile technique for surface patterning. In the remainder of this section, the main results obtained by this and other closely related techniques are summarized.

2.4.2 Dip pen nanolithography

Dip pen nanolithography employs a very sharp Si_xN_y AFM tip as a pen that is inked with an adsorbate, *e.g.* alkanethiols, and used to write onto a substrate, like Au. The delivery mechanism of the ink onto the surface probably relies on capillary transport of molecules from the AFM tip onto the substrate by a water meniscus (Scheme 2.5), and it allows the direct writing of submicron patterns.[17]

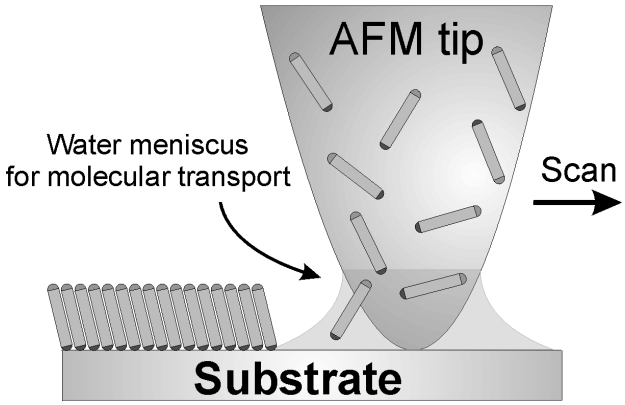

Scheme 2.5 Schematic representation of the ink transport from the tip to the substrate in DPN, via the water meniscus (adapted from ref. 17).

The chemical affinity of the ink for the "paper", i.e. the chemisorption of the sulfur atom of the adsorbate onto the gold surface, provides stability to the patterns, resulting in a new type of nanolithography. The high quality of the SAMs has been shown by the lattice-resolved AFM imaging of an octadecanethiol (ODT) SAM.[17]

The resolution of DPN depends on several parameters, and its ultimate limit is not yet clear. A parameter to be considered is the grain size of the substrate, while diffusion of the molecules after deposition can be limited by chemisorption and self-assembly. It has been shown that ODT patterns are stable whereas water forms metastable patterns, although no systematic studies on stability as a function of time and in the presence of a solvent have been reported. This fact limits the possibility to employ the DPN process in a reading/writing/erasing cycle, where the patterns can be removed at will. The ink transfer rate, and thus the pattern resolution, is a function of the tip-substrate contact time and of the scan speed,[92] but diffusion across an already formed SAM area can not be excluded, as observed in μCP. The dimensions of the pattern depend directly on the writing parameters, *e.g.* dots with different diameter have been created by keeping the tip in contact with the substrate, disabling the x-y scanning, and changing the contact times, while lines with different thickness have been produced by changing the scan speed. In addition the size of the water meniscus that bridges the tip and substrate depends on relative humidity, and thus it affects the resolution by influencing the rate of ink transport from the tip to the substrate. The rate of transport is also related to the ink employed and in particular to its polarity.[92]

Following this first example, many different applications have been reported, in which the substrate and the ink have been changed and a number of technical improvements now allow the formation of more sophisticated patterns. A common issue of concern for nanolithographic tools is related to the creation of overlaid structures with well-defined alignment together with the use of multiple inks within one single nanostructure, and this matter is usually addressed as pattern registry. DPN proved to be a viable option to create multicomponent nanostructures and it has been shown that chemically pure patterns of multiple different materials can be generated with near perfect alignment and nm spatial separation.[93] The registration capabilities of DPN have been demonstrated by generating a pattern of 15-nm-diameter SAM dots of 16-mercaptohexadecanoic acid (MHA) on a Au(111) substrate. A first set of nanosized dots was created by placing a MHA-coated tip in contact with the Au(111) surface for 10 s. By increasing the scan size, the pattern could be imaged with the same tip by lateral force microscopy (LFM). Based on the position of the first pattern, the coordinates of additional patterns could be determined for the precise placement of a second pattern of MHA dots.

The precise positioning of multiple-ink nanostructures on a Au substrate without cross-contamination has been demonstrated as well. An initial pattern of 50-nm parallel lines composed of MHA separated by 190 nm has been drawn with a 2-μm separation from exterior alignment marks. The tip has been replaced with an ODT-coated tip and used to

locate the alignment marks (not the first set of lines). Based on the position of these marks a second set of 50-nm parallel lines of ODT has been patterned onto the substrate. These lines were positioned in an interdigitated manner and with good registry with respect to the first set of MHA SAM lines.

Furthermore, the overwrite capability of DPN has been reported. This allows the generation of nanostructures and the subsequent filling in of the surrounding areas with a second type of ink. Different geometric structures, the linewidths of which can be tuned by changing the writing time, have been generated with an MHA-coated tip. The tip has been then changed, and a $3 \times 3\ \mu m^2$ area that comprised the original nanostructures has been overwritten by scanning across the surface with an ODT-coated tip. Increasing the scan size to $4.3 \times 4.3\ \mu m^2$ and imaging the patterned areas with an uncoated tip showed the MHA-patterned areas and the ODT-overwritten areas.

Mirkin also demonstrated parallel patterning using an eight-pen nanoplotter.[94] Multiple-pen experiments employ a cantilever array of which only one tip (the "imaging" tip) has a feedback system to monitor the tip position while writing the patterns. All other tips reproduce passively what occurs to the imaging tip. In this parallel approach, each tip can be coated with different inks and proof-of-concept experiments demonstrated up to eight-pen parallel writing.

2.4.3 Applications of DPN

Patterns created by DPN have been employed to direct successive adsorption steps of a variety of materials such as magnetic nanoparticles,[95] and to create combinatorial templates for 2D particle arrays.[96] As already shown for μCP, SAMs can direct specific adsorption processes of proteins and the same applies for patterned SAMs created by DPN. Protein nanoarrays have been generated and found to exhibit almost no detectable nonspecific binding of proteins to their passivated areas even in complex mixtures of proteins. Therefore they provide an opportunity to study a variety of surface-mediated biological recognition processes.[97] MHA has been patterned on a gold substrate in the form of dots and grids and the areas surrounding these features passivated with 11-mercaptoundecyl-tri(ethylene glycol). Proteins which have a high affinity for carboxylic acid–terminated monolayers at pH 7 and a relatively weak affinity for surfaces coated with 11-mercaptoundecyl-tri(ethylene glycol) have been adsorbed by immersing the substrate in a solution containing the desired proteins. Lysozyme cleanly assembled onto the MHA nanopatterns, as evidenced by AFM, while there was almost no non-specific protein adsorption on the array. Experiments carried out with rabbit immunoglobulin G (IgG) and multicomponent aqueous protein solutions showed that

regardless of the orientations of the IgG within the nanoscopic features the proteins maintained their biological activity. Direct writing of proteins and protein-related structures, such as collagen and a collagen-like peptide, using DPN has been reported as well, down to 30–50-nm linewidths, and the method preserves the triple-helical structure and biological activity of collagen.[98]

DPN has been employed to pattern modified oligonucleotides by the formation of covalently anchored nanoscale patterns on both metallic and insulating substrates.[99] To promote reliable adhesion of the DNA ink to the tip surface, a silicon nitride AFM cantilever has been modified with 3'-aminopropyltrimethoxysilane. Hexanethiol-modified oligonucleotides have been used to directly pattern gold substrates with features ranging from 50 nm to several μm in size and ODT has been used subsequently to passivate the substrates, in order to prevent the adsorption of DNA in subsequent steps. Hereafter, tapping-mode AFM images of the oligonucleotide patterns exhibited feature heights of 2 to 5 nm. The immobilized DNA retained its highly specific recognition properties, and the patterns could be used to direct the assembly of 13-nm-diameter oligonucleotide-modified gold nanoparticles.

The same approach has been extended to oxidized silicon wafers activated by treatment with 3'-mercaptopropyltrimethoxysilane (MPTMS). In this case oligonucleotides with 5'-terminal acrylamide groups have been used, which react with the thiol moieties of the MPTMS substrate to covalently link the DNA to the surface. After patterning, the substrate has been passivated by reaction with buffered acrylic acid monomer. The biological activity of the patterned oligonucleotides has been verified by exposing the surface to a solution containing both complementary and noncomplementary fluorophore-labeled DNA. The patterns have been characterized subsequently by epifluo-rescence microscopy and in all cases fluorescence has only been detected when the complementary target was used. These DNA nanostructures could be used to direct the assembly of complementary DNA-modified gold nanoparticles, and this methodology has been extended in an orthogonal approach.[100]

In another example by Mirkin, DPN has been employed to pattern semiconductor surfaces such as silicon and gallium arsenide with sub-100 nm features using hexamethyldisilazane (HMDS) as the ink.[101]

The combination of DPN and wet chemical etching is a viable approach to produce nanosized features on a silicon surface.[102] The "written" SAM protects the underlying layer from an etchant, while the Au, Ti, and SiO_2 that are not protected by the monolayer can be removed in a stepwise manner. The overall process yields all-Si features with at least one dimension of sub-100 nm size (Scheme 2.6a-e).

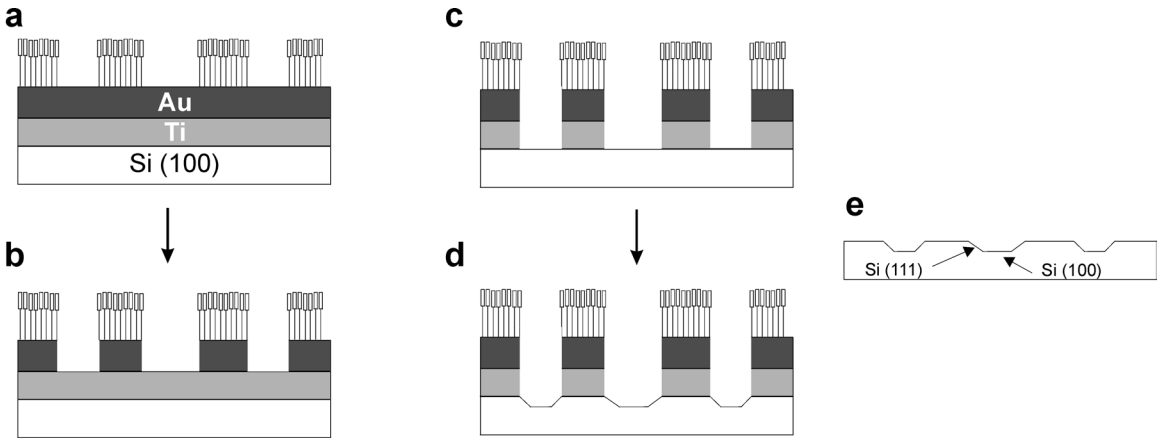

Scheme 2.6 Multistep scheme to produce Si features by combination of DPN and wet chemical etching (adapted from ref. 102).

By changing the writing parameters (contact time and/or writing speed) of the DPN step with an ODT-coated AFM tip pillar structures of increasing size as well as lines with different width were created.

Combining the nanoshaving approach with DPN results in a nanopen-reader-and-writer (NPRW).[103] In each NPRW experiment, a self-assembled monolayer serves as the resist, while an AFM tip displaces the resist molecules from desired locations by using a high shear force. The AFM tip is precoated with adsorbate molecules, which can adsorb to the newly exposed substrate areas.

Luminescent patterns have been created on glass surfaces by DPN and analyzed in situ by fluorescence confocal microscopy (Scheme 2.7 left) by using either a dilute solution of Rhodamine 6G (R6G) (Scheme 2.7 right) or of human chorionic gonadotropin (HCG) antibody tagged with a tetramethylrhodamine (TMR) dye.[104] The patterns produced using R6G are composed of a number of spots. They show features that are characteristic of single molecule emission patterns, such as striped patterns, and abrupt emission cessation, which is indicative of dye molecules switching to and from dark states, and of photobleaching.

Optically active and arbitrarily shaped nanostructures with dimensions well below 200 nm have been produced in a straightforward manner by patterning a number of organic dyes onto Si/SiO_x surfaces.[105]

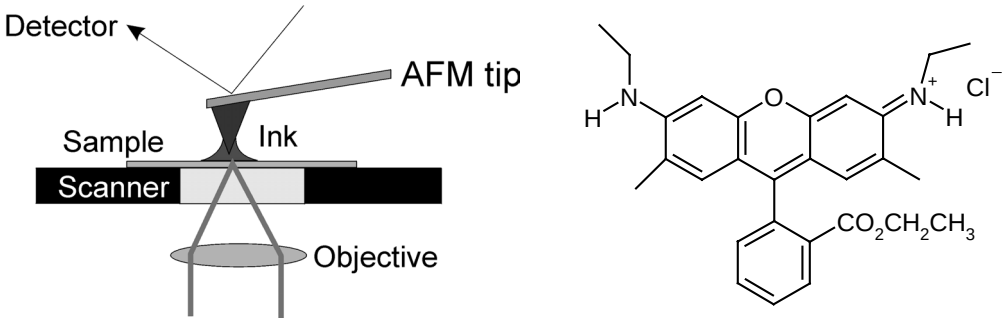

Scheme 2.7 DPN/confocal microscope setup (left) (adapted from ref. 104), and the ink R6G (right).

The possibility of patterning silicon and oxidized silicon substrates with sol-based inks has been demonstrated.[106] This approach is based on the hydrolysis of metal precursors in the water meniscus according to the reaction $2MCl_n + nH_2O \rightarrow M_2O_n + 2n$HCl. The inks are hybrid composites of inorganic salts with amphiphilic block copolymer surfactants. The copolymer surfactant is responsible for dispersing and stabilizing the inorganic ink precursor, for increasing the ink fluidity, and it acts as a structure-directing agent for the materials that constitute the patterned nanostructures. After removing the organic moieties, mesoporous metal oxides such as Al_2O_3, SiO_2, and SnO_2 are the resulting products. A similar approach developed by Liu and coworkers allows the creation of metal nanostructures and exploits a conductive AFM tip to locally perform electrochemistry within the water meniscus.[107] Deposition of dendrimers has been reported as well and patterns with 100 nm features (20 dendrimer molecules) have been generated on a Si/SiO_x surface. The dependence of the resolution on both surface chemistry and molecular weight of the dendrimer ink has been investigated.[108]

2.5 Single molecule detection and manipulation techniques

2.5.1 Introduction

The invention of Scanning Probe Microscopy (SPM),[109] such as Scanning Tunneling Microscopy (STM) in the early 1980s by Binnig, and Rohrer,[110] followed by Atomic Force Microscopy (AFM) in 1986 by Binnig, Quate, and Gerber,[111] represented a break-through for analytical techniques at the nanometer scale.[26d] Sensitivity and limits of detection have been pushed to new levels and in addition these techniques allow one to characterize a sample, such as a biological one, in its natural environment, with minimal perturbation by the probe.[112]

AFM reveals mostly topographical information, which can be difficult to interpret for samples with complicated morphology. The combination of the high resolution of SPM with the sensitivity, specificity, and flexibility afforded by optical techniques would further push the analytical technique's limits. This goal has driven the development of near-field scanning optical microscopy (NSOM or SNOM) which can be used to conduct optical measurements with a spatial resolution beyond the classical diffraction limit.[113]
Many biochemical processes involve recognition events between complementary biomolecules, such as DNA or proteins, based on specific, highly selective receptor-ligand interactions. The optical tweezers technique allows one to manipulate and investigate the biophysics and mechanical properties of single biomolecules or cells.[114] This powerful tool has been employed extensively in life sciences for the fundamental understanding of recognition processes, as well as to investigate the properties, events, and mechanisms, such as protein motion, which regulate complex functional structures at the single molecule level.

2.5.2 Scanning tunneling microscopy

STM is based on a tunneling current flowing between a conducting sample surface and a sharp tip when a voltage bias is applied (Scheme 2.8). When dealing with an organic monolayer in between, the interpretation of data is complicated because there is no theory that describes how the tunneling current propagates through these insulating films. Even though several experiments have been carried out in the last years with smaller tunneling currents[30b] than in the past, there still seems to be a significant effect of the tip being in contact with or penetrating into organic monolayers.[115]

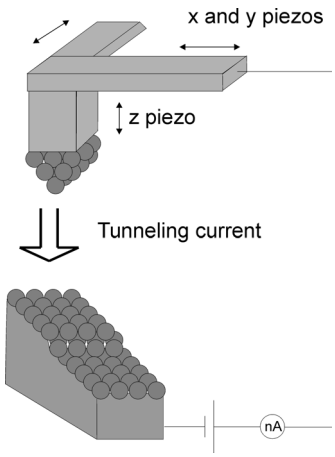

Scheme 2.8 Schematic representation of STM working principle.

The first attempts at imaging biological molecules using STM date back to 1983.[23] In 1987, individual molecules of phthalocyanine, lipid bilayers, and ascorbic acid were imaged.[116] Semiflexible molecules have been studied by direct real-space imaging with STM. For example, Cu-tetrakis(3,5-di-tertbutylphenyl)porphyrin (Cu-DTBPP) molecules have been shown to modify their conformation, adapting to different metallic substrates by principal *s*-type-bond rotations of the four di-tert-butylphenyl (DTBP) groups symmetrically bound to the central porphyrin ring of the molecule. These four bulky groups, imaged by STM as four lobes, determine the shape of the molecule, and define the interaction of the molecule with the substrate.[117]

Supramolecular assemblies have been characterized by STM as well. Kern *et al.* reported single molecule STM observations of chiral complexes generated by the assembly of achiral components and metal centers at a metal surface. Upon co-deposition of iron atoms and 1,3,5-tricarboxybenzoic acid (trimesic acid, TMA) on Cu(100), the molecules react with the metal centers to form chiral complexes $Fe(TMA)_4$ stabilized by metal-ligand interactions.[118]

Another example from the same group concerns supramolecular nanostructures of 4-[trans-2-(pyrid-4-yl-vinyl)]benzoic acid (PVBA) on surfaces based on hydrogen bonds (Figure 2.1).[119] The different morphological assemblies in situ observed on different single-crystal metal surfaces by temperature-controlled STM have been ascribed to a balance between the intermolecular and the surface-adsorbate interactions.

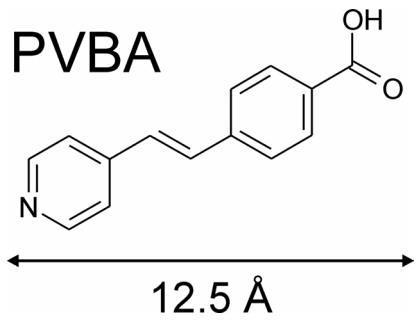

Figure 2.1 Molecular structure of 4-[trans-2-(pyrid-4-yl-vinyl)]benzoic acid (PVBA) with a pyridyl group at the head and a benzoic acid moiety at the tail.

STM has been employed extensively by the group of De Schryver to characterize the two-dimensional organization of monolayers, providing insights in fields such as chirality,[120] reactivity[121] and dynamics at interfaces.[122] It has been shown, *e.g.* that the 2,5-bis(dodecyloxy)terephthalic acid (Figure 2.2) on graphite forms a monolayer, which

displays stabilizing hydrogen bonding along the lamella axis, and the alkyl chains, perpendicularly oriented to the lamella axis, are interdigitated.[123]

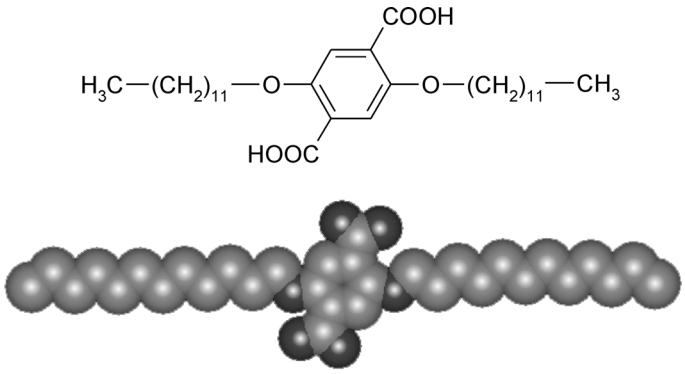

Figure 2.2 2,5-bis(dodecyloxy)terephthalic acid (top) and corresponding molecular model (bottom).

A number of examples have been reported in the literature from the group of Allara concerning the characterization of single conjugated molecules inserted into alkanethiol SAMs. Due to the higher conductivity of these wires with respect to the surrounding monolayer, visualization of the individual molecules was achieved.[124]

2.5.3 Atomic force microscopy

Despite the collective name used to indicate AFM techniques, several different instrumental modes can be defined. It is beyond the scope of this chapter to give an exhaustive overview on SFM-related techniques, and therefore only the most common instrumental modes related to the applications presented in this thesis are reported. The most popular mode is contact mode (CM) in which a very sharp tip (radius in the range of 10-100 nm) attached to the end of a flexible cantilever (spring constant k = 0.1 - 1 N/m) is brought into contact with the surface.[111,125] Either the sample or the tip can be moved, while an electronic feedback maintains preset scanning parameters to keep the vertical deflection of the cantilever constant (constant force mode), and a topographic image can be obtained by plotting the feedback signal (Scheme 2.9). If the sample is scanned under an appropriate angle (90°) also the lateral torsion of the tip can be monitored, probing the friction force existing between the tip and sample and collecting information on the chemical nature of the scanned area.[126]

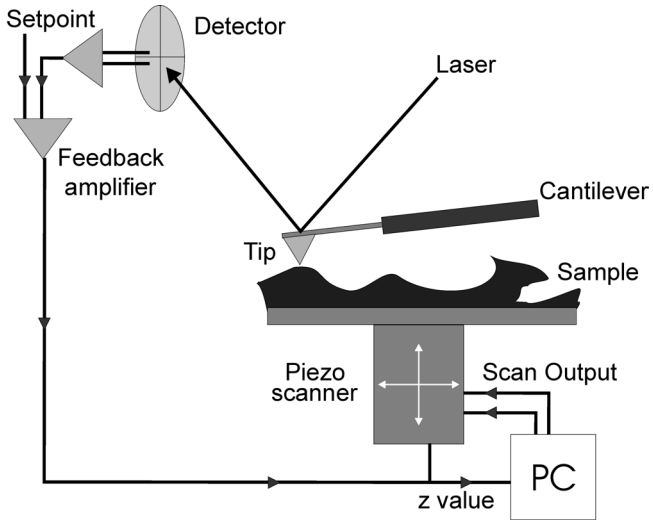

Scheme 2.9 Major components of an SFM apparatus.

When imaging soft samples, such as biological ones, the shear force applied during a contact mode experiment might exceed the mechanical properties of the specimen, causing perturbation or even irreversible damage. Tapping mode AFM (TM-AFM) avoids this difficulty by reducing the force applied by the tip onto the surface.[127] In a typical TM experiment, a cantilever stiffer than the one used in a CM setup (k = 20-80 N/m) is brought near its resonance frequency (cantilever resonance frequency f_0 = 280-320 kHz) by a piezoelectric crystal and it is used to tap periodically the surface. The feedback loop in this case is used to maintain a constant amplitude of oscillation, which decreases in close proximity of a sample. The changes in amplitude and/or phase oscillation are used to reconstruct the topography of the sample. Furthermore, by monitoring the phase shift of the oscillation, it is possible to obtain information on surface properties such as viscoelasticity or adhesion.[128]

Single molecule detection (SMD) by AFM has been shown by several groups. Crooks and coworkers[129] have measured the height of G4 and G8 polyamidoamine (PAMAM) dendrimers on gold using TM-AFM. The deviation in height and lateral size of the surface-confined dendrimers with respect to calculated values may arise from a distribution of molecular sizes resulting from the synthesis, tip-induced deformation of the dendrimers, and/or differences in adsorption geometry. The width of the nanosized features (20 nm) is much larger than the molecular dimensions due to convolution of the AFM tip. For both G8 and G4 the measured height of the dendrimers protruding above the thiol monolayer increases upon exposure of the samples to a hexadecanethiol

solution, from a loss of dendrimer amine-Au interactions in favor of the formation of stronger thiol-Au interactions.

However, absolute height measurements are difficult to carry out because they are affected by the adhesion and viscoelastic properties of the imaged material, which are different for *e.g.* the alkanethiol SAM and the dendritic structures, as in this case.

Similarly, Tomalia *et al.*[130] have measured the molecular diameter and height of individual G5-G10 PAMAM dendrimers on mica. De Schryver *et al.*[131] have used TM-AFM to measure the height of G4 polyphenylene dendrimer molecules spincoated on mica. Good agreement was found between the observed height and values calculated from molecular dynamics simulations.

The AFM spring constant k can vary between 10^{-1} - 10^{2} N/m and cantilever deflections Δz of 0.1 Å can be detected,[132] thus turning the AFM setup into an extremely sensitive force (F) measurement apparatus[133] with a detection limit between 10^{-12} and 10^{-9} N (Equation 2.1). Chemical Force Microscopy technique combines the resolution available through force microscopy, with attractive/repulsive forces taking place between the tip and the sample allowing accurate mapping of surfaces with different chemical functionalities on the basis of different adhesion properties.[134]

Equation 2.1 $$F = \Delta z \times k$$

While in TM and CM imaging modes the sample is scanned in the x-y plane, the only direction in which the piezo bearing the specimen can move during a force spectroscopy experiment is the z direction, i.e. perpendicular to the cantilever. The force-displacement curve (Figure 2.3) is an approach-retract cycle during which the sample first approaches the tip (*i.e.*, the sample moves in a positive z direction) and is subsequently retracted from the tip. A force curve can be divided into several regions:[26d] (a) At large tip-sample separations no interactions occur. (b) At a certain distance, the energy gradient of short-distance interactions overcomes the restoring force of the cantilever and brings the tip in contact with the surface. (c) Moving the sample further in the positive z-direction causes a positive, linear cantilever deflection and the tip and the sample move together. As the sample moves in the negative z-direction, a similar line is traced as the tip and the sample remain in contact. (d) Further moving the tip/sample system in the negative z-direction, the restoring force exerted by the bending of the cantilever overcomes the adhesive force and the tip breaks away from the sample. (e) The cantilever returns to its equilibrium position.

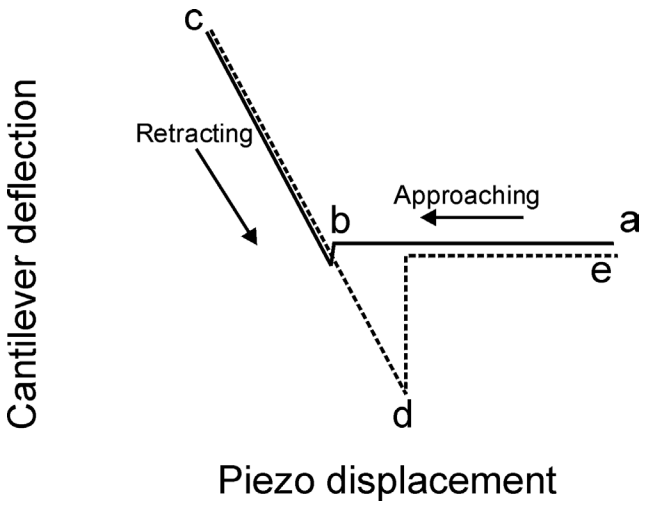

Figure 2.3 Typical force-displacement curve for adhesive contact (adapted from ref. 26d).

The possibility to functionalize individually the tip and the surface allows investigation of specific combinations of molecular pairs. Early force spectroscopy work mainly focused on biological systems,[135] *e.g.* by Gaub *et al*.[27,136] The adhesion force between an AFM tip derivatized with avidin and agarose beads functionalized with biotin, desthiobiotin, or iminobiotin was measured (Scheme 2.10).

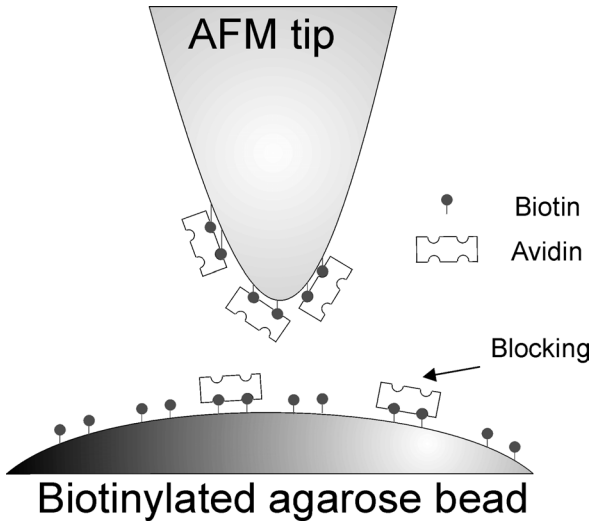

Scheme 2.10 Schematic picture of the avidin-functionalized AFM tip and the biotinylated agarose bead, partially blocked with avidin (adapted from ref. 136a).

At low ligand densities, only a limited number of molecular pairs are interacting. Autocorrelation analysis of the histograms of the adhesion plots showed that quantized forces were required to separate the tip and the bead, with force quanta of 160 ± 20 pN for biotin and 85 ± 15 pN for iminobiotin, respectively.[136a]

Interaction forces between single strands of DNA were measured with an atomic force microscope by a procedure in which DNA oligonucleotides were covalently attached to a spherical probe and surface.[137] Adhesive forces measured between complementary 20-base strands fell into three distinct distributions centered at 1.52, 1.11, and 0.83 nN, which are associated with the rupture of the interchain interaction between a single pair of molecules involving 20, 16 and 12 base pairs, respectively.

In an elegant example by McKendry *et al.* force spectroscopy demonstrated chiral discrimination, by exploiting the differences in adhesion between enantiomers self-assembled onto an AFM tip and the two enantiomers of mandelic acid bound to a gold surface.[138]

Molecular mechanics calculations have been carried out to determine the force required to rupture the streptavidin-biotin complex. The computed force is in agreement with that obtained by single molecule force spectroscopy experiments and these simulations suggested a detailed multiple-pathway rupture mechanism involving five major unbinding steps. Binding forces and specificity were attributed to a hydrogen bond network between the biotin ligand and residues within the binding pocket of streptavidin.[139]

The interpretation of the force value data and their relation to known thermodynamic data have remained inconclusive, however, since Evans and co-workers later showed that single molecule rupture forces for systems in far-from-equilibrium situations, such as biological ones, are highly unloading rate-dependent (for a detailed description cfr. Chapter 6).[140]

2.5.4 Single molecule fluorescence

Near-field scanning optical microscopy (NSOM)[113] is an optical technique based on a revolutionary idea that dates back to the early 20th century, when Synge proposed a new optical microscope with the objective to overcome the diffraction limits of traditional microscopy.[141] Diffraction limits in conventional microscopy arise from the size of the spot that a light beam can be focused to with normal lens elements.[142] It is beyond the scope of this chapter to give a comprehensive description of these phenomena. In short the maximal resolution is approximately equal to half the wavelength of the radiation used, which, for visible light applications, results in a spatial resolution of 200-300 nm.

The idea of Synge, depicted in Scheme 2.11A, is based on forcing the light to pass through a subwavelength aperture in an opaque screen. A specimen placed in the so-called near-field can be observed before the light diffracts with loss in resolution. Scheme 2.11B shows a schematic representation of a NSOM tip with submicron aperture.

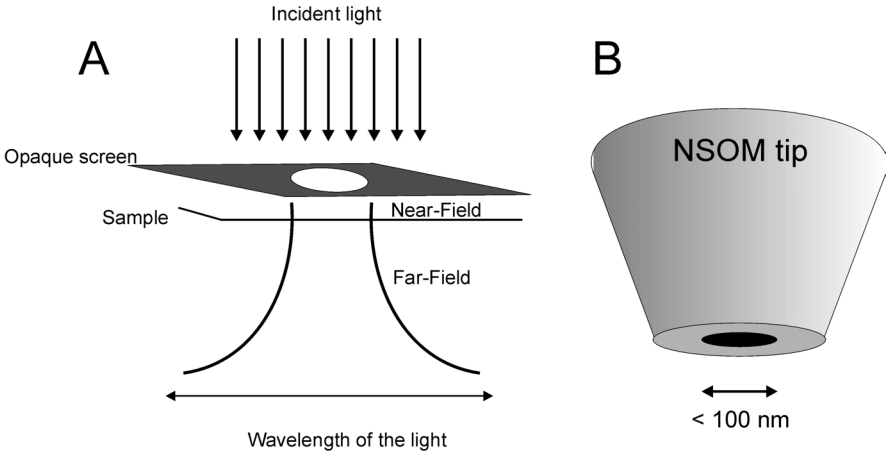

Scheme 2.11 Representation of Synge's ideas and introduction of the concept of near-field (A) and schematic representation of NSOM tip (B).

It took, however, almost half a century before these revolutionary ideas where confirmed at IBM research laboratories, where the first subdiffraction optical measurements with a resolution of λ/20 were performed,[143] representing the basis of modern NSOM.[144] The spatial resolution that can be obtained by NSOM makes it an attractive tool for single molecule detection. Single molecule studies allow identification and examination individual members of a heterogeneous population, while ensemble studies only yield information on the average properties of a system.[148b] Information on the orientation of the transition dipole can also be resolved. NSOM has been used to investigate the photophysical characteristics of first- to fourth-generation (G1 to G4) light-harvesting dendrimer thin films containing coumarin-343 and coumarin-2 as the core and peripheral chromophores, respectively. Thin film photoluminescence (PL) spectra exhibit a significant red shift for the lower generations (G1, G2, and G3) as compared to their respective solution PL spectra, implying the formation of excimers. Spatially resolved PL-NSOM images exhibit pronounced nanoscopic domains for G1, which become more homogeneous in higher generations due to site-isolation of the core chromophore. G4 exhibited complete site-isolation for these light-harvesting dendrimer films.[145]

Applications to semiconductor nanowires are related to their nonlinear optical response, which has potential application for frequency conversion in nanoscale optical circuitry.[146] Van Hulst *et al.* investigated the photodynamics of individual molecules embedded in ultrathin polymer layers, addressing rotational mobility of individual probe molecules in thin films, fluorescence lifetime trajectories and their spatial distribution, and real-time singlet-triplet dynamics.[147] Rotational and translational diffusion of single molecules using a near-field scanning optical microscope with two polarization detection channels has been observed.

Fluorescence spectroscopy[148] has been employed widely in life sciences to investigate biological processes related to proteins/nucleic acids dynamics, molecular recognition, and biological activity of enzymes.[149] RNA catalysis and folding has been reported using fluorescence resonance energy transfer (FRET) at the single molecule level.[150] This approach uses two fluorescent dyes attached to specific sites of a host molecule. Excitation energy can be transferred from the excited donor to the acceptor via dipole interactions. The efficiency of the energy transfer is a function of both distance and reciprocal orientation of the molecules; thus FRET can be correlated to conformational changes of the host molecules decorated with the two dyes,[151] in this case a ribozome.

In another example a green fluorescent donor dye and a red fluorescent acceptor were attached to the cysteine residues introduced at the amino and carboxy termini of the cold-shock protein, a 66-residue, five-stranded β-barrel protein, from the hyperthermophilic bacterium *Thermotoga maritima* (CspTm).[152] Upon addition of a denaturating agent the unfolding process of the protein, resulting in a larger average distance between the donor and acceptor dyes, could be monitored following the corresponding decrease of the FRET.

2.5.5 Optical tweezers

Optical tweezers are complementary tools in single molecule research, with the ability to uncover biophysical and mechanical properties of single biomolecules or polymers. They exploit the fact that light exerts force on matter. Dielectric particles, such as uniform beads or bacterial cells, are attracted to and trapped near the waist of a laser beam that has been focused through a microscope objective. Applied external forces will displace a trapped bead from the trap center, with a linear dependence of displacement on force. Such traps can be made sufficiently compliant so that they exert little resistance to the movement produced by single molecules. Silica and polystyrene beads with a diameter in the range of 1 μm are usually employed by decorating them with biomolecules. The

biophysical, mechanical, and structural properties can be tested by pulling apart the beads and recording the stretching curve.

This technique has been employed widely in systems such as molecular motors or machines. Myosin is a linear two-headed protein, which is responsible for muscle contraction, by interacting with actin filaments. Finer *et al.* used a "dumbbell" structure of an actin filament bound at either end to a polystyrene bead.[153] They trapped both beads, pulled the filament, and moved it near surface-bound silica spheres that were decorated sparsely with myosin molecules. They observed transient bead deflections parallel to the long filament axis and interpreted these as reflecting myosin binding and pulling the filament. Kinesin is structurally similar to myosin, being a linear two-headed linear motor protein as well, which is responsible for vesicle transport along microtubules.[154] A single kinesin molecule can move for several micrometers along a microtubule,[155] rendering it an excellent system for optical tweezer investigation. Silica beads have been modified with kinesin at a low density and, after being trapped they have been brought in close proximity to a microtubule fixed on a microscope coverslip. Steps of 8 nm were clearly distinguished from Brownian motion, separated by dwell periods of variable length.[156]

Instead the F_0F_1-ATPase can be referred to as a rotary motor. It is a multidomain complex consisting of a hydrophilic catalytic unit F_1 protruding into the mitochondria and a hydrophobic proton channel traversing the mitochondrial membrane. This complex is responsible for converting ADP into ATP, a process driven by phosphate and protons (Scheme 2.12A).

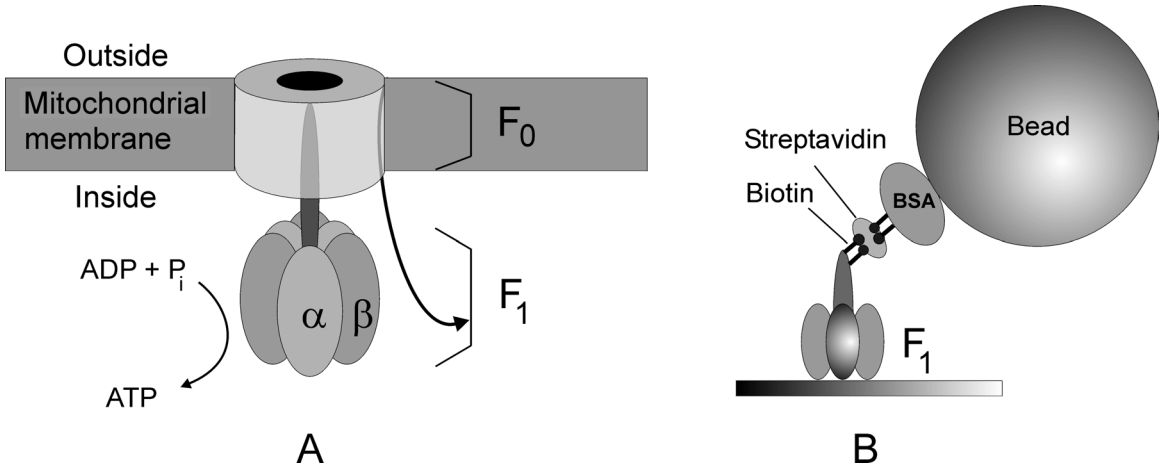

Scheme 2.12 (A) Schematic representation of the molecular motor F_0F_1-ATPase. (B) Experimental setup to probe rotary motion of theF_1 moiety of F_0F_1-ATPase (adapted from ref. 157).

Rotation of the F_1 moiety was detected by means of the setup depicted in Scheme 2.12B by Noij *et al.*[157] At low ATP concentrations, the motor rotates in discrete 120° steps, consistent with sequential ATP hydrolysis at the three β-subunits.[158] The mechanism of stepping is unknown. High-speed imaging shows that the 120° steps consist of roughly 90° and 30° substeps, each taking only a fraction of a millisecond. ATP binding drives the 90° substep, and the 30° substep is probably driven by release of a hydrolysis product. The two substeps are separated by two reactions of about 1 ms, which together occupy most of the ATP hydrolysis cycle.

Transcription of DNA into messenger RNA occurs via the enzyme RNA polymerase (RNAP). The protein moves along the DNA strand to be decoded by draining energy from the nucleotide condensation reaction. Surface-confined RNAP molecules were able to bind from solution with DNA-modified beads, pulling them towards the surface during the transcription process, as shown by Schafer *et al.*[159] The same measurement can be performed by trapping the bead and Yin *et al.* estimated the stall force against which the RNAP stops its movement to be 12.3 ± 3.5 pN.[160] In contrast to what has been observed for kinesin, many stalled complexes did not resume movement upon decreasing the stall force. The same system has been subject to more investigation and Wang *et al.* determined a stall force of 21-27 pN, by introducing a feedback system to enhance the trap strength, while decreasing the light exposure. It is interesting to note that this force value might convolute the disentanglement of secondary DNA structures.[161]

Beside protein motion, optical tweezers have found application in measuring biopolymer elasticity.[114] A single-parameter **A** (flexural persistence length, ca. 50 nm) model is usually employed to describe DNA biophysics, the worm-like chain model (WLC).[162] Optical tweezers have been employed to pull DNA strands[163] and direct measurements of force and extension were used to validate the WLC model with a good agreement between the experimental entropic force-extension data and the theoretical prediction.[163,164]

2.6 Conclusions

The increasing demand of miniaturization of devices has pushed research towards nanofabrication methods, alternative and/or complementary to the photolithographic top-down techniques currently employed in mass production. A valid alternative could arise by combination of traditional top-down approaches with the so called bottom-up one, which relies on building nanosized structures in a controlled manner by spontaneous assembly of properly designed atomic/molecular components. Scanning probe micros-

copy related techniques represent today the tool to achieve the ultimate lateral resolution in controlling position of matter, allowing single atom/molecule manipulation. Parallel to the development in nanofabrication techniques, analytical techniques follow the same trend, with increasing sensitivity and detection limits to characterize these nanostructures. The work presented in this thesis is directly related to nanotechnological issues, and is devoted to combinations of top-down/bottom up approaches, focusing in particular on AFM-related techniques. Specific aspects will be described in detail in the individual chapters.

2.7 References and notes

[1] Feynman, R. P. *Eng. Sci.* **1960**, *23*, 22-36.

[2] See the following technology roadmaps for micro and nanoelectronics: a) *The International Technology Roadmap for Semiconductors 2002*, to be found at http://public.itrs.net/Files/2002Update/Home.pdf. b) Compaño, R.; Molenkamp, L.; Paul, D. J. *Technology Roadmap for Nanoelectronics*, European Commission IST Programme: Future and Emerging Technologies, Microelectronics Advanced Research Initiative; http://nanoworld.org/NanoLibrary/nanoroad.pdf.

[3] a) Gittins, D. I.; Bethell, D.; Schiffrin, D. J.; Nichols, R. J. *Nature* **2000**, *408*, 67–69. b) Collier, C. P.; Mattersteig, G.; Wong, E. W.; Luo, Y.; Beverly, K.; Sampaio, J.; Raymo, F. M.; Stoddart, J. F.; Heath, J. R. *Science* **2000**, *289*, 1172–1175. c) Chen, J.; Reed, M. A.; Rawlett, A. M.; Tour, J. M. *Science* **1999**, *286*, 1550–1552. d) Lutwyche, M. I.; Despont, M.; Drechsler, U.; Dürig, U.; Häberle, W.; Rothuizen, H.; Stutz, R.; Widmer, R.; Binnig, G. K.; Vettiger, P. *Appl. Phys. Lett.* **2000**, *77*, 3299–3301. e) Mizutani, W.; Ishida, T.; Tokumoto, H. *Langmuir* **1998**, *14*, 7197–7202.

[4] For an overview on microelectromechanical systems see: a) Wise, K. D.; Najafi, K. *Science* **1991**, *254*, 1335-1342. b) Bryzek, J.; Peterson, K.; McCulley, W. *IEEE Spectrum* **1994**, *31*, 2-31. c) MacDonald, N. C. *Microelectron. Eng.* **1996**, *32*, 4-7. d) Kovacs, G. T. A.; Petersen, K.; Albin, M. *Anal. Chem.* **1996**, *68*, 407A-412A.

[5] For an overview on microanalytical systems see: a) Service, R. E. *Science* **1995**, *268*, 26-27. b) Manz, A. *Chimia* **1996**, *59*, 140-145. c) Craston, D.; Cowen, S. *Chem. Br.* **1996**, 31-33. d) Day, P. *Chem. Br.* **1996**, 29-31. e) Goffeau, A. *Nature* **1997**, *385*, 202-203.

[6] For an overview on combinatorial synthesis see: Szostak, J. W. *Chem. Rev.* **1997**, *97*, 347-509.

[7] For an overview on microsensors see: a) Galla, H.-J. *Angew. Chem. Int. Ed.* **1992**, *31*, 45-47. b) Kleinschmidt, P.; Hanrieder, W. *Sens. Actuators A* **1992**, *33*, 5-17. c) Vellekoop, M. J.; Lubking, G. W.; Sarro, P. M.; Venema, A. *Sens. Actuators A* **1994**, *44*, 249-263. d) Fuhr, G.; Müller, T.; Schnelle, T.; Hagedorn, R.; Voigt, A.; Fiedler, S.; Arnold, W. A.; Zimmermann, U.; Wagner, B.; Heuberger, A. *Naturwissenschaften* **1994**, *81*, 528-535. e) Bryzek, J. *Sensors* **1996**, *7*, 4-38.

[8] For an overview on microoptics see: a) Carts, Y. A. *Laser Focus World* **1994**, *30*, 67-71. b) Lee, S. S.; Lin, L. Y.; Wu, M. C. *Appl. Phys. Lett.* **1995**, *67*, 2135-2137. c) Wu, M. C.; Lin, L. Y.; Lee, S. S.; King, C. R. *Laser Focus World* **1996**, *32*, 64-68.

[9] a) Sundaram, M.; Chalmers, S. A.; Hopkins, P. F.; Gossard, A. C. *Science* **1991**, *254*, 1326-1335. b) Kastner, M. A. *Phys. Today* **1993**, *46*, 24-31. c) Reed, M. A. *Sci. Am.* **1993**, *270*, 118-123. d) Weller, H. *Angew. Chem. Int. Ed.* **1993**, *32*, 41-53. e) Likharev, K. K. *IBM J. Res. Dev.* **1988**, *32*, 144-158. f) Devoret, M. H.; Esteve, D.; Urbina, C. *Nature* **1992**, *360*, 547-553. g) Likharev, K. K.; Claeson, T. *Sci. Am.* **1992**, *269*, 80-85.

[10] For an overview on photolithography see: a) Ito, T.; Okazaki, S. *Nature* **2000**, *406*, 1027-1031. b) Walraff, G. M.; Hinsberg, W. D. *Chem. Rev.* **1999**, *99*, 1801-1821. c) Okazaki, S. *J. Vac. Sci. Technol. B* **1991**, *9*, 2829-2833. d) Jeong, H. J.; Markle, D. A.; Owen, G.; Pease, F.; Grenville, A.; von Bünau, R. *Solid State Technol.* **1994**, *37*, 39-47. e) Levenson, M. D. *Solid State Technol*. **1995**, *38*, 57-66. f) Geppert, L. *IEEE Spectrum* **1996**, *33*, 33-38.

[11] a) Moore, G. E. *Electronics* **1965**, *38*, 114-117. b) Moore, G. E. *IEDM Tech. Dig.* **1975**, 11-13.

[12] McCord, M.; Rooks, M. In *Handbook of Microlithography, Micromachining and Microfabrication*; SPIE Press: Bellingham, WA, 1997, Vol. 1, Chapter 2.

[13] Packman, P. A. *Science* **1999**, *285*, 2079-2081.

[14] For unconventional nanofabrication methods see: Xia, Y.; Rogers, J. A.; Paul, K. E.; Whitesides, G. M. *Chem. Rev.* **1999**, *99*, 1823-1848.

[15] For an overview of soft lithography, see: a) Xia, Y.; Whitesides, G. M. *Angew. Chem. Int. Ed.* **1998**, *37*, 550-575. b) Biebuyck, H. A.; Larsen, N. B.; Delamarche, E.; Michel, B. *IBM J. Res. Dev.* **1997**, *41*, 159-170. c) Kumar, A.; Whitesides, G. M. *Appl. Phys. Lett.* **1993**, *63*, 2002-2004. d) Xia, Y.; Kim, E.; Zhao, X.-M.; Rogers, J. A.; Prentiss, M.; Whitesides, G. M. *Science* **1996**, *273*, 347-349. e) Zhao, X.-M.; Xia, Y.; Whitesides, G. M. *Adv. Mater.* **1996**, *8*, 837-840. f) Kim, E.; Xia, Y.; Whitesides, G. M. *Nature* **1995**, *376*, 581-584. g) Kim, E.; Xia, Y.; Zhao, X.-M.; Whitesides, G. M. *Adv. Mater.* **1997**, *9*, 651-654. h) Zhao, X.-M.; Xia, Y.; Whitesides, G. M. *J. Mater. Chem.* **1997**, *7*, 1069-1074. i) Qin, D.; Xia, Y.; Rogers, J. A.; Jackman, R. J.; Zhao, X.-M.; Whitesides,

G. M. *Top. Curr. Chem.* **1998**, *194*, 1-20. j) Whitesides, G. M.; Xia, Y. *Annu. Rev. Mater. Sci.* **1998**, *28*, 153-184.

[16] a) Chou, S. Y.; Krauss, P. R.; Renstrom, P. J. *Science* **1996**, *272*, 85-87. b) Chou, S. Y.; Krauss, P. R.; Zhang, W.; Guo, L.; Zhuang, L. *J. Vac. Sci. Technol.* **1997**, *B15*, 2897-2904.

[17] a) Piner, R. D.; Zhu, J.; Xu, F.; Hong, S.; Mirkin, C. A. *Science* **1999**, *283*, 661-663. b) Mirkin, C. A.; Hong, S.; Levine, R. D. *ChemPhysChem* **2001**, *2*, 37-39.

[18] Greig, L. M.; Philip, D. *Chem. Soc. Rev.* **2001**, *30*, 287-302.

[19] a) Gracias, D. H.; Tien, J.; Breen, T. L.; Hsu, C.; Whitesides, G. M. *Science* **2000**, *289*, 1170-1172. b) Bowden, N. B.; Weck, M.; Choi, I. S.; Whitesides, G. M. *Acc. Chem. Res.* **2001**, *34*, 231-238.

[20] a) Ball, P. *Nature* **2000**, *406*, 118–120. b) Park, H.; Park, J.; Lim, A. K. L.; Anderson, E. H.; Alvisatos, A. P.; McEuen, P. L. *Nature* **2000**, *407*, 57-60. c) Collier, C. P.; Mattersteig, G.; Wong, E. W.; Luo, Y.; Beverly, K.; Sampaio, J.; Raymo, F. M.; Stoddart, J. F.; Heath, J. R. *Science* **2000**, *289*, 1172-1175. d) Chen, J.; Wang, W.; Reed, M. A.; Rawlett, A. M.; Price, D. W.; Tour, J. M. *Appl. Phys. Lett.* **2000**, *77*, 1224-1226. e) Balzani, V.; Credi, A.; Raymo, F. M.; Stoddart J. F. *Angew. Chem. Int. Ed.* **2000**, *39*, 3348-3391.

[21] Cramer, F. *Chaos and Order. The Complex Structure of Living Systems*; VCH: Weinheim, Germany, 1993.

[22] Service, R. F. *Science* **1999**, *283*, 1668–1669.

[23] Binnig, G.; Rohrer, H. *Rev. Mod. Phys.* **1987**, *59*, 615-625.

[24] Mehta, A. D.; Rief, M.; Spudich, J. A.; Smith, D. A.; Simmons, R. M. *Science* **1999**, *283*, 1689-1695.

[25] Bayburt, T. H.; Carlson, J. W.; Sligar, S. G. *Langmuir* **2000**, *16*, 5993-5997.

[26] a) Poirier, G. E. *Chem. Rev.* **1997**, *97*, 1117–1128. b) Dunn, R. C. *Chem. Rev.* **1999**, *99*, 2891–2927. c) Veerman, J. A.; Levi, S. A.; Van Veggel, F. C. J. M.; Reinhoudt, D. N.; Van Hulst, N. F. *J. Phys. Chem. A* **1999**, *103*, 11264–11270. d) Takano, H.; Kenseth, J. R.; Wong, S.-S.; O'Brien, J. C.; Porter, M. D. *Chem. Rev.* **1999**, *99*, 2845–2890. e) Ishii, Y.; Yanagida, T. *Single Mol.* **2000**, *1*, 5–13.

[27] a) Rief, M.; Oesterhelt, F.; Heymann, B.; Gaub, H. E. *Science* **1997**, *275*, 1295–1297. b) Rief, M.; Gautel, M.; Oesterhelt, F.; Fernandez, J. M.; Gaub, H. E. *Science* **1997**, *276*, 1109–1112.

[28] Nuzzo, R. G.; Allara, D. L. *J. Am. Chem. Soc.* **1983**, *105*, 4481-4483.

[29] For general reviews on SAMs see: a) Bain, C. D.; Whitesides G. M. *Angew. Chem. Int. Ed.* **1989**, *28*, 506-512. b) Whitesides, G. M.; Laibinis, P. E. *Langmuir* **1990**, *6*, 87-96. c)

Ulman, A. *Introduction to Thin Organic Films: From Langmuir-Blodgett to Self-Assembly*; Academic Press: Boston, MA, 1991. d) Swalen, J. D. *Annu. Rev. Mater. Sci.* **1991**, *21*, 373-408. e) Dubois, L. H.; Nuzzo, R. G. *Annu. Rev. Phys. Chem.* **1992**, *43*, 437-463. f) Ulman, A. *Characterization of Organic Thin Films*; Butterworth-Heinemann: Boston, MA, 1995. g) Allara, D. L. *Biosens. Bioelectron.* **1995**, *10*, 771-783.

[30] Grasserbauer, M.; Dudek, H. J.; Ebel, M. F. *Angewandte Oberflächenanalyse mit SIMS, AES, XPS*; Springer: Berlin, 1985, Chapter 1, p. 1. b) Gewirth, A. A.; Niece, B. K. *Chem Rev.* **1997**, *97*, 1129-1162.

[31] a) Chailapakul O.; Sun, L.; Xu, C.; Crooks, R. M. *J. Am. Chem. Soc.* **1993**, *115*, 12459-12467. b) Bishop, A. R.; Nuzzo, R. G. *Curr. Opin. Colloid Interface Sci.* **1996**, *1*, 127-136. c) Bain, C. D.; Whitesides, G. M. *J. Am. Chem. Soc.* **1988**, *110*, 3665-3666.

[32] a) Troughton, E. B.; Bain, C. D.; Whitesides, G. M.; Nuzzo, R. G.; Allara, D. L.; Porter, M. D. *Langmuir* **1988**, *4*, 365-385. b) Rubinstein, I.; Steinberg, S.; Tor, Y.; Shanzer, A.; Sagiv, J. *Nature* **1988**, *332*, 426-428. c) Steinberg S.; Rubinstein, I. *Langmuir* **1992**, *8*, 1183-1187. d) Hagenhoff, B.; Benninghoven, A.; Spinke, J.; Liley, M.; Knoll, W. *Langmuir* **1993**, *9*, 1622-1624. e) Zhang, M.; Anderson, M. R. *Langmuir* **1994**, *10*, 2807-2813. f) Huisman, B.-H.; Rudkevich, D. M.; Van Veggel, F. C. J. M.; Reinhoudt, D. N. *J. Am. Chem. Soc.* **1996**, *118*, 3523-3524. g) Friggeri, A.; Van Veggel, F. C. J. M.; Reinhoudt, D. N.; Kooyman, R. P. H. *Langmuir* **1998**, *14*, 5457-5463. h) Friggeri, A.; Van Veggel, F. C. J. M.; Reinhoudt, D. N. *Chem. Eur. J.* **1999**, *5*, 3595-3602. i) Van der Vegte, E. W.; Subbotin, A.; Hadziioannou, G.; Ashton, P. R.; Preece, J. A. *Langmuir* **2000**, *16*, 3249-3256.

[33] Nuzzo, R. G.; Zegarski, B. R.; Dubois, L. H. *J. Am. Chem. Soc.* **1987**, *109*, 733-740.

[34] Delamarche, E.; Michel, B.; Kang, H.; Gerber, Ch. *Langmuir* **1994**, *10*, 4103-4108.

[35] Schlenoff, J. B.; Li, M.; Ly, H. *J. Am. Chem. Soc.* **1995**, *117*, 12528-12536.

[36] a) Thoden Van Velzen, E. U.; Engbersen, J. F. J.; Reinhoudt, D. N. *J. Am. Chem. Soc.* **1994**, *116*, 3597-3598. b) Huisman, B.-H.; Schönherr, H.; Huck, W. T. S.; Friggeri, A.; Van Manen, H.-J.; Menozzi, E.; Vancso, G. J.; Van Veggel, F. C. J. M.; Reinhoudt, D. N. *Angew. Chem. Int. Ed.* **1999**, *38*, 2248-2251. c) Zehner, R.; Sita, L. R. *Langmuir* **1997**, *13*, 2973-2979. d) Friggeri, A.; Van Manen, H.-J.; Auletta, T.; Li, X.-M.; Zapotoczny, S.; Schönherr, H.; Vancso, G. J.; Huskens, J.; Van Veggel, F. C. J. M.; Reinhoudt, D. N. *J. Am. Chem. Soc.* **2001**, *123*, 6388-6395. e) Van Manen H.-J.; Auletta, T.; Dordi, B.; Schönherr, H.; Vancso, G. J.; Van Veggel, F. C. J. M.; Reinhoudt, D. N. *Adv. Funct. Mater.* **2002**, *12*, 811-818.

[37] a) Winslow, J. S. *IEEE Trans. Consumer Electron.* **1976**, 318-326. b) Lehmann, H. W.; Widmer, R.; Ebnoether, M.; Wokaun, A.; Meier, M.; Miller, S. K. *J. Vac. Sci. Technol. B*

1983, *1*, 1207-1210. c) Rodia, C. M. *Proc. SPIE Int. Soc. Opt. Eng.* **1985**, *529*, 69-75. d) Schlereth, K.-H.; Bötther, H. *J. Vac. Sci. Technol. B* **1992**, *10*, 114-117. e) Emmelius, M.; Pawlowski, G.; Vollmann, H. W. *Angew. Chem. Int. Ed.* **1989**, *28*, 1445-1471. f) Shvartsman, F. P. *Diffractive and Miniaturized Optics*; SPIE Optical Engineering Press: Bellingham, WA, 1993, pp. 165-186. g) Chou, S. Y.; Krauss, P. R.; Renstrom, P. J. *Appl. Phys. Lett.* **1995**, *67*, 3114-3116. h) Terris, B. D.; Mamin, H. J.; Best, M. E.; Logan, J. A.; Rugar, D. *Appl. Phys. Lett.* **1996**, *69*, 4262-4264. i) Gale, M. T. *Micro-Optics: Elements, Systems and Applications;* Taylor & Francis: London, 1997, pp. 153-179. j) Haverkorn Van Rijsewijk, H. C.; Legierse, P. E. J.; Thomas, G. E. *Philips Tech. Rev.* **1982**, *40*, 287-297. k) Kloosterboer, J. G.; Lippits, G. J. M.; Meinders, H. C. *Philips Tech. Rev.* **1982**, *40*, 198-309.

[38] Kumar, A.; Biebuyck, H.; Whitesides, G. M. *Langmuir* **1994**, *10*, 1498-1511.

[39] a) *Siloxane Polymers*; Prentice-Hall: Engleword, NJ, 1993. b) Künzler, J. F. *Trends Polym. Sci.* **1996**, *4*, 52-59.

[40] Biebuyck, H. A.; Whitesides, G. M. *Langmuir* **1994**, *10*, 4581-4587.

[41] Larsen, N. B.; Biebuyck, H.; Delamarche, E.; Michel, B. *J. Am. Chem. Soc.* **1997**, *119*, 3017-3026.

[42] Libioulle, L.; Bietsch, A.; Schmid, H.; Michel, B.; Delamarche, E. *Langmuir* **1999**, *15*, 300-304.

[43] Delamarche, E.; Schmid, H.; Bietsch, A.; Larsen, N. B.; Rothuizen, H.; Michel, B.; Biebuyck, H. A. *J. Phys. Chem. B* **1998**, *102*, 3324-3334.

[44] Liebau, M.; Huskens, J.; Reinhoudt, D. N. *Adv. Funct. Mater.* **2001**, *11*, 147-150.

[45] Bietsch A.; Michel, B. *J. Appl. Phys.* **2000**, *88*, 4310-4318. b) Delamarche, E.; Schmid, H.; Michel, B.; Biebuyck, H. *Adv. Mater.* **1997**, *9*, 741-746. c) Hui, C. Y.; Jagota, A.; Lin, Y. Y.; Kramer E. J. *Langmuir* **2002**, *18*, 1394-1407.

[46] a) Grzybowski, B. A.; Brittain, S. T.; Whitesides, G. M. *Rev. Sci. Instrum.* **1999**, *70*, 2031-2037. b) Schmid, H.; Michel, B. *Macromolecules* **2000**, *33*, 3042-3052.

[47] Rogers, A.; Paul, K. E.; Whitesides, G. M. *J. Vac. Sci. Technol. B*, **1998**, *16*, 88-97.

[48] a) Tormen, M.; Borzenko, T.; Steffen, B.; Schmidt, G.; Molenkamp, L. W. *Appl. Phys. Lett.* **2002**, *81*, 2094-2096. b) Odom, T. W.; Love, J. C.; Wolfe, D. B.; Paul, K. E.; Whitesides, G. M. *Langmuir*, **2002**, *18*, 5314-5320.

[49] Martin, B. D.; Brandow, S. L.; Dressick, W. J.; Schull, T. L. *Langmuir*, **2000**, *16*, 9944-9946.

[50] a) Yan, L.; Huck, W. T. S.; Zhao, X.-M.; Whitesides, G. M. *Langmuir* **1999**, *15*, 1208-1214. b) Lahiri, J.; Ostuni, E.; Whitesides, G. M. *Langmuir* **1999**, *15*, 2055-2060.

[51] a) Owen, M. J.; Fritz, J. L. in *Proc. Int. Conf. Front. Polym. Adv. Mater. 3rd;* Plenum: New York, 1995, p. 201. b) Murakami, T.; Kuroda, S.-L.; Osawa, Z. *J. Colloid Interface Sci.* **1998**, *202*, 37-44. c) Hilborg, H.; Ankner, J. F.; Gedde, U. W.; Smith, G. D.; Yasuda, H. K.; Wikström, K. *Polymer* **2000**, *41*, 6851-6863.

[52] Donzel, C.; Geissler, M.; Bernard, A.; Wolf, H.; Michel, B; Hilborn, J.; Delamarche, E. *Adv. Mater.* **2001**, *13*, 1164-1167.

[53] a) Wilbur, J. L.; Kumar, A.; Kim, E.; Whitesides, G. M. *Adv. Mater.* **1994**, *6*, 600-604. b) Kumar, A.; Abbott, N. L.; Kim, E.; Biebuyck, H. A.; Whitesides, G. M. *Acc. Chem. Res.* **1995**, *28*, 219-226. c) Whitesides, G. M.; Gorman C. B. *Handbook of Surface Imaging and Visualization*; CRC Press: Boca Raton, FL, 1995, pp. 713-733. d) Wilbur, J. L.; Kumar, A.; Biebuyck, H. A.; Kim, E.; Whitesides, G. M. *Nanotechnology* **1996**, *7*, 452-457. e) Xia, Y.; Zhao, X.-M.; Whitesides, G. M. *Microelectron. Eng.* **1996**, *32*, 255-268.

[54] Hidber, P. O.; Helbig, W.; Kim, E.; Whitesides, G. M. *Langmuir* **1996**, *12*, 1375-1380.

[55] a) López, G. P.; Biebuyck, H. A.; Frisbie, C. D.; Whitesides, G. M. *Science* **1993**, *260*, 647-649. b) López, G. P.; Biebuyck, H. A.; G. M. Whitesides, G. M. *Langmuir* **1993**, *9*, 1513-1516; c) López, G. P.; Biebuyck, H. A.; Härter, R.; Whitesides, G. M. *J. Am. Chem. Soc.* **1993**, *115*, 10774-10781.

[56] a) Wilbur, J. L.; Biebuyck, H. A.; MacDonald, J. C.; Whitesides, G. M. *Langmuir* **1995**, *11*, 825-831. b) Bar, G.; Rubin, S.; Prikh, A. N.; Swanson, B. I.; Zawodzinski, Jr. T. A.; Whangbo, M.-H. *Langmuir* **1997**, *13*, 373-377.

[57] Moss, S. J. in *The Chemistry of the Semiconductor Industry*; Chapman and Hall: New York, 1987, pp. 390-413.

[58] Xia, Y.; Zhao, X.-M.; Kim, E.; Whitesides, G. M. *Chem. Mater.* **1995**, *7*, 2332-2337.

[59] a) Kim, E.; Kumar, A.; Whitesides, G. M. *J. Electrochem. Soc.* **1995**, *142*, 628-633. b) Kim, E.; Whitesides, G. M.; Freiler, M. B.; Levy, M.; Lin, J. L.; Osgood, Jr., R. M. *Nanotechnology* **1996**, *7*, 266-269. c) Whidden, T. K.; Ferry, D. K.; Kozicki, M. N.; Kim, E.; Kumar, A.; Wilbur, J. L.; Whitesides, G. M. *Nanotechnology* **1996**, *7*, 447-451. d) Xia, Y.; Whitesides, G. M. *Adv. Mater.* **1996**, *8*, 765-768.

[60] Qin, D.; Xia, Y.; Black, A. J.; Whitesides G. M. *J. Vac. Sci. Technol. B* **1998**, *16*, 98-103.

[61] Zhao, X.-M.; Wilbur, J. L.; Whitesides, G. M. *Langmuir* **1996**, *12*, 3257-3264.

[62] Wang, A.; Zhao, J.; Green, M. A. *Appl. Phys. Lett.* **1990**, *57*, 602-604.

[63] Rajkumar, N.; McMullin, J. N. *Appl. Opt.* **1995**, *34*, 2556-2559.

[64] Gupta, V. K.; Abbott, N. L. *Science* **1997**, *276*, 1533-1536.

[65] a) Kumar, A.; Whitesides, G. M. *Science* **1994**, *263*, 60-62. b) Kim, E.; Whitesides, G. M. *Chem. Mater.* **1995**, *7*, 1257-1264.

[66] a) Bunker, B. C.; Rieke, P. C.; Tarasevich, B. J.; Campbell, A. A.; Fryxell, G. E.; Graff, G. L.; Song, L.; Liu, J.; Virden, J. W.; McVay, G. *Science* **1994**, *264*, 48-55. b) Rieke, P. C.; Tarasevich, B. J.; Wood, L. L.; Engelhard, M. H.; Baer, D. R.; Fryxell, G. E.; John, C. M.; Laken, D. A.; Jaehnig, M. C. *Langmuir* **1994**, *10*, 619-622. c) Abbott, N. L.; Whitesides, G. M. *Langmuir* **1994**, *10*, 1493-1497.

[67] a) Biebuyck, H. A.; Whitesides, G. M. *Langmuir* **1994**, *10*, 2790-2793. b) Gorman, C. B.; Biebuyck, H. A.; Whitesides, G. M. *Chem. Mater.* **1995**, *7*, 252-254.

[68] Kim, E.; Whitesides, G. M.; Lee, L. K.; Smith, S. P.; Prentiss, M. *Adv. Mater.* **1996**, *8*, 139-142.

[69] a) Stenger, D. A.; Georger, J. H.; Dulcey, C. S.; Hickman, J. J.; Rudolph, A. S.; Nielsen, T. B.; McCort, S. M.; Calvert, J. M. *J. Am. Chem. Soc.* **1992**, *114*, 8435-8442. b) DiMilla, P. A.; Folkers, J. P.; Biebuyck, H. A.; Haerter, R.; Lopez, G. P.; Whitesides, G. M. *J. Am. Chem. Soc.* **1994**, *116*, 2225-2226. c) Mrksich, M.; Whitesides, G. M. *Trends Biotechnol.* **1995**, *13*, 228-230.

[70] Palacin, S.; Hidber, P. C.; Bourgoin, J.-P.; Miramond, C.; Fermon, C.; Whitesides, G. M. *Chem. Mater.* **1996**, *8*, 1316-1325.

[71] Kaloyeros, A. E.; Fury, M. A. *MRS Bull.* **1993**, *28*, 22-28.

[72] a) Jeon, N. L.; Nuzzo, R. G.; Xia, Y.; Mrksich, M.; Whitesides, G. M. *Langmuir* **1995**, *11*, 3024-3026. b) Jeon, N. L.; Clem, P. G.; Nuzzo, R. G.; Payne, D. A. *J. Mater. Res.* **1995**, *10*, 2996-2999. c) Jeon, N. L.; Clem, P. G.; Payne, D. A.; Nuzzo, R. G. *Langmuir* **1996**, *12*, 5350-5355. d) Yang, H.; Coombs, N.; Ozin, G. A. *Adv. Mater.* **1997**, *9*, 811-814.

[73] a) Singhvi, R.; Kumar, A.; Lopez, G. P.; Stephanopoulos, G. N.; Wang, D. I. C.; Whitesides, G. M.; Ingber, D. E. *Science* **1994**, *264*, 696-698. b) Chen, C. S.; Mrksich, M.; Huang, S.; Whitesides, G. M.; Ingber, D. E. *Science* **1997**, *276*, 1245-1248. c) Gallant, N. D.; Capadona, J. R.; Frazier, A. B.; Collard, D. M.; Garcia, A. J. *Langmuir*, **2002**, *18*, 5579-5584.

[74] Mrksich, M.; Chen, C. S.; Xia, Y.; Dike, L. E.; Ingber, D. E.; Whitesides, G. M. *Proc. Natl. Acad. Sci. USA* **1996**, *93*, 10775-10778.

[75] Mrksich, M.; Dike, L. E.; Tien, J.; Ingber, D. E.; Whitesides, G. M. *Exp. Cell Res.* **1997**, *235*, 305-313.

[76] a) Moffat, T. P.; Yang, H. *J. Electrochem. Soc.* **1995**, *142*, L220-L222. b) Xia, Y.; Kim, E.; Mrksich, M.; Whitesides, G. M. *Chem. Mater.* **1996**, *8*, 601-603.

[77] a) Xia, Y.; Kim, E.; Whitesides, G. M. *J. Electrochem. Soc.* **1996**, *143*, 1070-1079. b) Yang, X. M.; Tryk, A. A.; Hasimoto, K.; Fujishima, A. *Appl. Phys. Lett.* **1996**, *69*, 4020-4022.

[78] Kittel, C. *Introduction to Solid State Physics*, *6th ed*.; Wiley: New York, 1986, p. 110.

[79] Ulman, A. *Chem. Rev.* **1996**, *96*, 1533-1554 and cited literature.

[80] a) Xia, Y.; Mrksich, M.; Kim, E.; Whitesides, G. M. *J. Am. Chem. Soc.* **1995**, *11*, 9576-9577. b) Wang, D.; Thomas, S. G.; Wang, K. L.; Xia, Y.; Whitesides, G. M. *Appl. Phys. Lett.* **1997**, *70*, 1593-1595.

[81] St. John, P. M.; Craighead, H. G. *Appl. Phys. Lett.* **1996**, *68*, 1022-1024.

[82] Jeon, N. L.; Finnie, K.; Branshaw, K.; Nuzzo, R. G. *Langmuir* **1997**, *13*, 3382-3391.

[83] Tan J. L.; Tien J.; Chen C. S. *Langmuir*, **2002,** *18*, 519-523.

[84] Inerowicz, H. D.; Howell, S.; Regnier, F. E.; Reifenberger, R. *Langmuir* **2002**, *18*, 5263-5268.

[85] Hidber, P. C.; Helbig, W.; Kim, E.; Whitesides, G. M. *Langmuir* **1996**, 12, 1375-1380.

[86] Kind, H.; Geissler, M.; Schmid, H.; Michel, B.; Kern, K.; Delamarche, E. *Langmuir* **2000**, *16*, 6367-6373.

[87] Eigler, D. M.; Schweizer, E. K. *Nature*, **1990**, *344*, 524-526.

[88] Crommie, M. F.; Lutz, C. P.; Eigler, D. M. *Science* **1993**, *262*, 218-220.

[89] a) Xu, S.; Liu, G.-Y. *Langmuir* **1997**, *13*, 127-129. b) Xu, S.; Laibinis, P. E.; Liu, G.-Y. *J. Am. Chem. Soc.* **1998**, *120*, 9356-9361. c) Xu, S.; Laibinis, P. E.; Liu, G.-Y. *Langmuir*, **1999**, *15*, 7244-7251.

[90] Wadu-Mesthrige, K.; Amro, N. A.; Garno, J. C.; Xu, S.; Liu G.-Y. *Biophys. J.* **2001**, *80*, 1891–1899.

[91] Zhao, J.; Uosaki, K. *Langmuir* **2001**, *17*, 7784-7788.

[92] Rozhok, S.; Piner, R.; Mirkin, C. A. *J. Phys. Chem.* **2003**, *107*, 751-757.

[93] Hong, S.; Jin, Z.; Mirkin, C. A. *Science* **1999**, *286*, 523-525.

[94] Hong, S.; Mirkin, C. A. *Science* **2000**, *288*, 1808-1811.

[95] Liu, X.; Fu, L.; Hong, S.; Dravid, V. P.; Mirkin, C. A. *Adv. Mater.* **2002**, *14*, 231-234.

[96] Demers, L. M.; Mirkin, C. A. *Angew. Chem. Int. Ed.* **2001**, *40*, 3069-3071.

[97] Lee, K.-B.; Park, S.-J.; Mirkin, C. A.; Smith, J. C.; Mrksich, M. *Science* **2002**, *295*, 1702-1705.

[98] Wilson, D. L.; Martin, R.; Hong, S.; Cronin-Golomb, M.; Mirkin, C. A.; Kaplan, D. L. *Proc. Natl. Acad. Sci. USA* **2001**, *98*, 13660-13664.

[99] Demers, L. M.; Ginger, D. S.; Park, S.-J.; Li, Z.; Chung, S.-W.; Mirkin, C. A. *Science* **2002**, *296*, 1836-1838.

[100] Demers, L. M.; Park, S.-J.; Taton, T. A.; Li, Z.; Mirkin, C. A. *Angew. Chem. Int. Ed.* **2001**, *40*, 3071-3073.
[101] Ivanisevic, A.; Mirkin, C. A. *J. Am. Chem. Soc.* **2001**, *123*, 7887-7889.
[102] Weinberger, D. A.; Hong, S.; Mirkin, C. A.; Wessels, B. W.; Higgins; T. B. *Adv. Mater.* **2000**, *12*, 1600-1603.
[103] Amro, N. A.; Xu, S. X.; Liu, G. Y. *Langmuir* **2000**, *16*, 3006-3009.
[104] Noy, A.; Miller, A. E.; Klare, J. E.; Weeks, B. L.; Woods, B. W.; DeYoreo, J. J. *Nano Lett.* **2002**, *2*, 109-112.
[105] Su, M.; Dravida, V. P. *Appl. Phys. Lett.* **2002**, *80*, 4434-4436.
[106] Su, M.; Liu, X.; Li, S.-H.; Dravid, P. D.; Mirkin, C. A. *J. Am. Chem. Soc.* **2002**, *124*, 1560-1561.
[107] Li, Y.; Maynor, B. W.; Liu, J. *J. Am. Chem. Soc.* **2001**, *123*, 2105-2106.
[108] McKendry, R.; Huck, W. T. S.; Weeks, B.; Fiorini, M.; Abell, C.; Rayment, T. *Nano Lett.* **2002**, *2*, 713-716.
[109] Gimzewski, J. K.; Joachim, C. *Science* **1999**, *283*, 1683–1688.
[110] Binnig, G.; Rohrer, H. *Helv. Phys. Acta* **1982**, *55*, 726-735.
[111] Binnig, G.; Quate, C. F.; Gerber, C. *Phys. Rev. Lett.* **1986**, *56*, 930-933.
[112] Müller, D. J.; Janoviak, H.; Lehto, T.; Kuerscher, L.; Anderson, K. *Prog. Biophys. Molec. Biol.* **2002**, *79*, 1-43.
[113] For an overview on NSOM see: Dunn, C. R. *Chem. Rev.* **1999**, *99*, 2891-2927.
[114] Bustamante, C.; Bryant, Z.; Smith, S. B. *Nature* **2003**, *421*, 423-427.
[115] Touzov, I.; Goran, C. B. *J. Phys. Chem.* **1997**, *101*, 5263-5276.
[116] a) Gimzewski, J. K.; Stoll, E. P.; Schlittler, R. R. *Surf. Sci.* **1987**, *181*, 267-277. b) Smith, D. P. E.; Kirk, M. D.; Quate, C. F. *J. Chem. Phys.* **1987**, *86*, 6034-6038.
[117] a) Jung, T. A.; Schlittler, R. R.; Gimzewski, J. K.; Tang, H.; Joachim, C. *Science* **1996**, *271*, 181-184. b) Jung, T. A.; Schlittler, R. R.; Gimzewski, J. K. *Nature* **1997**, *386*, 696-698.
[118] Messina, P.; Dmitriev, A.; Lin, N.; Spillmann, H.; Abel, M.; Barth, J. V.; Kern, K. *J. Am. Chem. Soc.* **2002**, 124, 14000-14001.
[119] Barth, J. V.; Weckesser, J.; Cai, C.; Günter, P.; Bürgi, L.; Jeandupeux, O.; Kern, K. *Angew. Chem. Int. Ed.* **2000**, *39*, 1230-1234.
[120] a) Stevens, F.; Dyer, D. J.; Walba, D. M. *Angew. Chem. Int. Ed.* **1996**, *35*, 900-901. b) Walba, D. M.; Stevens, F.; Clark, N. A.; Parks, D. C. *Acc. Chem. Res.* **1996**, *29*, 591-597. c) De Feyter, S.; Gesquière, A.; Grim, P. C. M.; De Schryver, F. C.; Valiyaveettil, S.; Meiners, C.; Sieffert, M.; Müllen, K. *Langmuir* **1999**, *15*, 2817-2822. d) De Feyter, S.; Grim, P. C. M.; Rücker, M.; Vanoppen, P.; Meiners, C.; Sieffert, M.; Valiyaveetiil, S.;

Müllen, K.; De Schryver, F. C. *Angew. Chem. Int. Ed.* **1998**, *37*, 1223-1226. e) Lopinski, G. P.; Moffatt, D. J.; Wayner, D. D. M.; Wolkow, R. A. *Nature* **1998**, *392*, 909-911. f) Fang, H.; Giancarlo, L. C.; Flynn, G. W. *J. Phys. Chem. B* **1998**, *102*, 7311-7315. g) Böhringer, M.; Morgenstern, K.; Schneider, W. D.; Berndt, R. *Angew. Chem. Int. Ed.* **1999**, *38*, 821-823. h) De Feyter, S.; Gesquière, A.; Wurst, K.; Amabilino, D. B.; Veciana, J.; De Schryver, F. C. *Angew. Chem. Int. Ed.* **2001**, *40*, 3217-3220.

[121] a) Heinz, R.; Stabel, A.; Rabe, J. P.; Wegner, G.; De Schryver, F. C.; Corens, D.; Dehaen, W.; Süling, C. *Angew. Chem. Int. Ed.* **1994**, *33*, 2080-2082. b) Vanoppen, P.; Grim, P. C. M.; Rücker, M.; De Feyter, S.; Moessner, G.; Valiyaveettil, S.; Müllen, K.; De Schryver, F. C. *J. Phys. Chem.* **1996**, *100*, 19636-19641. c) Grim, P. C. M.; De Feyter, S.; Gesquière, A.; Vanoppen, P.; Rücker, M.; Valiyaveettil, S.; Moessner, G.; Müllen, K.; De Schryver, F. C. *Angew. Chem. Int. Ed.* **1997**, *36*, 2601-2603. d) Takami, T.; Ozaki, H.; Kasuga, M.; Tsuchiya, T.; Mazaki, Y.; Fukushi, D.; Ogawa, A.; Uda, M. *Angew. Chem. Int. Ed.* **1997**, *36*, 2755-2757. e) Grim, P. C. M.; Vanoppen, P.; Rücker, M.; De Feyter, S.; Valiyaveettil, S.; Moessner, G.; Müllen, K.; De Schryver, F. C. *J. Vac. Sci. Technol. B* **1997**, *15*, 1419-1424.

[122] a) Stabel, A.; Heinz, R.; De Schryver, F. C.; Rabe, J. P. *J. Phys. Chem.* **1995**, *99*, 505-507. b) Venkataraman, B.; Breen, J. J.; Flynn, G. W. *J. Phys. Chem.* **1995**, *99*, 6608-6619. c) Buchholz, S.; Rabe, J. P. *J. Vac. Sci. Technol. B* **1991**, *9*, 1126-1128. d) Adkadskaya, L.; Rabe, J. P. *Phys. Rev. Lett.* **1992**, *69*, 1395-1398. e) Stabel, A.; Heinz, H.; Rabe, J. P.; Wegner, G.; De Schryver, F. C.; Corens, D.; Dehaen, W.; Süling, C. *J. Phys. Chem.* **1995**, *99*, 8690- 8697. f) Gesquière, A.; Abdel-Mottaleb, M.; De Schryver, F. C. *Langmuir* **1999**, *15*, 6821- 6824. g) De Feyter, S.; Grim, K.; Van Esch, J.; Kellogg, R. M.; Feringa, B. L.; De Schryver, F. C. *J. Phys. Chem. B* **1998**, *102*, 8981-8987. h) Baker, T. R.; Mougous, J. D.; Brackley, A.; Patrick, D. L. *Langmuir* **1999**, *15*, 4884-4891. i) Stevens, F.; Beebe, T. P. *Langmuir* **1999**, *15*, 6884-6889.

[123] De Feyter, S.; Gesquière, A.; Abdel-Mottaleb, M.; Grim, P. C. M.; De Schryver, F. C. *Acc. Chem. Res.* **2000**, *33*, 520-531.

[124] a) Cygan, M. T.; Dunbar, T. D.; Arnold, J. J.; Bumm, L. A.; Shedlock, N. F.; Burgin, T. P.; Jones, L.; Allara, D. L.; Tour, J. M.; Weiss, P. S. *J. Am. Chem. Soc.* **1998**, *120*, 2721-2732. b) Bumm, L. A.; Arnold, J. J.; Charles, L. F.; Dunbar, T. D.; Allara, D. L.; Weiss, P. S. *J. Am. Chem. Soc.* **1999**, *121*, 8017-8021. c) Dunbar, T. D.; Cygan, M. T.; Bumm, L. A.; McCarty, G. S.; Burgin, T. P.; Reinhert, W. A.; Jones, L.; Jackiw, J. J.; Tour, J. M.; Weiss, P. S.; Allara, D. L. *J. Phys. Chem. B* **2000**, *104*, 4880-4893.

[125] Binnig, G. *Ultramicroscopy* **1992**, *42-44*, 7-15.

[126] a) Bhushan, B. in *Handbook of Micro/Nano Tribology*; CRC Press: Boca Raton, FL, 1995; p 3. b) Ogletree, D. F.; Carpick, R. W.; Salmeron, M. *Rev. Sci. Instrum.* **1996**, *67*, 3298-3306.

[127] a) Magonov, S. N.; Reneker, D. H. *Annu. Rev. Mater. Sci.* **1997**, *27*, 175-222. b) Noy, A.; Sanders, C. H.; Vezenov, D. V.; Wong, S. S.; Lieber, C. M. *Langmuir* **1998**, *14*, 1508-1511. c) Finot, M. O.; McDermott, M. T. *J. Am. Chem. Soc.* **1997**, *119*, 8564-8565.

[128] a) Whangbo, M.-H.; Bar, G.; Brandsch, R. *Surf. Sci.* **1998**, *411*, L794-L801. b) Magonov, S. N.; Elings, V.; Whangbo, M.-H. *Surf. Sci.* **1997**, *375*, L385-L391.

[129] Hierlemann, A.; Campbell, J. K.; Baker, L. A.; Crooks, R. M.; Ricco, A. J. *J. Am. Chem. Soc.* **1998**, *120*, 5323–5324.

[130] Li, J.; Piehler, L. T.; Qin, D.; Baker Jr., J. R.; Tomalia, D. A. *Langmuir* **2000**, *16*, 5613–5616.

[131] Zhang, H.; Grim, P. C. M.; Foubert, P.; Vosch, T.; Vanoppen, P.; Wiesler, U.-M.; Berresheim, A. J.; Müllen, K.; De Schryver, F. C. *Langmuir* **2000**, *16*, 9009–9014.

[132] Putman, C. A. J.; DeGrooth, B. D.; Van Hulst, N. F.; Greve, J. *J. Appl. Phys.* **1992**, *72*, 6-12.

[133] a) Evans, E.; Ritchie, K.; Merkel, R. *Biophys. J.* **1995**, *68*, 2580-2587. b) Kuo, S. C.; Sheetz, M. P. *Science* **1993**, *260*, 232-234 and references cited herein.

[134] Frisbie, C. D.; Rozsnyai, L. F.; Noy, A.; Wrighton, M. S.; Lieber, C. M. *Science* **1994**, 265, 2071-2074. b) Noy, A.; Vezenov, D. V.; Lieber, C. M. *Annu. Rev. Mater. Sci.* **1997**, *27*, 381-421.

[135] For recent reviews see: a) Hugel, T.; Seitz, M. *Macromol. Rapid Commun.* **2001**, *22*, 989-1016. b) Zlatanova, J.; Lindsay, S. M.; Leuba, S. H. *Prog. Biophys. Molec. Biol.* **2000**, *74*, 37-61. c) Janshoff, A.; Neitzert, M.; Oberdörfer, Y.; Fuchs, H. *Angew. Chem. Int. Ed.* **2000**, *39*, 3212-3237.

[136] a) Florin, E.-L.; Moy, V. T.; Gaub, H. E. *Science* **1994**, *264*, 415-417. b) Moy, V. T.; Florin, E.-L.; Gaub, H. E. *Science* **1994**, *266*, 257-259. c) Grandbois, M.; Beyer, M.; Rief, M.; Clausen-Schaumann, H.; Gaub, H. E. *Science* **1999**, *283*, 1727-1730.

[137] Lee, G. U.; Chrisey, L. A.; Colton, R. J. *Science* **1994**, *266*, 771-773.

[138] McKendry, R.; Theoclitou, M.-E.; Rayment, T.; Abell, C. *Nature* **1998**, *391*, 566-568.

[139] Grumbmuller, H.; Heymann, B.; Tavan, P. *Science* **1996**, *271*, 997-999.

[140] a) Evans, E.; Ritchie, K. *Biophys. J.* **1997**, *72*, 1541-1555. b) Merkel, R.; Nassoy, P.; Leung, A.; Ritchie, K.; Evans, E. *Nature* **1999**, *397*, 50-53.

[141] a) Synge, E. H. *Philos. Mag.* **1928**, *6*, 356-362. b) Synge, E. H. *Philos. Mag.* **1931**, *11*, 65-80.

[142] Abbe, E. *Arch. Mikrosk. Anat.* **1873**, *9*, 413-468.

[143] a) Pohl, D. W.; Denk, W.; Lanz, M. *Appl. Phys. Lett.* **1984**, *44*, 651-653. b) Durig, U.; Pohl, D. W.; Rohner, F. *J. Appl. Phys.* **1986**, *59*, 3318-3327.

[144] Betzig, E.; Trautman, J. K.; Harris, T. D.; Weiner, J. S.; Kostelak, R. L. *Science* **1991**, *251*, 1468-1470.

[145] Lee, L. F.; Adronov, A.; Schaller, R. D.; Frechet, J. M. J.; Saykally, R. J. *J. Am. Chem. Soc.* **2003**, *125*, 536-540.

[146] Johnson, J. C.; Yan, H. Q.; Schaller, R. D.; Petersen, P. B.; Yang, P. D.; Saykally, R. J. *Nano Lett.* **2002**, *2*, 279-283.

[147] a) García-Parajó, M. F.; Veerman, J. A.; Bouwhuis, R.; Vallee, R.; Van Hulst, N. F. *ChemPhysChem* **2001**, *2*, 347-360. b) Ruiter, A. G. T.; Veerman, J. A.; García-Parajó, M. F.; Van Hulst, N. F. *J. Phys. Chem. A* **1997**, *101*, 7318-7323. c) García-Parajó, M. F.; Veerman, J.-A.; Ruiter, A. G. T.; Van Hulst, N. F. *Ultramicroscopy* **1998**, *71*, 311-319. d) García-Parajó, M. F.; Veerman, J.-A.; Van Noort, S. J. T.; de Grooth, B. G.; Greve, J.; Van Hulst, N. F. *Bioimaging* **1998**, *6*, 43-53. e) Van Hulst, N. F.; García-Parajó, M. F.; Moers, M. H. P.; Veerman, J.-A.; Ruiter, A. G. T. *J. Struct. Biol.* **1997**, *119*, 222-231.

[148] For an overview on fluorescence see: Basché, T.; Moerner, W. E.; Orritt, M.; Wild, U. P. *Single Molecule Optical Detection and Spectroscopy*; VCH: Weinheim, Germany 1997. b) Weiss, S. *Science* **1999**, *283*, 1676–1683.

[149] a) Mollova, E. T. *Curr. Opin. Biol. Chem.* **2002**, *6*, 823-828. b) Forkey, J. N.; Quinlan M. E.; Goldman, Y. E. *Prog. Biophys. Molec. Biol.* **2000**, *74*, 1-35. c) Pierce, D. W.; Vale, R. D. *Meth. Cell Biol.* **1999**, *58*, 49-73. d) Krishnan, R. V.; Varma, R.; Mayor, S. *J. Fluoresc.* **2001**, *11*, 211-226.

[150] a) Zhuang, X.; Bartley, L. E.; Babcock, H. P.; Russell, R.; Ha, T.; Herschlag, D.; Che, S. *Science* **2000**, *288*, 2048-2051. b) Berglund, A. J.; Doherty, A. C.; Mabuchi H. *Phys. Rev. Lett.* **2002**, *89*, 068101.

[151] a) Ha, T.; Enderle, T.; Ogletree, D. F.; Chemla, D. S.; Selvin. P. R.; Weiss, S. *Proc. Natl. Acad. Sci. U.S.A.* **1996**, *93*, 6264-6268. b) Ha, T.; Enderle, Th.; Chemla, D. S.; Weiss, S. *IEEE J. Sel. Top. Quantum Electron.* **1996**, *2*, 1115-1128. c) Schutz, G. J.; Trabesinger, W.; Schmidt, T. *Biophys. J.* **1998**, *74*, 2223-2226.

[152] Schuler, B.; Lipman, E. A.; Eaton, W. A. *Nature*, **2002**, *419*, 743-747.

[153] Finer, J. T.; Simmons, R. M.; Spudich, J. A. *Nature* **1994,** *368*, 113-119.

[154] Kull, F. J.; Sablin, E. P.; Lau, R.; Fletterick, R. J.; Vale, R. D. *Nature* **1996**, *380*, 550-555.

[155] a) Howard, J.; Hudspeth, A. J.; Vale, R. D. *Nature* **1989**, *342*, 154-158. b) Block, S. M.; Goldstein, L. S.; Schnapp, B. J. *Nature* **1990**, *348*, 348-352.

[156] Svoboda, K.; Schmidt, C. F.; Schnapp, B. J.; Block, S. M. *Nature* **1993**, *365*, 721-727.

[157] a) Noji, H.; Yasuda, R.; Yoshida, M.; Kinosita Jr., K. *Nature*, **1997**, *386*, 299-302. b) Yasuda, R.; Noji, H.; Yoshida, M.; Kinosita, K.; Itoh, H. *Nature* **2001**, *401*, 898-904.

[158] Yasuda, R.; Noji, H.; Kinosita Jr., K.; Yoshida, M. *Cell* **1998**, *93*, 1117-1124.

[159] Schafer, D. A.; Gelles, J.; Sheetz, M. P.; Landick, R. *Nature*, **1991** *353*, 444-448.

[160] Yin, H.; Wang, M.; Svoboda, K.; Landick, R.; Block, S. M.; Gelles, J. *Science* **1995**, *270*, 1653-1657.

[161] Wang, M. D.; Schnitzer, M. J.; Yin, H.; Landick, R.; Gelles, J.; Block, S. M. *Science* **1998**, *282*, 902-907.

[162] Kratky, O.; Porod, G. *Recl. Trav. Chim. Pays-Bas* **1949**, *68*, 1106–1123.

[163] a) Smith, S. B.; Finzi, L.; Bustamante, C. *Science* **1992**, *258*, 1122-1126. b) Smith, S. B.; Cui, Y.; Bustamante, C. *Science* **1996** *271*, 795-799. c) Cluzel P.; Lebrun, A.; Heller, C.; Lavery, R.; Viovy, J. L.; Chatenay, D.; Caron, F. *Science* **1996**, *271*, 792-794.

[164] Wang, M. D.; Yin, H.; Landick, R.; Gelles, J.; Block, S. M. *Biophys. J.* **1997**, *72*, 1335–1346. b) Bustamante, C.; Marko, J. F.; Siggia, E. D.; Smith, S. *Science* **1994**, *265*, 1599–1600.

Chapter 3

Non-Covalent Chemistry on Surface-Confined, Isolated Dendrimers*

In this chapter a "bottom-up" fabrication of nanometer-scale dendritic structures via the growth of isolated, nanosized supramolecular architectures on gold surfaces is presented. A dendritic wedge containing four peripheral pyridines, and a thioether chain was synthesized. Its coordination chemistry in solution was addressed by reaction with a second generation Fréchet dendron functionalized with a sulfur-carbon-sulfur (SCS) Pd^{II} pincer moiety. Based on these results the analogous surface-confined reaction on a gold substrate was studied. The dendritic molecules with the reactive pyridine groups at the periphery were first isolated spatially by inserting them into self-assembled monolayers (SAMs) of decanethiol on a gold surface, via the thioether group. The isolated molecules were resolved by ex-situ tapping mode atomic force microscopy (TM-AFM). Subsequently, the pyridines were reacted via metal-ligand coordinative interactions by exposing the monolayer to a solution of the (SCS) Pd^{II} dendron. The Pd^{II}-pyridine coordination resulted in a significant growth of the individually resolved molecules as a result of specific metal-ligand interactions.

3.1 Introduction

3.1.1 General introduction

Miniaturization of technological devices is of critical importance, especially in the microelectronics industry,[1] to continue improving device performance and speed.[2,3] For decades, "top-down" technology has proven highly successful for reproduction of features on a substrate, traditionally employing photolithography.[4] In order to further scale down the reproduced pattern size, techniques have been developed that allow an increased lateral resolution for master production (*e.g.* deep UV, X-ray, electron-beam

---

* This chapter has been published in: Van Manen H.-J.; Auletta, T.; Dordi, B.; Schönherr, H.; Vancso, G. J.; Van Veggel, F. C. J. M.; Reinhoudt, D. N. *Advanced Functional Materials* **2002**, *12*, 811-818.

lithography[5]). However, the decrease in pattern size poses several problems. Besides the increase of production costs, several issues must be addressed. These include mask alignment in multistep processes, homogeneity in the composition of the employed materials, or serial production techniques such as e-beam lithography.[3] At present, other non-photolithographic "top-down" methods, such as “soft” lithography,[6] imprint lithography,[7] and dip-pen nanolithography[8] are being investigated as complements or alternatives for microfabrication.

In contrast to the top-down fabrication, “bottom-up” nanofabrication should involve the self-assembly of appropriately designed molecules to give discrete aggregates. The final structure of these aggregates is encoded in the functionalities built into the molecular building blocks.[9] The central paradigm in self-assembly is that the final superstructure is close to or at thermodynamic equilibrium, so it forms spontaneously and is prone to error correction. The requirement for such aggregates is to achieve a size large enough to be employed in nanofabrication. The challenge becomes the design of suitable building blocks to synthesize assemblies in the 10-100 nanometers range, dimensions that are comparable to natural counterparts such as DNA and proteins.

Dendrimers are promising candidates as building blocks in nanofabrication owing to their regular, highly branched three-dimensional structure, and their ease of synthesis and functionalization of the core and/or the periphery.[10] Self-assembled monolayers (SAMs) of sulfur-containing molecules on gold have been exploited for the spatial confinement on surfaces of dendritic structures or Au nanoparticles[11,12] by coordination to SCS Pd^{II} pincer molecules.[13] These can be visualized as isolated species inserted into 11-mercapto-1-undecanol and decanethiol SAMs on gold (Chapter 4).[14] The mechanism of surface-confinement relies on the formation of defects in the alkanethiol monolayer upon exposure to a solvent and the subsequent insertion of individual dendrimers via their thioether chain.[12]

This chapter describes an alternative and complementary strategy which consists of the insertion of dendritic wedges containing peripheral pyridine groups into SAMs of decanethiol and the subsequent coordination of SCS Pd^{II} pincer dendritic molecules to these adsorbates, leading to isolated nanosized species (Scheme 3.1). The whole growth process was studied using atomic force microscopy (AFM).

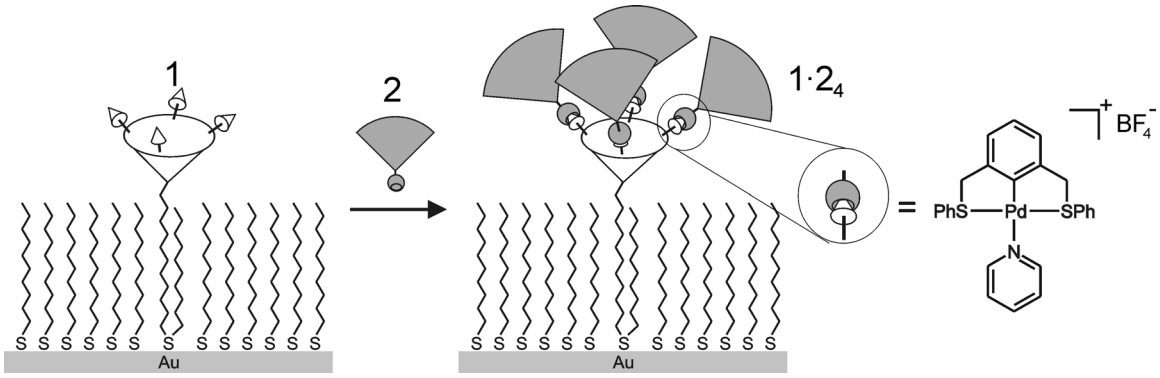

Scheme 3.1 Schematic representation of the non-covalent chemistry on surface-confined dendrimers.

3.1.2 Strategy and building blocks

In order to employ individual isolated molecules inserted into SAMs as a platform for further reactions, a dendritic wedge containing peripheral pyridines and a thioether chain at the focal point (**1**) and a Fréchet dendron with a SCS Pd^{II} pincer moiety at the focal point (**2**) were synthesized (Chart 3.1).[15]

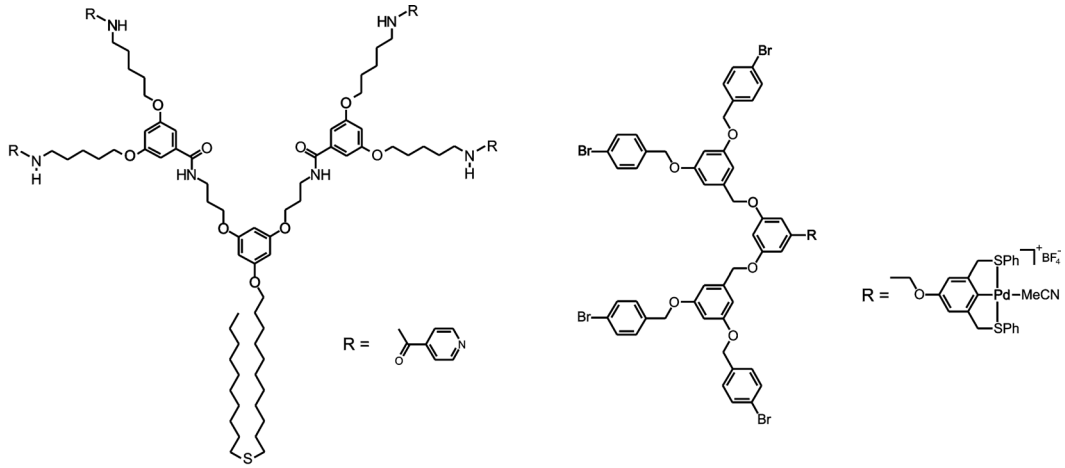

1 **2**

Chart 3.1 Building blocks **1** and **2**.

Pyridines bind strongly to SCS Pd^{II} pincer moieties via metal-ligand coordination.[13,16] Therefore, coordination of each pyridine group of **1** to the Pd^{II} center of dendron **2** (by substitution of the labile acetonitrile ligand) converts the second generation dendritic

wedge **1** into the fourth generation metallodendron **1·2₄** in one step. The advantage of using metal-ligand coordination instead of covalent coupling is that coordination of ligands to Pd^{II} pincers is fast, quantitative, proceeds under mild condition and liberates only a solvent molecule, without further side-products.[13]

3.2 Coordination of dendritic wedges in solution

The coordination of a variety of pyridines to SCS Pd^{II} pincer systems has been studied by our group[13] and others.[16] Pyridine complexes of SCS Pd^{II} pincers are synthesized from the corresponding acetonitrile complexes by a fast and quantitative exchange. It was reasoned that quantitative exchange of the acetonitrile ligand in **2** by the *p*-amide-substituted pyridine end groups of adsorbate **1** might be inhibited for both steric and/or electronic reasons. Therefore, coordination of isonicotinoyl benzylamide to the pincer moiety of dendron **2** was first investigated as a model. As shown in Figure 3.1, significant shifts in the ^1H NMR spectrum are observed upon addition of 1 equiv. of isonicotinoyl benzylamide to **2** in $CDCl_3$. The large upfield shift of the α-pyridyl protons upon coordination to the SCS Pd^{II} pincer is diagnostic for pyridine coordination.[13] The absence of a signal around 8.6 ppm (Figure 3.1b) indicated quantitative substitution of acetonitrile for isonicotinoyl benzylamide.

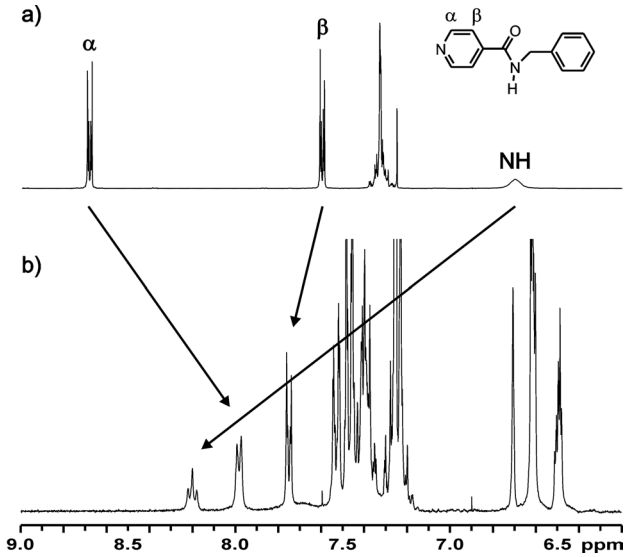

Figure 3.1 ^1H NMR spectra (300 MHz, $CDCl_3$, 298 K) of isonicotinoyl benzylamide before (a), and after addition of 1 equiv. of acetonitrile pincer complex **2** (b).

Similarly ^{1}H NMR spectra proved that upon titration of **1** to **2** in $CDCl_3$ adsorbate **1** can accommodate four dendritic wedges to give **1·2$_4$**. Upon coordination, similar shifts for the pyridyl groups of **1** in **1·2$_4$** were observed as for the isonicotinoyl benzylamide model as displayed in Figure 3.1. There was a minor interference (± 5%, as judged from the NMR spectrum) from coordination of the sulfide moiety of **1** to the pincer in **2**. As observed before, the coordination strengths of pyridine and sulfide groups to SCS Pd^{II} pincers are of the same magnitude.[14] Sulfide interference will of course be absent when the pyridine coordination is carried out with a surface-confined **1**, since in that case the sulfide group is strongly bound to the gold substrate.

3.3 Coordination of dendritic wedges to surface-confined isolated platforms

3.3.1 Surface confinement of dendritic structures by insertion into decanethiol SAMs

Insertion of dendritic adsorbate **1** into SAMs was achieved by exposing a decanethiol SAM to a 0.1 mM solution of **1** in CH_2Cl_2 for 3 h. After rinsing, tapping mode atomic force microscopy (TM-AFM) experiments in air revealed isolated features, well separated and randomly distributed over the surface, with an average height of 3.3 ± 0.5 nm (Figure 3.2 and Figure 3.3A).

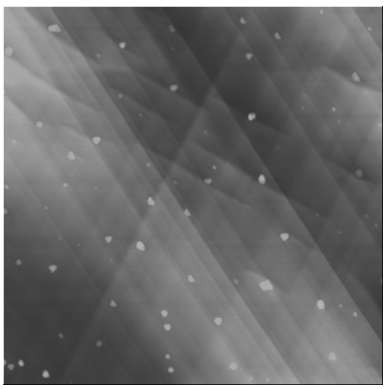

Figure 3.2 TM-AFM height image in air of a decanethiol SAM exposed to a 0.1 mM solution of **1** in CH_2Cl_2 for 3 h (image size 1.5 × 1.5 μm^2, z-scale = 30 nm).

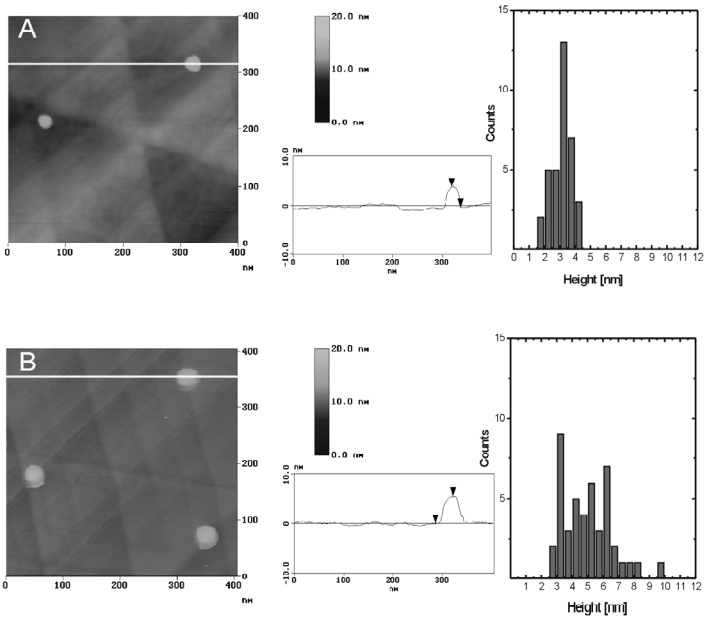

Figure 3.3 TM-AFM height images in air, height profiles, and height histogram plots of a decanethiol SAM exposed to a 0.1 mM solution of **1** in CH_2Cl_2 for 3 h (A), followed by exposure to a 0.3 mM solution of dendritic wedge **2** in CH_2Cl_2 for 10 min (B). The height profiles correspond to the lines drawn in the images on the left side.

From a computer-generated model, the maximum protrusion of adsorbate **1** above the decanethiol monolayer was estimated to be 2.8 nm. Thus the average height, as determined by TM-AFM, is in reasonable agreement with the calculated value for the single dendritic molecules. A direct quantitative comparison of the two values cannot be made even though very soft tapping conditions were employed in the TM-AFM experiments. Although these imaging conditions are considered to yield topographical information closest to the actual height,[17] flattening of the molecules due to compression and height artifacts due to adhesive interactions[18] cannot be excluded. The width of the dendrimers as seen in Figure 3.2 is certainly overestimated due to tip convolution.[19] The average number of nanometer-sized features counted in a 500×500 nm^2 area of the decanethiol SAM exposed to sulfide adsorbate **1** is 4 ± 2. This is in the same order of magnitude as previously found for insertion of other dendritic adsorbates under similar conditions *i.e.* reaction time, concentration, and solvent.[11-14]

3.3.2 Growth of isolated features by pincer coordination chemistry

Substrates with spatially isolated molecules of **1** were immersed in a 0.3 mM CH_2Cl_2 solution of Pd^{II} pincer-functionalized dendritic wedge **2** for 10 min, followed by rinsing

with pure solvents. TM-AFM images in air show the presence of a number of nanosize features, comparable to the above reported results, but now with height values ranging from 3.1 to 7.5 nm (Figure 3.3B).

Several reference experiments were carried out to support the interpretation that the increase in feature size is due to metal-ligand interactions. First, to rule out interactions between the pyridine moieties and the gold surface, a decanethiol monolayer was exposed to a dendritic adsorbate similar to adsorbate **1** but having a long (C22) alkyl chain instead of a thioether chain. After rinsing, no features on the SAM could be detected by TM-AFM imaging (Figure 3.4), indicating the necessity for the thioether in the anchoring step.

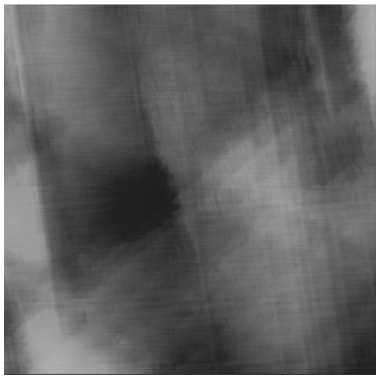

Figure 3.4 TM-AFM image in air of a decanethiol SAM exposed to a solution of the C22-analog of adsorbate **1** (*i.e.*, **1** with a C22 hydrocarbon chain instead of a thioether chain) (image size 500 × 500 nm^2, z-scale = 10 nm).

Next, in order to prove that the size growth is due to coordination of the pyridines of adsorbate **1** to the Pd^{II} center of dendron **2**, a decanethiol monolayer was directly exposed to dendron **2** for 10 min without insertion of **1**. Also in this case, TM-AFM images showed no features on the layer (not shown here). Therefore, aspecific interactions (*i.e.* physisorption) between the monolayer and dendritic wedge **2** can be ruled out.

By comparing Figures 3A and 3B, it is obvious that the average height of the features increased after coordination. However, the size distribution after growth is much broader than before growth as shown by the height histograms, and there are features which have the same height as the isolated molecules of **1**. This may suggest that not all inserted adsorbates have reacted with four molecules of **2** and that a distribution of dendrimers with 0 to 4 wedges of **2** was obtained.

These observations seem to contradict the results obtained in solution where adsorbate **1** can coordinate four wedges of **2** (see Section 3.2). However, it should be realized that coordination of four dendritic wedges to adsorbate **1** is sterically more demanding on a gold surface than in solution. Whereas the conformation of adsorbate **1** can freely be adjusted in solution in order to accommodate all four dendrons, the space available for coordination to isolated molecules of **1** inserted into SAMs is restricted, as a rough approximation, to a hemisphere. The sizes of both adsorbate **1** and dendron **2** were therefore estimated in order to predict the number of dendrons that can be coordinated to adsorbate **1** on a gold surface. From a computer-generated model, the hemisphere defined by the part of adsorbate **1** which protrudes above the decanethiol monolayer was estimated to have a radius of approximately 2 nm. This leads to a surface area of 25 nm^2 for the hemisphere. To accommodate four dendrons of **2** on a hemisphere of this size, the surface area occupied by a single dendron of **2** must not exceed 5-6 nm^2. Using the hydrodynamic radii of poly(arylether) dendrimers and dendrons reported by Mourey *et al.*,[20] a surface area of 3.1 nm^2 was estimated for the structure of dendron **2**, with the Pd^{II} in the center of the flat side. This suggests that the reaction of **1** on the surface with up to four dendrons of **2** is, in principle, possible.

To obtain quantitative information on the size of the surface-confined supramolecular architecture containing all four Pd wedges coordinated to the pyridine moieties, the following reference experiment was carried out. A decanethiol monolayer was exposed for 3 h to a 1 mM solution of the complex $\mathbf{1{\cdot}2}_4$, in order to compare the growth in solution with results obtained on the monolayer. In this case, however, TM-AFM imaging in air showed no distinctive features on the layer (Figure 3.5).

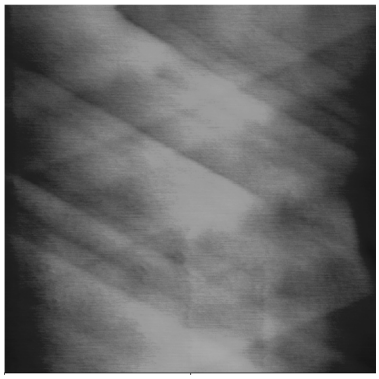

Figure 3.5 TM-AFM image in air of a decanethiol SAM exposed to a solution of the preformed dendritic complex $\mathbf{1{\cdot}2_4}$ (image size 500 × 500 nm^2, z-scale = 10 nm).

This is probably due to the large globular shape of the dendritic complex **1**·**2**$_4$ in solution, which effectively encapsulates the sulfur and restricts or prevents its access to the gold surface.
A kinetic inhibitive effect can also not be ruled out for the access of the sulfide to the surface. Furthermore, the insertion process of the complete assembly **1**·**2**$_4$ might require larger defects in the preformed decanethiol monolayer with respect to the smaller adsorbate **1**. This result supports our earlier interpretation of the partial derivatization of surface confined **1** by **2** (see above).

3.4 Conclusions

The feasibility of non-covalent chemistry on surface-confined, isolated dendrimers has been demonstrated. A second-generation dendritic adsorbate having four peripheral pyridines and a thioether chain at the focal point was synthesized in a convergent manner. The coordination of second generation dendritic wedges containing a SCS Pd^{II} pincer moiety at the focal point to this dendritic adsorbate was studied both in solution and on a monolayer. Isolated dendrimers inserted into a decanethiol SAM on gold with an average height of 3.3 nm could be converted by metal-ligand coordination into larger dendritic structures with heights ranging from 3.1 to 7.5 nm. Considering the broad range of heights obtained, it is likely that not all isolated dendritic adsorbates have four dendritic wedges coordinated to them.

3.5 Experimental

General Procedures. Melting points were determined with a Reichert melting point apparatus and are uncorrected. NMR spectra were recorded in $CDCl_3$ (unless stated otherwise) on a Varian Unity 300 at 300.1 (^{1}H) and 75.5 (^{13}C) MHz. ^{1}H chemical shifts are given relative to tetramethylsilane (TMS). FAB-MS spectra were recorded on a Finnigan MAT 90 spectrometer with *m*-nitrobenzyl alcohol (NBA) as the matrix. Elemental analyses were performed using a Carlo Erba EA1106. The presence of solvents in the analytical samples was confirmed by ^{1}H NMR spectroscopy. Column chromatography was performed using silica gel (SiO_2, E. Merck, 230-240 mesh).
Materials. CH_2Cl_2 was freshly distilled from $CaCl_2$. Acetone, EtOH, THF and $CHCl_3$ were used as received (p.a. from Merck). MeCN (p.a.) was stored over molecular sieves (4 Å). Water was purified by Millipore membrane units. All other reagents and decanethiol were purchased from Aldrich and used without further purification. Synthesis

of compounds **1** and **2** has been carried out by Henk-Jan Van Manen, as well as the ^{1}H NMR experiment to prove the formation of **1·2**$_4$ in solution.[15]

Methods. All glassware used to prepare monolayers was immersed in piraña solution (conc. H_2SO_4 and 33% H_2O_2 in a 3:1 ratio). **(Warning piraña should be handled with caution; it has detonated unexpectedly)**.[21] Next, the glassware was rinsed with large amounts of Milli-Q water.

Substrate preparation. Gold substrates were obtained from Metallhandel Schröer GmbH (Lienen, Germany). Immediately before use, the substrates were rinsed with Milli-Q water and then flame-annealed in a H_2 flame (purity 6) as described previously.[22] After the annealing procedure, the substrates were placed in p.a. ethanol for 10 min[23] and then immersed into the adsorbate solution for the desired time. All adsorbate solutions were prepared just before use. After each adsorption step the samples were removed from the solutions and rinsed thoroughly with dichloromethane, ethanol, and Milli-Q water. SAMs of decanethiol were prepared by immersing the gold substrates in the corresponding 1 mM solutions in ethanol at room temperature. They were exposed for 3 h to solutions of adsorbate **1**, and for 10 min to solutions of dendron **2**, and then rinsed by placing them three times in 20 ml CH_2Cl_2 for 5 min. Preformed decanethiol SAMs were exposed for 3 h to a solution of the complex **1·2**$_4$ and rinsed following the same procedure reported above.

Atomic force microscopy. The AFM measurements were carried out in tapping mode with a NanoScope III multimode AFM (Digital Instruments, Santa Barbara, CA, USA) as described previously[11,12,14] using silicon cantilevers/tips (Nanosensors, Wetzlar, Germany; cantilever resonance frequency f_0 = 280-320 kHz). The piezo scanner was calibrated in lateral directions using a grid with repeat distances of 1.0 μm, as well as self-assembled monolayers of thiols on Au(111) (*e.g.* octadecanethiol, repeat distance 0.51 nm),[22] and in z-direction by measuring step heights of Au(111) (2.355 Å). The number of nanometer-sized features and their standard deviations were determined by counting the features on at least four areas of the same sample (5 samples were investigated).

3.6 References and notes

[1] Peercy, P. S. *Nature* **2000**, *406*, 1023-1026.

[2] Lieber, C. M. *Sci. Am.* **2001**, *9*, 58-64.

[3] See the following technology roadmaps for micro- and nanoelectronics: a) *The International Technology Roadmap for Semiconductors 2002*, to be found at http://public.itrs.net/Files/2002Update/Home.pdf. b) Compaño, R.; Molenkamp, L.; Paul, D. J. *Technology Roadmap for Nanoelectronics*, European Commission IST Programme: Future and Emerging Technologies, Microelectronics Advanced Research Initiative; http://nanoworld.org/NanoLibrary/nanoroad.pdf

[4] For recent reviews, see: a) Ito, T.; Okazaki, S. *Nature* **2000**, *406*, 1027-1031. b) Walraff, G. M.; Hinsberg, W. D. *Chem. Rev.* **1999**, *99*, 1801-1821.

[5] McCord, M.; Rooks, M. In *Handbook of Microlithography, Micromachining and Microfabrication*; SPIE Press: Bellingham, WA, 1997; Vol. 1, Chapter 2.

[6] For an overview of soft lithography, see: Xia, Y.; Whitesides, G. M. *Angew. Chem. Int. Ed.* **1998**, *37*, 550-575.

[7] a) Chou, S. Y.; Krauss P. R.; Renstrom P. J. *Science* **1996**, *272*, 85-87. b) Chou, S. Y.; Krauss, P. R.; Zhang W.; Guo L.; Zhuang L. *J. Vac. Sci. Technol.* **1997**, *B15*, 2897-2904.

[8] a) Piner, R. D.; Zhu, J.; Xu, F.; Hong, S.; Mirkin, C. A. *Science* **1999**, *283*, 661-663. b) Mirkin, C. A.; Hong, S.; Levine, R. D. *ChemPhysChem* **2001**, *2*, 37-39.

[9] a) Steed, J. W.; Atwood, J. L. *Supramolecular Chemistry*; Wiley: Chichester, UK, 2000, Chapter 7. b) Templating, Self-Assembly, and Self-Organization. *Comprehensive Supramolecular Chemistry*; Pergamon: Oxford, UK, 1987-1996; Vol. 9. c) Philp, D.; Stoddart, J. F. *Angew. Chem. Int. Ed.* **1996**, *35*, 1154-1196.

[10] For recent overviews on dendrimers, see: a) Van Manen, H.-J.; Van Veggel, F. C. J. M.; Reinhoudt, D. N. *Top. Curr. Chem.* **2001**, *217*, 121-162. b) Grayson, S. M.; Fréchet, J. M. J. *Chem. Rev.* **2001**, *101*, 3819-3867. c) Newkome, G. R.; He, E.; Moorefield, C. N. *Chem. Rev.* **1999**, *99*, 1689-1746. d) Bosman, A. W.; Janssen, H. M.; Meijer, E. W. *Chem. Rev.* **1999**, *99*, 1665-1688. e) Fischer, M.; Vögtle, F. *Angew. Chem. Int. Ed.* **1999**, *38*, 884-905. f) Matthews, O. A.; Shipway, A. N.; Stoddart, J. F. *Prog. Polym. Sci.* **1998**, *23*, 1-56. g) Chow, H.-F.; Mong, T. K.-K.; Nongrum, M. F.; Wan, C.-W. *Tetrahedron* **1998**, *54*, 8543-8660. h) Zeng, F.; Zimmerman, S. C. *Chem. Rev.* **1997**, *97*, 1681-1712. i) Newkome, G. R.; Moorefield, C. N.; Vögtle, F. *Dendritic Macromolecules: Concepts, Syntheses, Perspectives*; VCH: Weinheim, Germany, 1996.

[11] Huisman, B.-H.; Schönherr, H.; Huck, W. T. S.; Friggeri, A.; Van Manen, H.-J.; Menozzi, E.; Vancso, G. J.; Van Veggel, F. C. J. M.; Reinhoudt, D. N. *Angew. Chem. Int. Ed.* **1999**, *38*, 2248-2251.

[12] Friggeri, A.; Schönherr, H.; Van Manen, H.-J.; Huisman, B.-H.; Vancso, G. J.; Huskens, J.; Van Veggel, F. C. J. M.; Reinhoudt, D. N. *Langmuir* **2000**, *16*, 7757-7763.

[13] The coordination chemistry of SCS Pd^{II} pincer systems was discussed in: Van Manen, H.-J.; Nakashima, K.; Shinkai, S.; Kooijman, H.; Spek, A. L.; Van Veggel, F. C. J. M.; Reinhoudt, D. N. *Eur. J. Inorg. Chem.* **2000**, 2533-2540.

[14] Friggeri, A.; Van Manen, H.-J.; Auletta, T.; Li, X.-M.; Zapotoczny, S.; Schönherr, H.; Vancso, G. J.; Huskens, J.; Van Veggel, F. C. J. M.; Reinhoudt, D. N. *J. Am. Chem. Soc.* **2001**, *123*, 6388-6395.

[15] Van Manen, H.-J. *Ph.D. Thesis*, University of Twente, the Netherlands 2001.

[16] a) Kickham, J. E.; Loeb, S. J.; Murphy, S. L. *Chem. Eur. J.* **1997**, *3*, 1203-1213. b) Cameron, B. R.; Loeb, S. J.; Yap, G. P. A. *Inorg. Chem.* **1997**, *36*, 5498-5504. c) Kickham, J. E.; Loeb, S. J. *Inorg. Chem.* **1995**, *34*, 5656-5665.

[17] Brandsch, R.; Bar, G.; Whangbo, M.-H. *Langmuir* **1997**, *13*, 6349-6353.

[18] Van Noort, S. J. T.; Van der Werf, K. O.; De Grooth, B. G.; Van Hulst, N. F.; Greve, J. *Ultramicroscopy* **1997**, *69*, 117-127.

[19] Schönherr, H. *Ph.D. Thesis*, University of Twente, the Netherlands, 1999.

[20] Mourey, T. H.; Turner, S. R.; Rubinstein, M.; Fréchet, J. M. J.; Hawker, C. J.; Wooley, K. L. *Macromolecules* **1992**, *25*, 2401-2406.

[21] a) Dobbs, D. A.; Bergman, R. G.; Theopold, K. H. *Chem. Eng. News* **1990**, 68, (17), 2. b) Wnuk, T. *Chem. Eng. News* **1990**, 68 (26), 2. c) Matlow, S. L. *Chem. Eng. News* **1990**, 68, (30), 2.

[22] Schönherr, H.; Vancso, G. J.; Huisman, B.-H.; Van Veggel, F. C. J. M.; Reinhoudt, D. N. *Langmuir* **1999**, *15*, 5541-5546.

[23] Ron, H.; Rubinstein, I. *Langmuir* **1994**, *10*, 4566-4573.

Chapter 4

Surface-Anchored Dendritic Structures on Gold Substrates: Growth and Lateral Confinement of Nanosized Functions*

This chapter describes the spatial confinement of Au nanoparticles by attachment to single Pd^{II} pincer adsorbate molecules embedded as isolated species into self-assembled monolayers (SAMs) of decanethiol on gold, similar to the dendrimer insertion presented in Chapter 3. The coordination of monolayer-protected Au nanoclusters bearing phosphine moieties at the periphery, to SAMs containing individual sulfur-carbon-sulfur (SCS) Pd^{II} pincer molecules was monitored by tapping mode atomic force microscopy (TM-AFM). The insertion of a thioether dendrimer into SAMs of n-alkanethiols was directed by using gold substrates patterned with two alkanethiols of different chain length. Microcontact printed substrates with well separated areas of octadecanethiol and decanethiol were prepared and exposed to a solution of the thioether dendrimer, and resulted in insertion exclusively into the decanethiol areas.

4.1 Introduction

Nanofabrication has a fundamental relevance for numerous application fields such as electronic devices,[1] high-density data storage,[2] and analytical chemistry.[3] One of the ultimate goals of nanofabrication/nanotechnology is computation by individual molecules.[4] In order to achieve single molecule computation one must rely on the understanding and thus study of individual molecules. Single molecule studies allow individual members of a heterogeneous population to be identified and studied, while ensemble studies only yield information on the average properties of a system.[5]

Single molecule research began with biomolecules, in particular DNA, not only because they are the "building blocks of life", but also because of their large size, which facilitates their visualization.[6] The first imaging attempts, using scanning tunneling microscopy, date back to 1983.[7] In recent years, the development of optical tweezers has made the

---

* Part of this chapter has been published in: Friggeri, A.; Van Manen, H.-J.; Auletta, T.; Li, X.-M.; Zapotoczny, S.; Schönherr, H.; Vancso, G. J.; Huskens, J.; Van Veggel, F. C. J. M.; Reinhoudt, D. N. *Journal of the American Chemical Society* **2001,** *123,* 6388-6395.

manipulation of single biomolecules possible,[8] and techniques such as scanning near-field optical microscopy (SNOM) and atomic force microscopy (AFM) can be used to study the physical,[9] dynamic,[10] and mechanical[11] properties of single molecules.

Nowadays, the dimensions of some synthetic molecular and supramolecular structures, *e.g.* dendrimers[12] and nanoparticles,[13] are in the same range as those of biological systems, and they have the desired dimensions of nanoelectronic devices. Therefore, the "bottom-up" alternative, which consists of the controlled construction of complex structures of nanometer dimensions starting from the molecular level, is becoming an increasingly realistic tool for nanofabrication.[7]

Self-assembled monolayers (SAMs) are useful starting platforms for the development of nanometer-scale devices,[14] since they are highly ordered and have uniform film thicknesses.[15] As already reported in Chapter 3, we developed an approach, called monolayer insertion, to immobilize a number of thioether functionalized dendritic molecules onto gold substrates, exploiting the partial replacement of a preexisting thiol self-assembled monolayer.[16,17]

Studies on the properties of single dendrimer molecules have recently been reported by several groups. Crooks and coworkers[18] have measured the height of G4 and G8 polyamidoamine (PAMAM) dendrimers on gold using TM-AFM. Similarly, Tomalia and coworkers[19] have measured the molecular diameter and height of individual G5-G10 PAMAM dendrimers on mica, also using TM-AFM. However, AFM images of individual dendrimers smaller than G5 could not easily be obtained. De Schryver and coworkers[20] have used TM-AFM to measure the height of G4 polyphenylene dendrimer molecules spincoated on mica. Good agreement was found between the observed height and values calculated from molecular dynamics simulations. In our group have been observed single metallodendrimer molecules containing a rhodamine B core, using the SNOM technique.[10c]

The interest in using dendritic structures as surface-confined species has already been addressed in Chapter 3. However, complementary contributions to the bottom-up approach originate from the use of metal or semiconductor nanoparticles, which can furthermore act as nanosized model systems for more complex molecular structures. Monolayer-protected nanoparticles have shown to be versatile materials in several fields[21] due to their unique optical[22] and electronic properties[23] related to quantum size effects. Moreover, their straightforward synthesis allows introduction of a variety of functional groups at the outer organic monolayer shell.[24]

In this chapter, we expand on the possibilities related to the use of the insertion method described in Chapter 3. Phosphine-containing Au nanoclusters (MPCs) were anchored by

a coordination reaction to isolated SCS Pd^{II} pincer adsorbate molecules that are inserted into alkanethiol monolayers.

The insertion process usually occurs in a random fashion across the whole surface. Here we present a combination of this "bottom-up" fabrication approach with the "top-down" microcontact printing technique (μCP)[25] in order to direct the insertion of a thioether dendrimer to predefined surface areas of substrates patterned with SAMs of alkanethiols of different chain length.

4.2 Results and discussion

4.2.1 Anchoring of Au nanoparticles onto SAMs

The attachment of the Au nanoparticles has been carried out using building blocks that are able to coordinate to SCS Pd^{II} pincer moieties. The main reasons are the quantitative yield of the ligand exchange reactions involved,[26] the short reaction times required,[26,27] and the absence of solid byproducts that could contaminate the surface.

The synthesis of SCS Pd^{II} pincer adsorbate molecules (**1**) and phosphine-containing Au nanoclusters (**2**) (Chart 4.1) has been described previously.[28,29] The anchoring of Au nanoparticles on planar gold was performed on isolated Pd^{II} pincer adsorbate molecules **1** that are inserted in SAMs of decanethiol on gold (Scheme 4.1). Adsorbate **1** was prepared from the corresponding chloride by exchange with a pyridine ligand in solution. Pincer molecules **1** were then inserted into decanethiol SAMs by exposing the latter to a 1 mM dichloromethane solution of **1** for 3 h (Scheme 4.1A-C). This procedure avoids the use of $AgBF_4$ on a monolayer.[30]

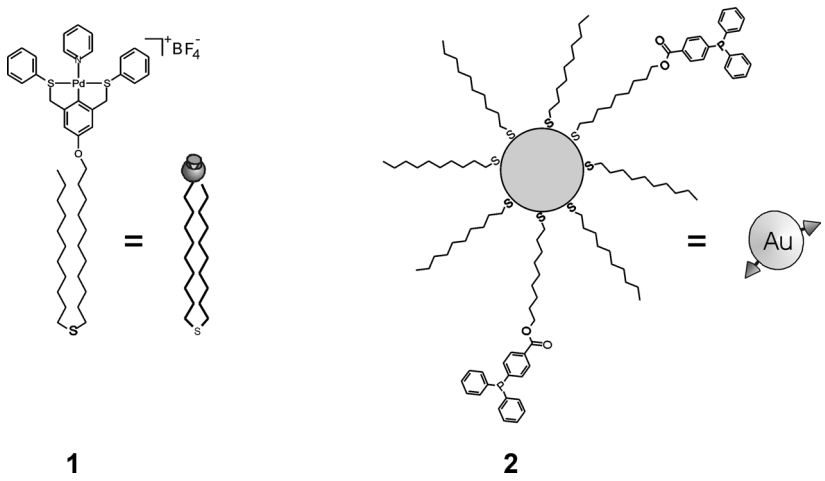

1 **2**

Chart 4.1 SCS Pd^{II} pincer adsorbate **1** and phosphine-functionalized MPCs **2** and their schematic representations.

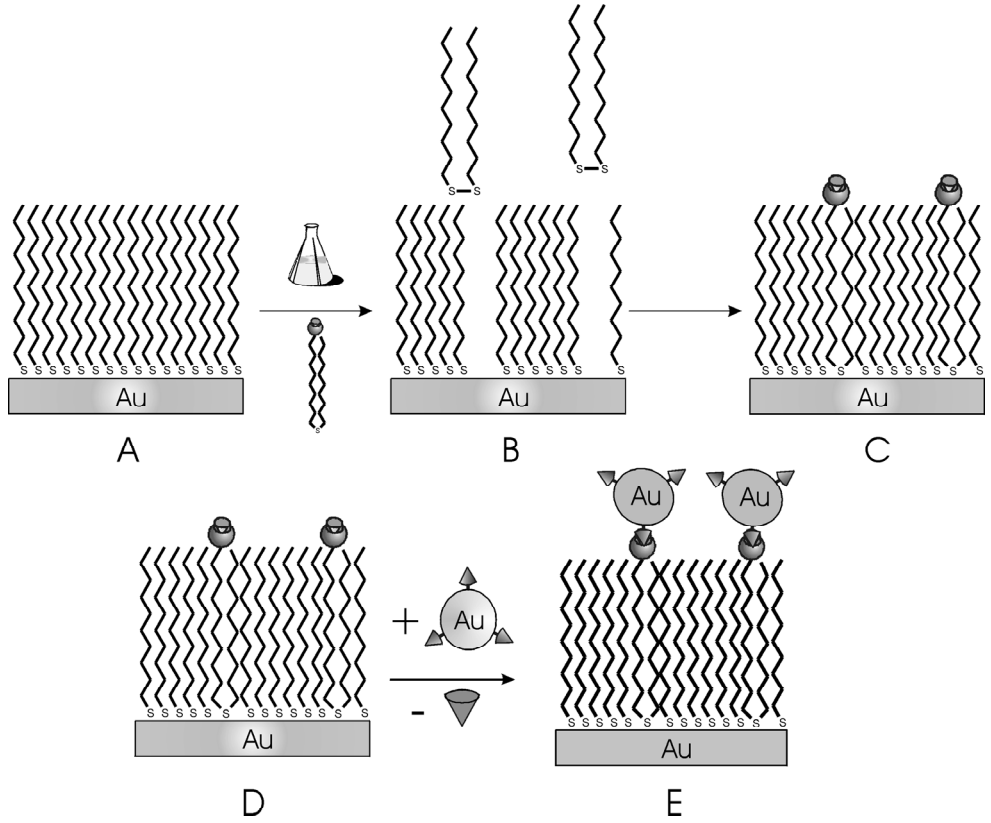

Scheme 4.1 Schematic representation of the insertion process of **1** into preformed decanethiol SAM and anchoring of **2**.

As expected, TM-AFM images of these layers showed only very few nanosized features due to the small size of the Pd^{II} pincer moiety protruding from the SAM (Figure 4.1A). Subsequently, these substrates were immersed into a phosphine-functionalized colloid **2** solution (0.4 mM in dichloromethane) for 10 min at r.t. followed by rinsing (Scheme 4.1D-E). TM-AFM (Figure 4.1B) showed the presence of nanosized features with a height of 3.5 ± 0.7 nm. This value correlates well with the average size of the gold core of 2.0 ± 0.5 nm obtained by TEM, taking into account that the thickness of the monolayer shell can be measured by AFM, while TEM gives exclusively information about the metal core.[31] The particles do not form a complete monolayer, but are instead well separated and randomly distributed over the entire surface.

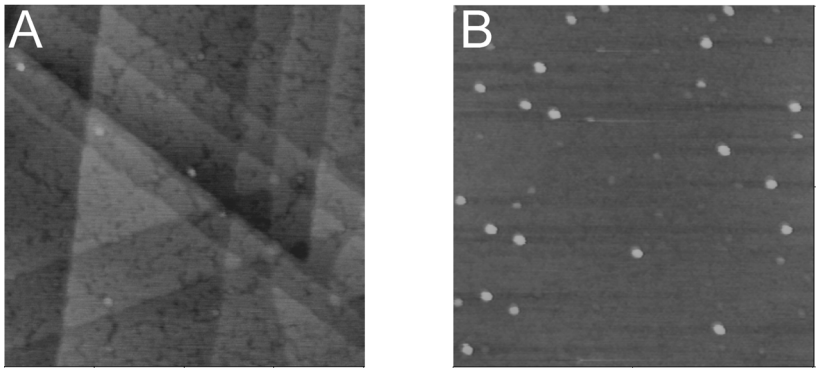

Figure 4.1 TM-AFM images in air of (A) decanethiol monolayer after exposure to a 1 mM solution of **1** (image size 400 × 400 nm^2, z-scale = 5 nm), and (B) after subsequent reaction with phosphine-derivatized gold colloids **2** (image size 500 × 500 nm^2, z-scale = 10 nm).

To rule out aspecific interactions or physisorption processes, two different types of control experiments were performed. In one case, Au nanoparticles stabilized exclusively with mixed monolayers of decanethiol and 11-mercapto-1-undecanol in a 4/1 ratio, and therefore lacking of the phosphine moiety, were brought into contact with the inserted pincer molecules **1**. In another experiment, phosphine-derivatized MPCs **2** were contacted with a decanethiol SAM. The absence of any adsorbed particles on either of these control layers clearly demonstrates that both the phosphine moiety on the colloidal particles *and* the pincer molecules in the layers are necessary for the anchoring/expression process. The overall behavior is consistent with specific metal-ligand interactions between the phosphine moieties of the Au nanoparticles and isolated Pd^{II} moieties in the layer.

4.2.2 Insertion into SAMs patterned by microcontact printing

To investigate possible ways to control the position of the dendritic structures on monolayer-protected gold surfaces the insertion of thioether dendrimer **3** (Chart 4.2, Scheme 4.3) was studied using patterned SAMs of alkanethiols with different chain length prepared by μCP. The use of **3** allows visualization of the nanosized features immediately after the insertion and does not require the expression stage.

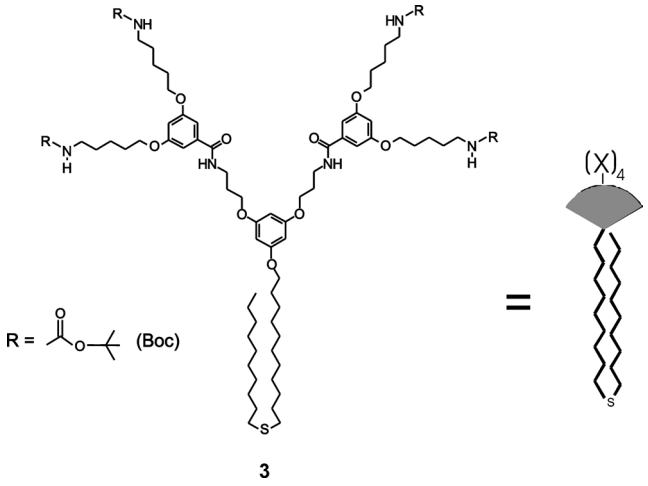

Chart 4.2 Dendritic thioether **3** and its schematic representation.

The synthesis of **3** has been reported previously.[29] Patterned substrates were prepared by microcontact printing[25,39] of octadecanethiol on gold-covered silicon substrates, in stripes of 5 μm width and separated by 2.5 μm. These substrates were immersed into a ferro/ferricyanide etching solution for 3 min, followed by rinsing with water and ethanol. The etching step allows an immediate and easy recognition of the two different areas. The grooves in between the printed areas were then filled by immersing the substrates in a decanethiol solution (1 mM in EtOH) for 2 h **(**Scheme 4.2**)**.

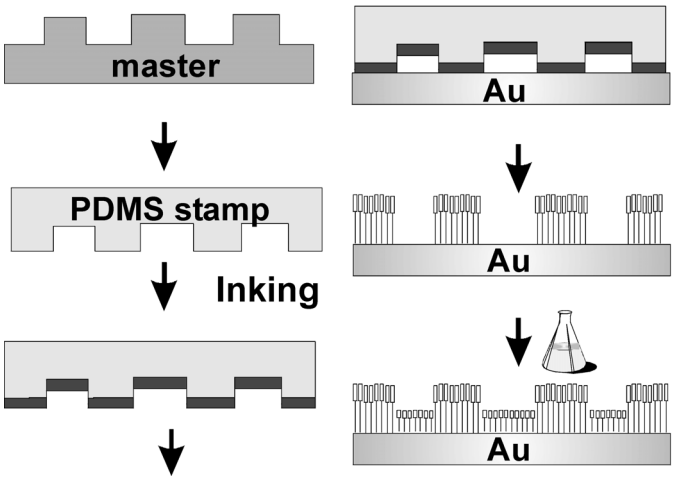

Scheme 4.2 Schematic representation of μCP to prepare patterned surface with two alkanethiols of different chain length.

TM-AFM allowed the identification of the octadecanethiol (brighter) and decanethiol areas (darker), as shown in Figure 4.2A. A zoomed-in AFM image of the decanethiol area is also shown (Figure 4.2B).[32]

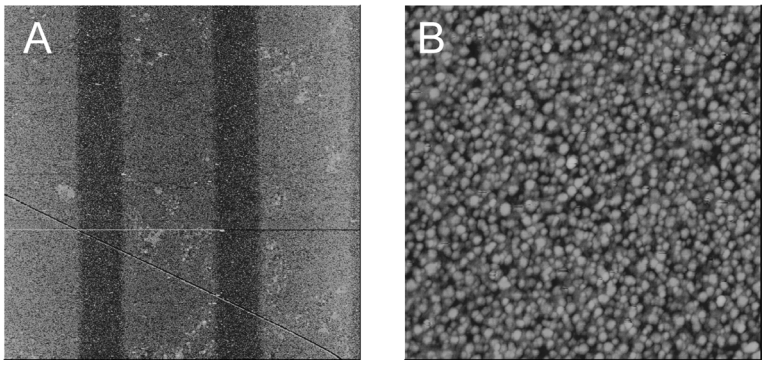

Figure 4.2 TM-AFM images in air of (A) an octadecanethiol/decanethiol patterned substrate with intermittent etching (image size 20 × 20 μm^2, z-scale = 10 nm); and (B) of a decanethiol area of the same substrate, with gold grain structure clearly visible (image size 1 × 1 μm^2, z-scale = 10 nm).

Subsequently, the substrates were exposed to a 0.01 mM solution of dendrimer **3**, and thoroughly rinsed. During this step defects are formed in the monolayer, that allow the molecular species **3** to interact with the gold surface via its thioether moiety.
TM-AFM images in air showed the presence of nanosized features that give a contrast in phase with respect to the granular gold structure, characterized by an average height of 7.0 ± 1.5 nm. These occurred *exclusively* in the decanethiol areas (Figure 4.3A).

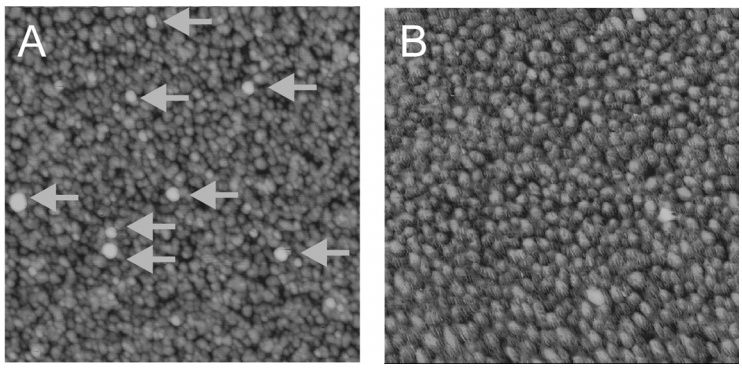

Figure 4.3 TM-AFM images in air of (A) decanethiol area after exposure to a 0.01 mM solution of **3** (image size 1 × 1 μm^2, z-scale = 10 nm; arrows point at single dendritic molecules inserted), and (B) of an octadecanethiol area of the same substrate (image size 1 × 1 μm^2, z-scale = 10 nm).

The height values measured for the inserted molecules were in the same order of magnitude as previously reported for homogeneous decanethiol SAMs.[16,17] No tip deconvolution has been performed, thus no systematic evaluation of the width of the dendrimers is reported.[33] The average number of nanometer-sized features counted in a 500×500 nm^2 area of the decanethiol SAM exposed to thioether adsorbate **3** was 7 ± 2, which is in good agreement with results obtained for the insertion of similar structures.[17] As expected, TM-AFM imaging of the octadecanethiol areas did not show any nanosized features corresponding to single isolated dendritic structures (Figure 4.3B).

The number of pinholes created in a layer by exposure to a solvent, which is necessary for the insertion of the dendron thioether to occur, is related to the stability of the self-assembled monolayer itself. Thus, it is a function of the chain length of the employed thiol. In general, the longer the alkyl moiety, the more stable is the layer due to stronger Van der Waals interactions between adjacent chains (in the order of a few kcal mol^{-1} per methylene unit).[34,35] The octadecanethiol SAM shows, therefore, a lower degree of defect formation, owing to this enhanced stability towards desorption. Moreover, adsorbate **3** contains an alkyl spacer between the dendritic moiety and the sulfur atom of only 10 carbon atoms, which is much smaller than the octadecanethiol SAM in which it would need to insert, and has a sterically demanding head-group (Scheme 4.3).

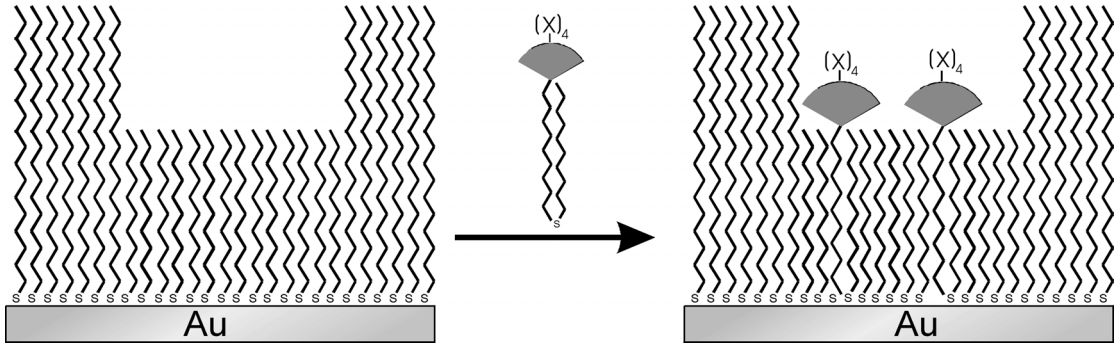

Scheme 4.3 Schematic representation of lateral control of the insertion process of **3** on μCP substrates.

Therefore, even if defects were created in the octadecanethiol layer, the molecules surrounding the pinhole will act as a physical barrier, preventing the sulfur moiety of the thioether dendrimer for reaching the gold surface.

4.3 Conclusions

In this chapter, a methodology has been shown to address single SCS Pd^{II} pincer receptor molecules embedded into a preformed decanethiol monolayer by using phosphine-derivatized MPCs. This "expression" relies on coordination chemistry reactions, and allows a fast and quantitative evaluation of the number of surface-confined molecular receptor via TM-AFM. These molecules are otherwise difficult to detect with conventional surface analysis techniques, due to the very low amount of material involved in the process. We can conclude that the insertion method combined with the "expression" stage allows us to monitor chemical reactions at the single molecule level. In principle, this technique can be applied to any suitably designed nanosized object incorporating specific functions (*e.g.* semi-conductor or magnetic nanoparticles).
The insertion process, however, occurs randomly on a surface, according to the formation of pinholes into a preformed alkanethiol monolayer. To achieve control over the position of the receptor molecules onto a certain surface the self-assembly methodology has been combined with the soft-lithographic technique microcontact printing. This methodology relies on using substrates that are patterned with SAMs of alkanethiols of different chain length, to perform the insertion process. This combination of top-down and bottom up approach proved to be successful to achieve lateral control over the position where the insertion of dendritic architectures occurs, as shown by TM-AFM analysis.

4.4 Experimental

Materials. CH_2Cl_2 was freshly distilled from $CaCl_2$. Acetone, EtOH, THF, and $CHCl_3$ were used as received (p.a. from Merck). MeCN (p.a. from Merck) was stored over molecular sieves (4 Å). Water was purified by Millipore membrane units. $HAuCl_4 \cdot xH_2O$ (99.99%, from Acros) and tetraoctylammonium bromide (from Fluka) were used as received. All other reagents, including octadecanethiol and decanethiol were purchased from Aldrich and used without further purification. Synthesis of compounds **1** and **3** was carried out by Henk-Jan Van Manen.[28,29]
Synthesis of gold nanoparticles was carried by Xue-Mei Li:[28] Au nanoparticles stabilized by a mixed monolayer of decanethiol and 11-mercapto-1-undecanol in a 4/1 ratio were prepared in a one-pot synthesis following the Brust method.[24a] ^1H NMR spectroscopy ($CDCl_3$) showed that the percentage of the two thiols in the monolayer is the same as in the solution from which the nanoparticles are formed (ca. 20 OH moieties per nanoparticle), indicating that the layer formation is under kinetic control. After purification of the product, the hydroxyl moieties were coupled with 4-(diphenylphosphino)benzoic acid in

the presence of 1-(3-dimethylaminopropyl)-3-ethyl-carbodiimide hydrochloride (EDC) and 4-(dimethylamino)pyridine (DMAP) in CH_2Cl_2. ^1H NMR spectroscopy proved that ester formation had occurred (disappearing of the C*H*$_2$OH signal). Transmission electron microscopy (TEM) analysis provided an average size of the gold core of 2.0 ± 0.5 nm.

Methods. All glassware used to prepare monolayers was immersed in piraña solution (conc. H_2SO_4 and 33% H_2O_2 in a 3:1 ratio). **(Warning piraña should be handled with caution; it has detonated unexpectedly)**.[36] Next, the glassware was rinsed with large amounts of Milli-Q water.

Substrate preparation. Gold substrates were obtained from Metallhandel Schröer GmbH (Lienen, Germany). Immediately before use, the substrates were rinsed with Milli-Q water and then flame-annealed with a H_2 flame (purity 6) as described previously.[37] After the annealing procedure, the substrates were placed in p.a. ethanol for 10 min[38] and then immersed into the adsorbate solution for the desired time. After each adsorption step the samples were removed from the solutions and rinsed thoroughly with dichloromethane, ethanol, and Milli-Q water. All adsorbate solutions were prepared freshly before use. SAMs of decanethiol were prepared by immersing the gold substrates in the corresponding 1 mM ethanol solutions at room temperature, for 3 h. Insertion of thioether **1** and **3** into a preformed decanethiol monolayer was achieved by immersing substrates into a 1 mM and 0.01 mM solution in CH_2Cl_2,respectively. 0.4 mM solutions of **2** in CH_2Cl_2 were deoxygenated prior to immersion of the monolayers by bubbling nitrogen through the solutions for 10 min, and were kept under argon during the insertion experiments. After immersion into a 1 mM solution of **2**, the samples were rinsed by placing them three times in CH_2Cl_2 for 5 min. Two other rinsing procedures were attempted: (a) CH_2Cl_2 (20 ml, 5 min), followed by EtOH (20 ml, 5 min), and H_2O (20 ml, 5 min), and (b) 15 min in CH_2Cl_2 during sonication, but some physisorbed material remained on the layers. All layers were dried under a nitrogen stream. All experiments were repeated 3 or 4 times.

Microcontact printing. Gold substrates were prepared by evaporating 20 nm of gold on a 3" silicon wafer with a 2 nm titanium layer to improve adhesion. Just before use, the substrates were cut in the desired size and shape and cleaned in an oxygen plasma reactor for 5 min. The substrates were then placed in p.a. ethanol for 10 min.[38] Microcontact printed substrates were prepared according to literature procedures.[25,39] Stamps were prepared by pouring PDMS (Sylgard silicon elastomer 184) on a silicon master patterned with grooves of 5 μm width separated 2.5 μm. A 1 mM solution of octadecanethiol was used to ink the stamp, and after drying in a stream of nitrogen it was applied by hand for 30 s on a gold-coated silicon substrate and subsequently carefully removed.

After printing, the substrates were thoroughly washed with EtOH and then subjected to a ferro/ferricyanide etchant for 3 min.[40] The etchant was prepared right before use by mixing an aqueous solution of $Na_2S_2O_3$ (0.1 M) and an aqueous solution containing KOH (1M), $K_3Fe(CN)_6$ (0.01 M), $K_4Fe(CN)_6$ (0.001 M) in a 1:1 ratio. After washing with Milli-Q water the substrates were immersed in a 1 mM solution of decanethiol in EtOH for 2h. The samples were removed from the solution, rinsed thoroughly with dichloromethane, ethanol, and Milli-Q water, immersed for 2 h in a 0.01 mM solution of adsorbate **1** and rinsed by placing them three times in 20 ml CH_2Cl_2, each time for 5 min.

Atomic force microscopy. The AFM measurements were carried out with a NanoScope III multimode AFM (Digital Instruments, Santa Barbara, CA, USA). Tapping mode AFM scans were performed in air using silicon cantilevers/tips (Nanosensors, Wetzlar, Germany; cantilever resonance frequency f_0 = 280-320 kHz). The free amplitude was kept constant for all experiments and the amplitude damping (setpoint) ratio was adjusted to ≈ 0.90. Prior to the measurements, the set-up was thermally equilibrated for several hours in order to minimize the drift and to ensure a constant temperature (≈ 30 °C). The piezo scanner was calibrated in the lateral directions using a grid with repeat distances of 1.0 μm, as well as self-assembled monolayers of thiols on Au(111) (*e.g.* octadecanethiol, repeat distance 0.51 nm),[37] and in the z-direction by measuring step heights of Au(111) (2.355 Å).[33] The number of nanometer-sized features and their standard deviations were determined by counting the features on at least three areas of the same sample, and taking the average.

4.5 References and notes

[1] a) Gittins, D. I.; Bethell, D.; Schiffrin, D. J.; Nichols, R. J. *Nature* **2000**, *408*, 67–69. b) Collier, C. P.; Mattersteig, G.; Wong, E. W.; Luo, Y.; Beverly, K.; Sampaio, J.; Raymo, F. M.; Stoddart, J. F.; Heath, J. R. *Science* **2000**, *289*, 1172–1175. c) Chen, J.; Reed, M. A.; Rawlett, A. M.; Tour, J. M. *Science* **1999**, *286*, 1550–1552.

[2] a) Lutwyche, M. I.; Despont, M.; Drechsler, U.; Dürig, U.; Häberle, W.; Rothuizen, H.; Stutz, R.; Widmer, R.; Binnig, G. K.; Vettiger, P. *Appl. Phys. Lett.* **2000**, *77*, 3299–3301. b) Mizutani, W.; Ishida, T.; Tokumoto, H. *Langmuir* **1998**, *14*, 7197–7202.

[3] Martin, C. R.; Mitchell, D. T. *Anal. Chem. A-Pages* **1998**, *70*, 322 A–327 A.

[4] Ball, P. *Nature* **2000**, *406*, 118–120.

[5] Weiss, S. *Science* **1999**, *283*, 1676–1683.

[6] Service, R. F. *Science* **1999**, *283*, 1668–1669.

[7] Gimzewski, J. K.; Joachim, C. *Science* **1999**, *283*, 1683–1688.
[8] Mehta, A. D.; Rief, M.; Spudich, J. A.; Smith, D. A.; Simmons, R. M. *Science* **1999**, *283*, 1689–1695.
[9] Bayburt, T. H.; Carlson, J. W.; Sligar, S. G. *Langmuir* **2000**, *16*, 5993–5997.
[10] a) Poirier, G. E. *Chem. Rev.* **1997**, *97*, 1117–1127. b) Dunn, R. C. *Chem. Rev.* **1999**, *99*, 2891–2927. c) Veerman, J. A.; Levi, S. A.; Van Veggel, F. C. J. M.; Reinhoudt, D. N.; Van Hulst, N. F. *J. Phys. Chem. A* **1999**, *103*, 11264–11270. d) Takano, H.; Kenseth, J. R.; Wong, S.-S.; O'Brien, J. C.; Porter, M. D. *Chem. Rev.* **1999**, *99*, 2845–2890; e) Ishii, Y.; Yanagida, T. *Single Mol.* **2000**, *1*, 5–13.
[11] a) Rief, M.; Oesterhelt, F.; Heymann, B.; Gaub, H. E. *Science* **1997**, *275*, 1295–1297. b) Rief, M.; Gautel, M.; Oesterhelt, F.; Fernandez, J. M.; Gaub, H. E. *Science* **1997**, *276*, 1109−1112.
[12] For recent reviews of dendrimers, see: a) Fischer, M.; Vögtle, F. *Angew. Chem. Int. Ed.* **1999**, *38*, 884-905. b) Bosman, A. W.; Janssen, H. M.; Meijer, E. W. *Chem. Rev.* **1999**, *99*, 1665-1688. c) Smith, D. K.; Diederich, F. *Chem. Eur. J.* **1998**, *4*, 1353-1361. d) Newkome, G. R.; Moorefield, C. N.; Vögtle, F. *Dendritic Molecules: Concepts, Syntheses and Perspectives*; VCH: Weinheim, Germany, 1996.
[13] a) Schmid, G.; Bäumle, M.; Geerkens, M.; Ingo, H.; Osemann, C.; Sawitowski, T. *Chem Soc. Rev.* **1999**, *28*, 179-185. b) Templeton, A. C.; Wuelfing, W. P., Murray, R. W. *Acc. Chem. Res.* **2000**, *22*, 27-36.
[14] a) Moav, T.; Hatzor, A.; Cohen, H.; Libman, J.; Rubinstein, I.; Shanzer, A. *Chem. Eur. J.* **1998**, *4*, 502–507. b) Hatzor, A.; Moav, T.; Cohen, H.; Matlis, S.; Libman, J.; Vaskevich, A.; Shanzer, A.; Rubinstein, I. *J. Am. Chem. Soc.* **1998**, *120*, 13469−13477.
[15] a) Ulman, A. *Introduction to Thin Organic Films: From Langmuir-Blodgett to Self-Assembly*; Academic Press: Boston, MA, 1991. b) Ulman, A. *Chem. Rev*. **1996**, *96*, 1533-1554.
[16] a) Huisman, B.-H.; Schönherr, H.; Huck, W. T. S.; Friggeri, A.; Van Manen, H.-J.; Menozzi, E.; Vancso, G. J.; Van Veggel, F. C. J. M.; Reinhoudt, D. N. *Angew. Chem. Int. Ed.* **1999**, *38*, 2248–2251. b) Friggeri, A.; Schönherr, H.; Van Manen, H.-J.; Huisman, B.-H.; Vancso, G. J.; Huskens, J.; Van Veggel, F. C. J. M.; Reinhoudt, D. N *Langmuir* **2000**, *16*, 7757–7763.
[17] Van Manen, H.-J.; Auletta, T.; Van Veggel, F. C. J. M.; Reinhoudt D. N. *Adv. Funct. Mater*. **2002**, *12*, 811-818.
[18] Hierlemann, A.; Campbell, J. K.; Baker, L. A.; Crooks, R. M.; Ricco, A. J. *J. Am. Chem. Soc.* **1998**, *120*, 5323–5324.

[19] Li, J.; Piehler, L. T.; Qin, D.; Baker, Jr., J. R.; Tomalia, D. A. *Langmuir* **2000**, *16*, 5613–5616.

[20] Zhang, H.; Grim, P. C. M.; Foubert, P.; Vosch, T.; Vanoppen, P.; Wiesler, U.-M.; Berresheim, A. J.; Müllen, K.; De Schryver, F. C. *Langmuir* **2000**, *16*, 9009–9014.

[21] a) Bartz, M.; Küther, J.; Seshadri, R.; Tremel, W. *Angew. Chem. Int. Ed.* **1998**, *37*, 2466–2468. b) Labande, A.; Astruc, D. *Chem. Commun.* **2000**, 1007–1008. c) Patolsky, F.; Ranjit, K. T.; Lichtenstein, A.; Willner, I. *Chem. Commun.* **2000**, 1025–1026.

[22] Thomas, K. G.; Kamat, P. V. *J. Am. Chem Soc.* **2000**, *122*, 2655–2656.

[23] a) Elghanian, R.; Storhoff, J. J.; Mucic, R. C.; Letsinger, R. L.; Mirkin, C. A. *Science* **1997**, *277*, 1078–1081. b) Schmid, G.; Bäumle, M.; Geerkens, M.; Heim, I.; Osemann, C.; Sawitowski, T. *Chem. Soc. Rev.* **1999**, *28*, 179–185. c) Andres, R. P.; Bein, T.; Dorogi, M.; Feng, S.; Henderson, J. I.; Kubiak, C. P.; Mahoney, W.; Osifchin, R. G.; Reifenberger, R. *Science* **1996**, *272*, 1323–1325.

[24] a) Brust, M.; Walker, M.; Bethell, D.; Schiffrin, D. J.; Whyman, R. *J. Chem. Soc., Chem. Commun*. **1994**, 801–802. b) Brust, M.; Fink, J.; Bethell, D.; Schiffrin, D. J.; Kiely, C. *J. Chem. Soc., Chem. Commun*. **1995**, 1655–1656. c) Liu, J.; Alvarez, J.; Kaifer, A. E. *Adv. Mater.* **2000**, *12*, 1381–1383.

[25] a) Xia, Y.; Whitesides, G. M. *Angew. Chem. Int. Ed.* **1998**, *37*, 550-575. b) Biebuyck, H. A.; Larsen, N. B.; Delamarche, E.; Michel, B. *IBM J. Res. Dev.* **1997**, *41*, 159-170.

[26] Huck, W. T. S.; Van Veggel, F. C. J. M.; Reinhoudt, D. N. *Angew. Chem. Int. Ed.* **1996**, *35*, 1213–1215.

[27] a) Huck, W. T. S.; Van Veggel, F. C. J. M.; Kropman, B. L.; Blank, D. H. A.; Keim, E. G.; Smithers, M. M. A.; Reinhoudt, D. N. *J. Am. Chem. Soc.* **1995**, *117*, 8293–8294. b) Huck, W. T. S.; Van Veggel, F. C. J. M.; Reinhoudt, D. N. *J. Mater. Chem.* **1997**, *7*, 1213–1219.

[28] Friggeri, A.; Van Manen, H.-J.; Auletta, T.; Li, X.-M.; Zapotoczny, S.; Schönherr, H.; Vancso, G. J.; Huskens, J.; Van Veggel, F. C. J. M.; Reinhoudt, D. N. *J. Am. Chem. Soc.* **2001**, *123*, 6388-6395.

[29] Van Manen, H.-J. *Ph.D. Thesis*, University of Twente, the Netherlands, 2001.

[30] Deprotection with $AgBF_4$ of the corresponding coordinated chloride ligands of **1** inserted in a decanethiol monolayer gave rise to an insoluble residue (probably AgCl), which remained on the substrate, thereby hindering scanning force microscopy measurements.

[31] Reetz, M. T.; Helbig, W.; Quaiser, S. A.; Stimming, U.; Vogel, R. *Science* **1995**, *267*, 367–370.

[32] To allow a good contact between the PDMS stamps and the gold surface in the microcontact printing step over an area of at least tens of square microns, substrates were prepared by evaporation of a very thin layer (20 nm) of gold on a silicon wafer, without any further treatment (*e.g.* high temperature annealing). This approach allows one to prepare gold layers that retain the flatness of the underlying silicon wafer, leading to a very low roughness (<1 nm over a 1 × 1 μm^2). However, on a nm scale the granular structure of the evaporated gold with a grain size of about 5 nm is clearly seen. This structure does not allow one to set a unique zero level to be taken as reference in the section analysis measurements. As a consequence, both the average and standard deviation of the height values measured for **3** after insertion are higher than the one reported for similar structures.[16,17] In previous studies, all measurements were carried out on H_2 flame annealed substrates characterized by monoatomically flat regions of 200-300 nm^2. The absence of granular structures allows a more accurate zero level to which the height values are correlated and, therefore, a more accurate section analysis.

[33] Schönherr, H. *Ph.D. Thesis*, University of Twente, the Netherlands, 1999.

[34] Schreiber, F. *Progr. Surf. Sci.* **2000**, *65*, 151-256.

[35] Dubois, L. H.; Nuzzo, R. G. *Ann. Rev. Phys. Chem.* **1992**, *43*, 437-463.

[36] a) Dobbs, D. A.; Bergman, R. G.; Theopold, K. H. *Chem. Eng. News* **1990**, 68, (17), 2. b) Wnuk, T. *Chem. Eng. News* **1990**, 68 (26), 2. c) Matlow, S. L. *Chem. Eng. News* **1990**, 68, (30), 2.

[37] Schönherr, H.; Vancso, G. J.; Huisman, B.-H.; Van Veggel, F. C. J. M.; Reinhoudt, D. N. *Langmuir* **1999**, *15*, 5541–5546.

[38] Ron, H.; Rubinstein, I. *Langmuir* **1994**, *10*, 4566–4573.

[39] a) Kumar, A.; Whitesides, G. M. *Appl. Phys. Lett.* **1993**, *63*, 2002-2004. b) Lopez, G. P.; Biebuyck, H. A.; Whitesides, G. M. *Langmuir* **1993**, *9*, 1513-1516. c) Kumar, A.; Biebuyck, H. A.; Whitesides, G. M. *Langmuir* **1994**, *10*, 1498-1511. d) Wilbur, J. L.; Kim, E.; Xia, Y.; Whitesides, G. M. *Adv. Mater.* **1995**, *7*, 649-652. e) Xia, Y.; Whitesides, G. M. *Adv. Mater.* **1995**, *7*, 471-473.

[40] Xia, Y.; Zhao, X-M.; Kim, E.; Whiteside, G. M. *Chem. Mater.* **1995**, *7*, 2332-2337.

Chapter 5

Mixed Self-Assembled Monolayers on Gold of Ferrocene-Terminated Thiols and Hydroxyalkanethiols[*]

In this chapter, a study on the formation of mixed self-assembled monolayers (SAMs) using two different combinations of thiols, $Fc(CH_2)_6SH/HO(CH_2)_2SH$ and $Fc(CH_2)_{16}SH/HO(CH_2)_{11}SH$ (Fc=Ferrocene), is presented. The behavior at low Fc concentration was studied in order to prepare surfaces with isolated ferrocenyl-alkanethiols embedded in shorter ω-hydroxyalkanethiols. This type of architecture is required to perform AFM force spectroscopy experiments on host-guest supramolecular complexes, as shown in Chapter 6.

Several SAMs were prepared on polycrystalline gold electrodes from 1 mM thiol solutions, with different ferrocenylalkanethiol/hydroxyalkanethiol ratios. The amount of Fc immobilized on the electrode was determined by cyclic voltammetry and compared to the composition of the solution. The general trend appeared to be preferential adsorption by the longer chain component. However, significant differences in the layer formation and composition were observed for the two systems. $Fc(CH_2)_{16}SH$ is adsorbed to a larger extent, compared to $Fc(CH_2)_6SH$ for the same solution composition, as shown by the higher charge densities observed upon electrochemical oxidation. Furthermore, the redox peak position shifts to more positive values for the $Fc(CH_2)_{16}SH/HO(CH_2)_{11}SH$ system upon the increase of the ferrocenylalkanethiol fraction in solution, indicating that phase segregation may occur. The differences between the two systems were related to chain length effects from which favorable enthalpic contributions to the adsorption of the longer-chain component may arise.

---

[*] This chapter has been published in: Auletta, T.; Van Veggel, F. C. J. M.; Reinhoudt, D. N. *Langmuir* **2002,** *18,* 1288-1293.

5.1 Introduction

Self-assembled monolayers (SAMs) of sulfur-containing molecules on gold substrates provide an easy and fast way to form homogeneous monomolecular films with well defined surface properties. They have been prepared both from the solution and the gas phase.[1,2,3,4,5] The adsorption process of monolayers can basically be divided into two different steps. In a first, fast step, molecules are physisorbed and lie with their axis almost parallel to the surface (Scheme 5.1A-B).[6] This process can be described by a Langmuir adsorption isotherm. A second slower step follows, during which the molecules reorient and organize their alkyl chains in an all-trans conformation with their axis close to the surface normal and the sulfur headgroups bound to the gold (chemisorption) (Scheme 5.1C-D). The realignment process starts from the boundaries of domains and therefore the process seems to be driven by lateral interactions.
Recently, the two-step formation mechanism of SAMs of alkanethiols on gold has been confirmed by STM and AFM techniques.[7,8,9]

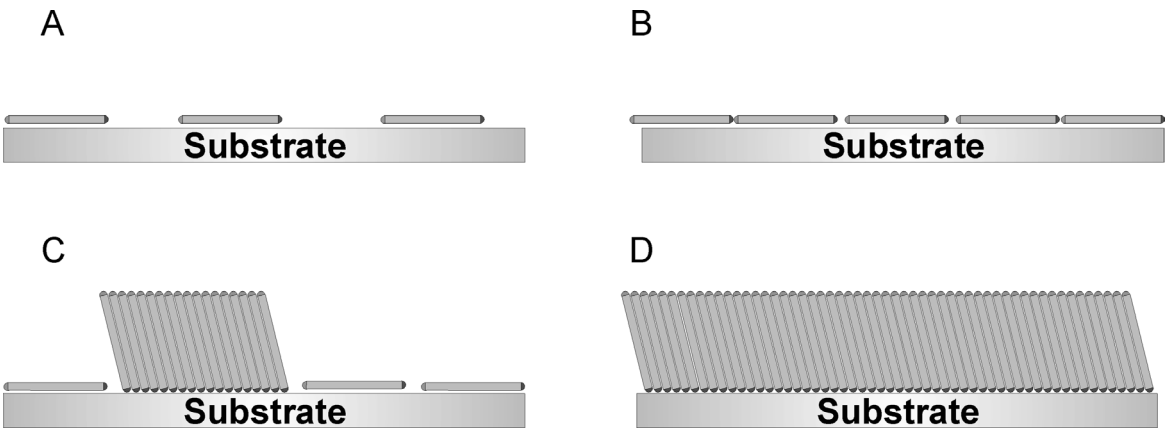

Scheme 5.1 Adsorption stages of monolayer formation (adapted from ref. 7).

By using a mixture of adsorbates, it is possible to introduce different chemical functionalities on a surface.[10,11] The adsorbate composition and distribution at the surface is a function of many different factors such as solution composition, chain length, and temperature. In general, when mixtures of thiols with different chain lengths are used, the longer chain component is preferentially adsorbed with respect to the solution composition.[12] Phase segregation in mixed monolayers is related to the difference in chain length of the two components (the stability of phases for mixed monolayers with a long and a short chain component decreases from long-long, to short-short, to

long-short).[13,14,15] Phase segregation may be induced by specific functional groups such as hydrogen bond donor/acceptor pairs.[16] At increasing temperatures at which the layers are formed, phase segregation is suppressed or drastically reduced, depending on the chain length difference between the two components.[17]

Thus, to achieve control over the layer composition, both the kinetics and thermodynamics of the adsorption process have to be taken into consideration. The interactions that lead to the formation of a stable monomolecular film can in general be separated into two main contributions: the binding force between the headgroup (sulfur) and gold (S-Au bond energy: 45 kcal mol^{-1})[18] and the interchain interactions (Van der Waals attractions of a few kcal mol^{-1} per CH_2).[3a]

Essential in studies of mixed SAMs, especially when containing small amounts of one of the two adsorbates, is the quantification and surface distribution of the adsorbed components. Electrochemistry provides a straightforward way to quantify the amount of electroactive centers adsorbed on a gold electrode and thus allows an indirect evaluation of the layer composition. In particular, mixed SAMs of Fc-containing thiols and *n*-alkanethiols have been widely investigated.[19,20,21,22,23] The redox properties of ferrocenylalkanethiols coadsorbed with *n*-alkanethiols have been studied as a function of the chain length of the coadsorbate and of the presence of polar groups (*e.g.* amide). The electron transfer rate between the ferrocene moieties and the gold electrode has been correlated to the nature of the different linking moieties between the redox center and the alkyl chain. In addition, the double layer effects on the interfacial redox reaction have been investigated.

The aim of this work is the preparation of surfaces with a low fraction of ferrocenylalkanethiols, embedded in a SAM of a hydroxyl-terminated thiol in order to produce surfaces with isolated Fc moieties available for complexation by β-cyclodextrin. Such substrates are required to perform AFM force spectroscopy measurements on single host-guest complexes as described in Chapter 6.[24] The alkyl chains of these ferrocenylalkanethiols must be longer than the coadsorbed hydroxyalkanethiols and the Fc headgroups homogeneously distributed over the surface. The hydroxyl moieties are required so as to reduce possible aspecific interactions between the SAMs on the substrate and on the AFM tip. Moreover, the electrochemical properties of the ferrocene units allow a direct comparison of the average concentration of surface-confined guests with the number of complexes detected in the tip-sample contact area by force spectroscopy experiments.

This chapter describes a study on the formation of mixed monolayers of ferrocenylalkanethiols and hydroxyalkanethiols with different chain lengths. Cyclic

voltammetry and contact angle measurements were carried out to determine the amount of electroactive component adsorbed on the electrode. The results are compared with the fractions of the two components in solution.

5.2 Results and discussion

5.2.1 Electrochemical characterization of mixed monolayers

Self-assembly of thiols containing an electroactive center can provide well-defined electrochemical systems in which all redox centers are at the same distance from the electrode and therefore the entire monolayer can be addressed in a single scan. Moreover, the redox current of such systems is linearly dependent on the scan rate. Thus, by integrating the current evolved in a redox cycle, the surface coverage of the electroactive component can be determined and related to the composition of the solution from which the layer is prepared.

The full-width at half-maximum of the anodic voltammetric wave, ΔE_{fwhm}, provides an indication of the interactions taking place between different redox centers. In the ideal situation, when there are no interactions between the redox centers, $\Delta E_{fwhm} = 3.53RT/nF$ (90.3/n mV at 24°C)[25] and deviations towards higher and smaller values have been attributed to interacting redox centers.

5.2.2 6-Ferrocenylhexanethiol/2-mercaptoethanol

Mixed monolayers with varying amounts of 6-ferrocenylhexanethiol and 2-mercaptoethanol ($Fc(CH_2)_6SH/HO(CH_2)_2SH$) were prepared from solutions in which the total thiol concentration was kept constant at 1 mM. Cyclic voltammetry (CV) measurements were performed in the presence of 0.1 M $NaClO_4$ as the background electrolyte. The cyclic voltammograms recorded at a scan rate of 0.1 V/s for SAMs formed from different solution compositions are reported in Figure 5.1.

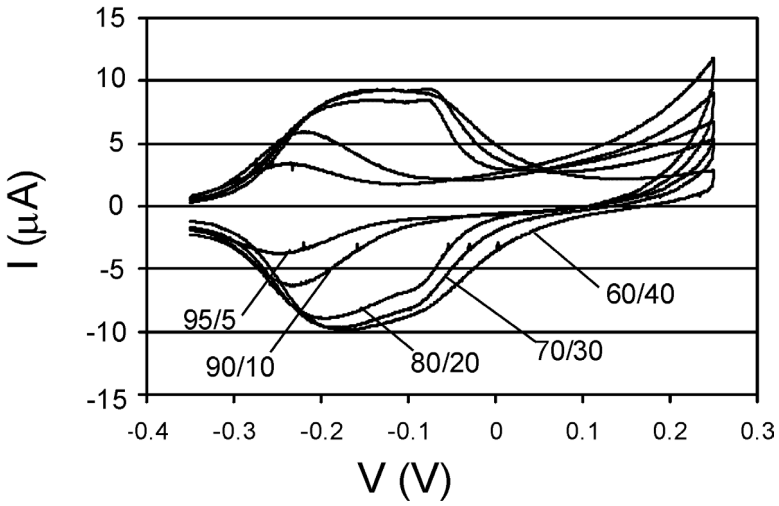

Figure 5.1 Cyclic voltammograms of mixed SAMs of 2-mercaptoethanol and 6-ferrocenylhexanethiol (molar ratios of the components in solution given) (0.1 M $NaClO_4$; scan rate = 0.1 V/s; potential vs. V_{MSE} = +0.61 V_{NHE}).

Significant changes in the shape and features of the CV curves were observed upon increase of the fraction of the Fc adsorbate in solution. In particular, the single, symmetric peak observed for ferrocene fractions in solution of 5 and 10% (ΔE_{fwhm} = 120 mV) broadens to ΔE_{fwhm} = 204 mV for Fc = 20%, showing even multiple peaks for larger Fc fractions. Upon increasing the Fc fraction in solution, the peak position shifts to more positive values from -0.234 V_{MSE} up to -0.136 V_{MSE}. At low ferrocene coverage, there is no difference in the peak position between the anodic and cathodic sweeps because of fast electron transfer kinetics while an increase of the Fc fraction led to a peak splitting up to 30 mV.

These results indicate that below 10% of Fc in solution each surface-confined redox center experiences almost the same environment independent of the progress of the redox process. Thus, the peak position and the absence of peak splitting can be ascribed to isolated ferrocene molecules inserted in the 2-mercaptoethanol environment. Upon increasing the amount of adsorbed ferrocenylthiol on the electrode, the electroactive centers start interacting, causing the broadening of the CV curves and the appearance of new peaks. However, it is difficult to assign uniquely all peaks to well-defined electrochemical species, due to the presence of the co-component and of other redox centers, which provide different chemical surroundings. Oxidation of a ferrocene center creates a positive charge and the oxidation process of any other ferrocene molecule in close proximity, with formation of yet another positive ferrocenium ion, will be more

difficult, thus requiring a more anodic potential. Furthermore the peak position is also affected by the creation of a less polar environment, due to the presence of the longer alkyl chains, also unfavorable for the creation of a positive charge.

Figure 5.2 shows a plot of the charge density versus the solution composition, together with a trendline expected for non-preferential adsorption (statistical mixing and equal adsorption rate).

This trend was estimated on the basis of geometrical assumptions, considering that an alkyl chain occupies around 20 $Å^2$,[26] while the ferrocene headgroup was treated as a hard sphere with a diameter of 6.6 Å.[19,27] Thus a straight line with f Fc_{SAM} = f Fc_{sol} describes the adsorption process up to a critical concentration of about 50%. Above this value no more ferrocene can be adsorbed due to sterical reasons, and the charge density reaches a plateau value. The corresponding surface coverage for such a full ferrocene layer is 2.7×10^{14} molecules/cm^2.[19]

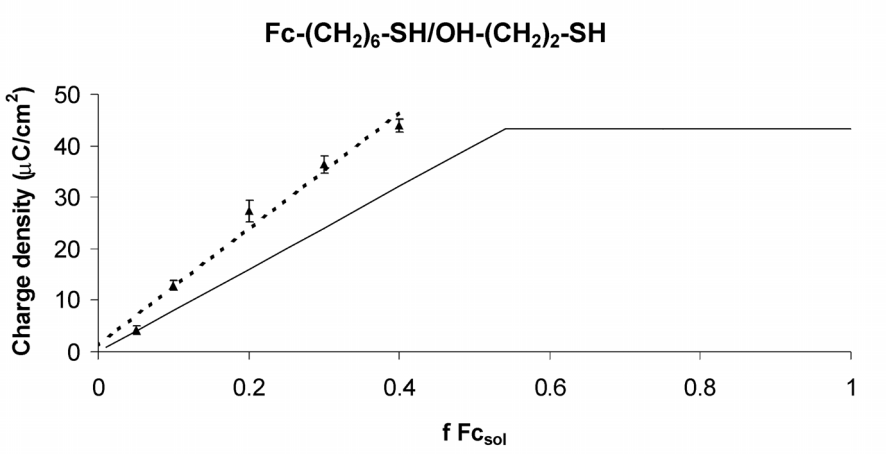

Figure 5.2 Charge density of mixed SAMs of 6-ferrocenylhexanethiol and 2-mercaptoethanol (▲) versus Fc molar fraction in solution, experimental fit (dashed line), and trendline expected for non-preferential adsorption (solid line).

The experimental data show an increase of the charge density upon increasing the percentage of the electroactive component in solution, and the maximum surface coverage was already reached at a Fc percentage in solution of 40% (2.74×10^{14} molecules/cm^2). Below 10 % of ferrocene in solution, the experimental data were in good agreement with the trendline for no preferential adsorption. However, above this value, higher charge densities were observed than predicted by the theoretical trend, indicating that the Fc component is preferentially adsorbed. Surface roughness of the polycrystalline

gold, which may lead to an increased surface area of 20% at most,[28] cannot explain this difference. The observed charge densities for Fc $\leq$ 30% can be fitted to a linear model (R^2 = 0.983) (Figure 5.2 dashed line). Deviation from linearity, in particular at high ferrocene coverage is attributed to saturation, as described above.

These results are in agreement with the general features reported in previous studies where the coadsorption of electroactive molecules with alkanethiol monolayers has been investigated[23c] and the chemical and physical properties of the shorter chain component seem to be not relevant in determining the layer composition. Using a polar hydroxyl-terminated thiol instead of an alkanethiol as a co-component, apparently does not modify the trend for the longer chain component to be adsorbed preferentially. Not only the difference in chain length but also the chain length itself might play a role in determining the driving forces for the layer formation, in particular for chain lengths longer than 10-12 methylene units, due to enhanced Van der Waals interactions acting both in the first physisorption stage of the SAM and in the following lateral interaction driven step that leads to the formation of the densely packed monolayer.

5.2.3 16-Ferrocenylhexadecanethiol/11-mercapto-1-undecanol

On the basis of the results reported above it was anticipated that the use of longer chain adsorbates could provide a more detailed picture of the layer formation process, focusing in particular on possible phase segregation phenomena. Mixed SAMs were prepared from solutions containing varying ratios of 11-mercapto-1-undecanol and 16-ferrocenylhexa-decanethiol keeping the total thiol concentration at 1 mM ($Fc(CH_2)_{16}SH/HO(CH_2)_{11}SH$).

The cyclic voltammograms recorded for these SAMs at a scan rate of 0.1 V/s are shown in Figure 5.3. Upon increasing the amount of electroactive component, a remarkable broadening of the peak towards a more positive potential is seen, up to Fc = 75% in solution; for this composition, instead, a very sharp peak (ΔE_{fwhm} = 62 mV) was observed. However, below 15% of ferrocene in solution (Figure 5.3b), the peaks are symmetric (ΔE_{fwhm} = 105 mV and 129 mV for Fc = 1% and 10% respectively) and show only a gradual change in the peak position.

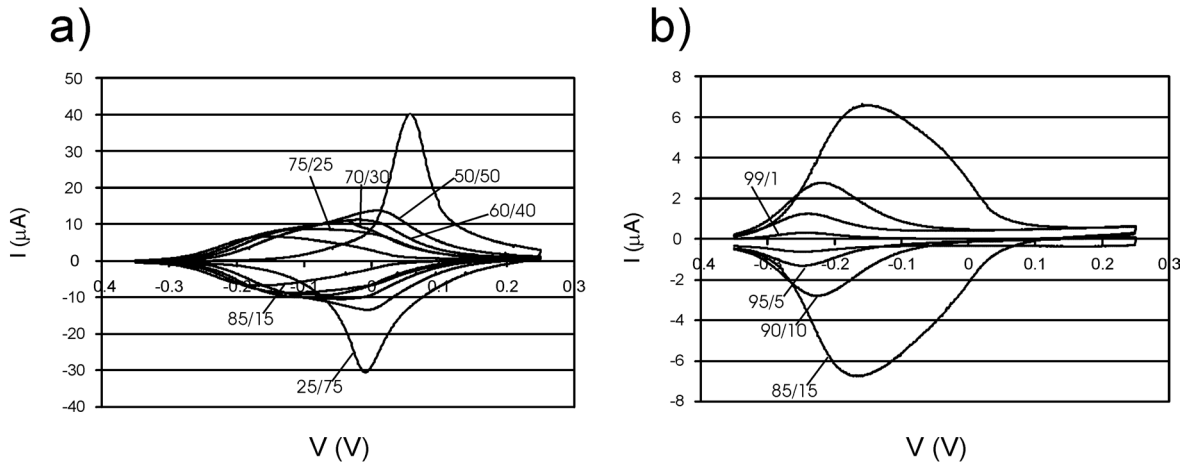

Figure 5.3 Cyclic voltammograms of mixed SAMs of 11-mercapto-1-undecanol and 16-ferrocenylhexadecanethiol (molar ratios of the components in solution given) (0.1 M $NaClO_4$; scan rate = 0.1 V/s; potential vs. V_{MSE} = +0.61 V_{NHE}): (a) 16-ferrocenylhexadecanethiol ≥ 15%; (b) ≤ 15%.

At low percentages of Fc in solution the electrochemical properties of the layers indicate that the surface-confined redox units can be treated as isolated species, as was already observed for the previous system. Upon increasing the Fc molar fraction in solution, the Fc moieties start interacting (ΔE_{fwhm} = 212 mV for 20% Fc) and strongly coupled centers are present at Fc = 75% as proven by the ΔE_{fwhm} = 62 mV characteristic of densely packed electroactive SAMs.[29]

The plot of the peak potential shift versus the solution composition (Figure 5.4) exhibits an S-shaped curve with an inflection at about 20% of ferrocene in solution. Upon increase of the fraction of the ferrocene component in solution, the redox potential peaks shift towards more anodic values starting from a value of –0.234 V_{MSE} (1% of $Fc(CH_2)_{16}SH$ in solution), corresponding to isolated ferrocene species similar to the $Fc(CH_2)_6SH/HO(CH_2)_2SH$ system, up to a final value of +0.059 V_{MSE} (100% of ferrocene in solution).

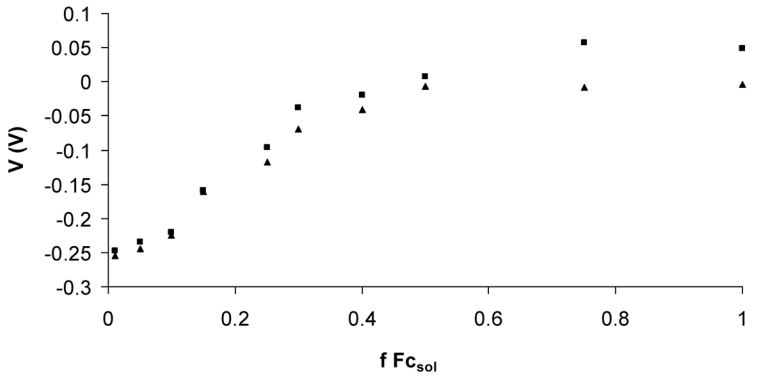

Figure 5.4 Oxidation (■) and reduction (▲) peak position versus Fc molar fraction in solution of mixed SAMs of 16-ferrocenylhexadecanethiol and 11-mercapto-1-undecanol (0.1 M $NaClO_4$; scan rate = 0.1 V/s; potential vs. V_{MSE} = +0.61 V_{NHE}).

The ferrocene component adsorbed on the gold electrode has been quantified by means of CV and the charge densities have been plotted vs. the solution fraction (Figure 5.5).

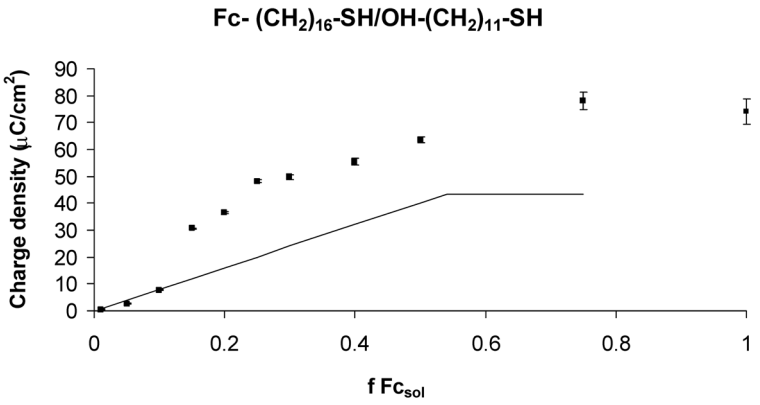

Figure 5.5 Charge density of mixed SAMs of 16-ferrocenylhexadecanethiol and 11-mercapto-1-undecanol (♦), versus Fc molar fraction in solution, and trendline (solid line).

At low concentration ($Fc(CH_2)_{16}SH$ in solution < 15%), the data are in good agreement with the trendline corresponding to a statistical composition of the layer. This suggests that other factors, such as surface roughness, are not relevant in determining the amount of electroactive component. Above this "threshold" the longer chain component is preferentially adsorbed and in this case the charge density values can not be fitted by a

single linear trend as for the 6-ferrocenylhexanethiol. Moreover, the measured charge densities are even higher than observed for 6-ferrocenylhexanethiol coadsorbed with 2-mercaptoethanol, and increase to a coverage of 4.6×10^{14} cm^{-2}, which corresponds to 1.7 times more than for a densely packed monolayer.[30] Chidsey and coworkers have already reported this phenomenon for long chain ferrocenylalkanethiols coadsorbed with n-alkanethiols with comparable chain length (15 carbon atoms) and attributed it to the possibility of the ferrocene moieties to backfold into the poorly packed alkyl chains.[19]
The advancing and the receding contact angle for monolayers adsorbed from solution with different composition are reported in Figure 5.6. The advancing contact angles and the hysteresis values (difference between advancing and receding contact angles) increase upon increase of the ferrocene fraction in solution. The former indicates a change in the surface properties of the layer towards a more hydrophobic system. The hysteresis increase suggests that the preferential adsorption of the longer component introduces a higher degree of disorder in the SAM. This behavior may be related to domain formation of the ferrocene component, leading to a decrease of the overall molecular ordering.

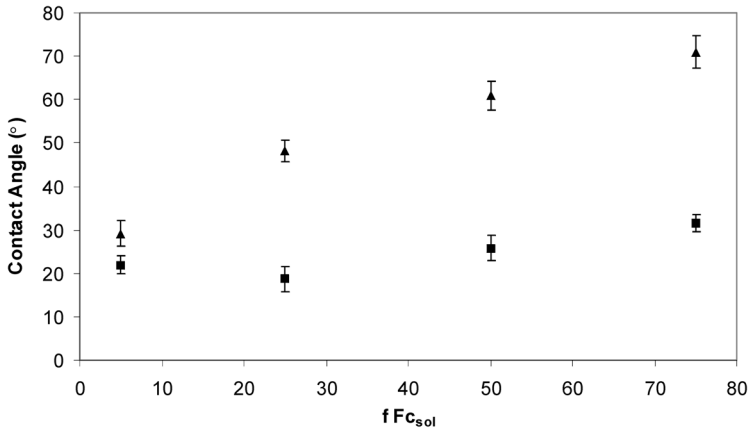

Figure 5.6 Advancing (▲) and receding (■) contact angles of mixed SAMs of 16-ferrocenylhexadecanethiol and 11-mercapto-1-undecanol versus Fc molar fraction in solution.

5.2.4 Comparison of the two systems

From a comparison of the peak positions (Table 5.1) for the two systems it is clear that for the same solution composition the peak shift occurs to a larger extent in the $Fc(CH_2)_{16}SH/HO(CH_2)_{11}SH$ system, supporting the conclusion of more strongly interacting redox centers. Even domain formation may occur at high Fc percentages.

Table 5.1 Oxidation peak position of mixed SAMs of 6-ferrocenylhexanethiol/2-mercaptoethanol and 16-ferrocenylhexadecanethiol/11-mercapto-1-undecanol (potential vs. V_{MSE} = +0.61 V_{NHE}).

Ferrocene (% in solution)	**Potential (V_{MSE}) $Fc(CH_2)_{16}SH$**	**Potential (V_{MSE}) $Fc(CH_2)_6SH$**
0	---	---
0.05	-0.234	-0.234
0.10	-0.220	-0.224
0.30	-0.038	-0.155
0.40	-0.019	-0.136

The difference in the peak position between the anodic and cathodic sweeps depends on the solution composition and below 15% it does not exceed 30 mV, as observed for the short Fc system. However, above this critical concentration it rises up to a maximum of 65 mV, for a percentage of ferrocene > 75% (Figure 5.4).

From the above reported data for the system $Fc(CH_2)_{16}SH/HO(CH_2)_{11}SH$ it is possible to define a critical ratio of the two components in solution that determines a change in the balance of the driving forces that rule the adsorption process, leading to a highly preferential adsorption of the longer component. On the basis of the plots of the charge density versus the solution composition (Figure 5.5) and of the peak position shift (Figure 5.4) this critical composition lies between 10 and 15% of ferrocene in solution. As shown by the overlap with the trendline in Figure 5.5, below 10% the layer composition is almost statistical, indicating that the layer formation is mainly ruled by the S-Au interaction, equal for both molecules. Above this composition threshold the longer component is preferentially adsorbed even in a more pronounced extent for $Fc(CH_2)_{16}SH$ than $Fc(CH_2)_6SH$. The main difference between the two systems is related to the absolute chain length of the alkyl spacer bearing the ferrocene moiety. The additional factor that rules the adsorption equilibrium is therefore correlated to the enhanced Van der Waals interactions, affecting both the first physisorption stage and increasing the role played by interchain packing, thus enhancing the tendency for the longer chain component to be adsorbed.[31]

5.3 Conclusions

In this chapter, the formation of mixed SAMs has been addressed, focussing on the chain length factor as a fundamental parameter of the adsorption process. By means of cyclic

voltammetry, the amount of the electroactive component in mixed monolayers has been investigated and related to the ratio of the adsorbates in the solutions from which the layers are formed. The contact angle data did not allow a quantitative evaluation of the layer composition, but, in combination with the electrochemical data, provided a consistent picture of the adsorption process. The use of a polar co-component in the layer formation did not affect the general trend for the longer chain component to be preferentially adsorbed, indicating favorable contributions from Van der Waals interactions between the alkyl chains. The preferential adsorption of the longer chain component is enhanced for even longer chain lengths. However, by using very low percentages (<5%) of the longer chain component in solution it is possible to obtain single isolated ferrocene functionalities embedded in a hydroxyalkanethiol background. As such, these layers are suitable for performing force spectroscopy experiments as reported in Chapter 6.

5.4 Experimental

General. 2-Mercaptoethanol and 11-mercapto-1-undecanol were purchased from Aldrich and used without any further purification. 6-Ferrocenylhexanethiol and 16-ferrocenyl-hexadecanethiol were synthesized according to literature procedures.[19,23b] All solvents used in monolayer preparation were of p.a. grade.

Gold Substrates. Gold substrates were prepared by evaporating 200 nm of gold on a glass slide of 25 mm diameter with a 2 nm titanium layer for adhesion. Just before use, the substrates were cleaned in an oxygen plasma reactor for 5 min and the resulting oxide layer was removed by immersing the substrates for 10 min in EtOH.[32]

Monolayer Preparation. All glassware used to prepare monolayers was immersed in piraña solution (conc. H_2SO_4 and 33% H_2O_2 in a 3:1 ratio). **(Warning: piraña should be handled with caution; it has detonated unexpectedly)**.[33] Next, the glassware was rinsed with large amounts of Milli-Q water. Monolayers were prepared by immersing the gold substrates in a 1 mM solution of adsorbate (total concentration of both components) in ethanol at ambient conditions (20 ± 3 ºC) for 16 h. The samples were removed from the solution and rinsed with large amounts of dichloromethane, ethanol, and water to remove any physisorbed material.

Electrochemistry. Electrochemical measurements were performed with an AUTOLAB PGSTAT10, in a custom built electrochemical cell equipped with a platinum counter electrode, a mercury sulfate reference electrode (V_{MSE} = +0.61 V_{NHE}) and a screw cap holding the gold working electrode (area exposed to the solution = 0.44 cm^2). The cyclic voltammograms were performed in 0.1 M $NaClO_4$ at scan rates of 0.1, 0.2, and 0.5 V/s.

The charge values for the electroactive species adsorbed on the electrode and the corresponding standard deviations were calculated by averaging the redox peaks at different scan rates.

Contact Angle Goniometry (CA). The advancing and receding contact angles with Milli-Q water were measured on a Krüss G10 Contact Angle Measuring Instrument, equipped with a CCD camera. Measurements with a drop of water, the volume of which was gradually increased (advancing CA) and then decreased (receding CA), were repeated on three different sites of the sample. For each adsorbate composition three samples were measured for a total of 12 drops, of which the average values and the corresponding errors are reported.

5.5 References and notes

[1] Chailapakul, O.; Sun, L.; Xu, C.; Crooks, R. M. *J. Am. Chem. Soc.* **1993**, *115*, 12459-12467.

[2] Ulman, A. *Introduction to Thin Organic Films: From Langmuir-Blodgett to Self-Assembly*; Academic Press: Boston, MA, 1991.

[3] a) Dubois, L. H.; Nuzzo, R. G. *Ann. Rev. Phys. Chem.* **1992**, *43*, 437-463. b) Allara, D. L. *Biosens. Bioelectron.* **1995**, *10*, 771-783. c) Bishop, A. R.; Nuzzo, R. G. *Curr. Opin. Coll. Interface Sci.* **1996**, *1*, 127-136.

[4] a) Ulman, A. *Chem. Rev.* **1996**, *96*, 1533-1554. b) Ulman, A. *Characterization of Organic Thin Films*; Butterworth-Heinemann: Boston, MA, 1995. c) Rubinstein, I.; Steinberg, S.; Tor, Y.; Shanzer, A.; Sagiv, J. *Nature* **1988**, *332*, 426-429.

[5] Nuzzo, R. G.; Allara, D. L. *J. Am. Chem. Soc.* **1983**, *105*, 4481-4483.

[6] Camillone III, N.; Leung, T. Y. B.; Schwartz, P.; Eisenberger, P.; Scoles, G. *Langmuir* **1996**, *12*, 2737-2746.

[7] Poirier, G. E.; Pylant, E. D. *Science* **1996**, *272*, 1145-1148.

[8] Yamada, R.; Uosaki, K. *Langmuir* **1997**, *13*, 5218-5221.

[9] Tamada, K.; Hara, M.; Sasabe, H.; Knoll, W. *Langmuir* **1997**, *13*, 1558-1566.

[10] a) Bain, C. D.; Whitesides, G. M. *J. Am. Chem. Soc.* **1988**, *110*, 6560-6561. b) Bain, C. D.; Whitesides, G. M. *J. Am. Chem. Soc.* **1988**, *110*, 3665-3666. c) Whitesides, G. M.; Laibinis, P. E. *Langmuir* **1990**, *6*, 87-96. d) Pale-Grosdemange, C.; Simon, E. S.; Prime, K. L.; Whitesides, G. M. *J. Am. Chem. Soc.* **1991**, *113*, 12-20. e) Laibinis, P. E.; Fox, M. A.; Folkers, J. P; Whitesides, G. M.; Deutch, J. *Langmuir* **1991**, *7*, 3167-3173. f) Bertilsson, L.; Liedberg, B. *Langmuir*, **1993**, *9*, 141-149. g) Folkers, J. P.; Laibinis, P. E.; Whitesides, G. M.; Deutch, J. *J. Phys. Chem.* **1994**, *98*, 563-571.

[11] Kakiuchi, T.; Iida, M.; Gon, N.; Hobara, D.; Imabayashi, S.-I.; Niki, K. *Langmuir* **2001**, *17*, 1599-1603.
[12] a) Bain, C. D.; Whitesides, G. M. *J. Am. Chem. Soc.* **1989**, *111*, 7164-7175. b) Labinis, P. E.; Nuzzo, R. G.; Whitesides, G. M. *J. Phys. Chem.* **1992**, *96*, 5097-5105.
[13] Folkers, J. P.; Laibinis, P. E.; Whitesides, G. M. *Langmuir* **1992**, *8*, 1330-1334.
[14] Offord, D. A.; John, C. M.; Linford, M. R.; Griffin, J. H. *Langmuir* **1994**, *10*, 883-889.
[15] Hobara, D.; Ota, M.; Imabayashi, S.-I.; Niki, K.; Kakiuchi, T. *J. Electroanal. Chem.* **1998**, *444*, 113-119.
[16] a) Chen, S.; Li, L.; Boozer, C. L.; Jiang, S. *J. Phys. Chem. B* **2001**, *105*, 2975-2980. b) Smith, R. K.; Reed S. M.; Lewis, P. A.; Monnell, J. D.; Clegg, R. S.; Kelly, K. F.; Bumm, L. A.; Hutchinson, J. E.; Weiss, P. S. *J. Phys. Chem. B* **2001**, *105*, 1119-1122. c) Stranick, S. J.; Parikh, A. N.; Tao, Y.-T.; Allara, D. L.; Weiss, P. S. *J. Phys. Chem.* **1994**, *98*, 7636-7646. d) Stranick, S. J.; Atre, S. V.; Parikh, A. N.; Wood, M. C.; Allara, D. L.; Winograd, N.; Weiss, P. S. *Nanotechnology* **1996**, *7*, 438-442.
[17] Chen, S.; Li, L.; Boozer, C. L.; Jiang, S. *Langmuir* **2000**, *16*, 9287-9293.
[18] Nuzzo, R. G.; Zegarski, B. R.; Dubois, L. H. *J. Am. Chem. Soc.* **1987**, *109*, 733-740.
[19] Chidsey, E. D.; Bertozzi, C. R.; Putwinski, T. M.; Mujsce, A. M. *J. Am. Chem. Soc.* **1990**, *112*, 4301-4306.
[20] Smalley, J. F.; Feldberg, S. W.; Chidsey, C. E. D.; Linford, M. R.; Newton, M. D.; Liu, Y.-P. *J. Phys. Chem.* **1995**, *99*, 13141-13149.
[21] Sabapathy, R. C.; Bhattacharyya, S.; Leavy, M. C.; Cleland, W. E.; Hussey, C. L. *Langmuir* **1998**, *14*, 124-136.
[22] Sek. S.; Misicka, A.; Bilewicz, R. *J. Phys. Chem. B* **2000**, *104*, 5399-5402.
[23] a) Creager, S. E.; Rowe, G. K. *Anal. Chim. Acta* **1991**, *246*, 233-239. b) Creager, S. E.; Rowe, G. K. *J. Electroanal. Chem.* **1994**, *370*, 203-211. c) Rowe, G. K.; Creager, S. E. *Langmuir* **1991**, *7*, 2307-2312. d) Weber, K; Hockett, L.; Creager, S. E. *J. Phys. Chem. B* **1997**, *101*, 8286-8291. e) Sumner, J. J.; Weber, K. S.; Hockett, L. A.; Creager, S. E. *J. Phys. Chem. B* **2000**, *104*, 7449-7454.
[24] a) Zapotoczny, S.; Auletta, T.; De Jong, M. R.; Schönherr, H.; Huskens, J.; Van Veggel, F. C. J. M.; Reinhoudt, D. N.; Vancso, G. J. *Langmuir* **2002**, *18*, 6988-6994. b) Schönherr, H.; Beulen, M. W. J.; Bügler, J.; Huskens, J.; Van Veggel, F. C. J. M.; Reinhoudt, D. N.; Vancso, G. J. *J. Am. Chem. Soc.* **2000**, *122*, 4963-4967. c) Bügler, J.; Beulen, M. W. J.; Lammerink, B.; Geurts, F. A. J.; Biemond, E. M. E. F.; Van Leerdam, K. G. C.; Van Veggel, F. C. J. M.; Engberts, J. F. J.; Reinhoudt, D. N. *Langmuir* **1998**, *14*, 6424-6429. d) Beulen, M. W. J.; Bügler, J.; De Jong, M. R.; Lammerink, B.;

Huskens, J.; Schönherr, H.; Vancso, G. J.; Boukamp, B. A.; Wieder, H.; Offenhauser, A.; Knoll, W.; Van Veggel, F. C. J. M.; Reinhoudt, D. N. *Chem. Eur. J.* **2000**, *6*, 1176-1183.

[25] Bard, A. J.; Faulkner, L. R. *Electrochemical Methods: Fundamentals and Applications*; John Wiley & Sons: New York, 1980; p.522.

[26] a) Chidsey, C. E. D.; Liu, G.-Y.; Rowntree, P.; Scoles, G. *J. Chem. Phys.* **1989**, *91*, 4421-4423. b) Camillone III, N.; Chidsey, C. E. D.; Liu, G.-Y.; Putvinki, T. M.; Scoles, G. *J. Chem. Phys.* **1991**, *94*, 8493-8502. c) Fenter, P.; Eisenberger, P.; Liang, K. S. *Phys. Rev. Lett.* **1993**, *70*, 2447-2450. d) Widrig, C. A.; Alves, C. A.; Porter, M. D. *J. Am. Chem. Soc.* **1991**, *113*, 2805-2810.

[27] Seiler, P.; Dunitz, J. D. *Acta Crystallogr.* **1979**, *B35*, 1068-1074.

[28] a) Rodriguez, J. F.; Mebrahtu, T.; Soriaga, M. P. *J. Electroanal. Chem.* **1987**, *233*, 283-289. b) Schneider, T. W.; Buttry, D. A. *J. Am. Chem. Soc.* **1993**, *115*, 12391-12397. c) Walczak, M. M.; Alves, C. A.; Lamp, B. D.; Porter, M. D. *J. Electroanal. Chem.* **1995**, *396*, 103-114.

[29] Sato, Y.; Uosaki, K. *Redox Mechanisms and Interfacial Properties of Molecules of Biological Importance*; The Electrochemical Society: Pennington, 1993, p 299-311.

[30] A densely packed monolayer is a SAM in which all the ferrocene moieties are well packed and no more can fit due to steric interactions. Even if the headgroups are well packed, a certain degree of disorder can be found in the underlying alkyl chains, due to the difference in size between the ferrocene moieties and the alkyl chains, as shown in the calculation for the trendline of the charge densities vs. the solution composition.

[31] These results are not in contradiction with the work of Chidsey and co-workers[19] where the increase of chain length of both components (ferrocenylalkanethiol and unsubstituted thiol) did not affect the ferrocene surface coverage. In that case, both components had a comparable chain length, therefore, no discrimination could be expected on the basis of different Van der Waals interaction.

[32] Ron, H.; Rubinstein, I. *Langmuir* **1994**, *10*, 4566-4573.

[33] a) Dobbs, D. A.; Bergman, R. G.; Theopold, K. H. *Chem. Eng. News* **1990**, 68, (17), 2. b) Wnuk, T. *Chem. Eng. News* **1990**, 68 (26), 2. c) Matlow, S. L. *Chem. Eng. News* **1990**, 68, (30), 2.

Chapter 6

Force Spectroscopy of β-Cyclodextrin Host-Guest Complexes Probed under Thermodynamic Equilibrium*

The rupture forces of individual host-guest complexes between a surface-confined β-cyclodextrin derivative (β-CD) and AFM tip-immobilized guests were measured in aqueous medium by atomic force microscope (AFM) dynamic single molecule force spectroscopy. The interactions between a thiol-derivatized ferrocene guest immobilized in mixed self-assembled monolayers (SAMs) with 2-mercaptoethanol on gold-coated AFM tips and the heptathioether β-CD SAM on atomically flat Au(111) substrates were probed. Depending on the concentration of ferrocene moieties on the AFM tip, multiple or predominantly single pull-off events were observed. A statistical analysis showed a periodic distribution of force with a force quantum of 55 ± 10 pN, independent of the number of host-guest pairs, of the unloading rate, and of the spacer length, which is attributed to the rupture of a single host-guest complex. These results indicate that the host-guest complex rupture forces were probed under conditions of thermodynamic equilibrium. Exploiting the same thiol chemistry, an anilyl, a toluidyl, a tert-butylphenyl, and an adamantyl derivative were immobilized onto AFM tips. Force displacement curves showed the characteristic multiple pull-off events in all cases and the statistical analysis showed periodic distributions of the force values, with force quanta of 39 ± 15, 45 ± 15, 89 ± 19, and 102 ± 25 pN, respectively. The force values follow the same trend as the complexation constants measured for model guest compounds in solution or on β-CD monolayers, as probed by microcalorimetry and surface plasmon resonance spectroscopy, respectively. A descriptive model has been developed to quantitatively correlate the pull-off force values with the ΔG^{o} of the complexes, based on the evaluation of the energy potential landscape of tip-surface interaction.

---

* Part of this chapter has been published in: Zapotoczny, S.; Auletta, T.; De Jong, M. R.; Schönherr, H.; Huskens, J.; Van Veggel, F. C. J. M.; Reinhoudt, D. N.; Vancso, G. J. *Langmuir* **2002**, *18*, 6988-6994.

6.1 Introduction

Inspired by the lock and key principle in nature,[1,2,3] the binding and unbinding processes of host-guest complexes, as well as assemblies based on hydrogen-bonding interactions, are located at the heart of supramolecular chemistry. Based on many *cooperative*, weak, reversible, and sometimes short-lived interactions, self-assembled structures can be thermodynamically stable or may even become kinetically stable, depending on the number of interactions. Outstanding examples are supramolecular capsules,[4,5] rosette structures,[6] and non-covalent supramolecular polymers.[7]

β-cyclodextrin (β-CD) is a cyclic sugar formed by seven glucose units linked via α-1-4 glycosidic bonds, and is characterized by a polar outer surface and an apolar cavity. It is able to form inclusion complexes in aqueous solutions with a variety of organic molecules, both neutral and charged.[8] The driving force that rules the recognition process is mainly due to hydrophobic interactions, even if other effects such as Van der Waals forces, hydrogen bond formation and release of water molecules from the apolar cavity into the bulk solution also contribute to the host–guest complex stability.[9]

A fundamental understanding of the behavior of assemblies, such as non-covalent supramolecular polymers, in situations of both thermodynamic equilibrium and non-equilibrium is required in order to develop materials with predictable properties.[10] Non-equilibrium behavior is particularly interesting under the influence of external forces (vide infra).

Expanding on the rapid technical development of ultrasensitive force probe techniques,[11,12,13] the study of host-guest chemistry at the fundamental level of individual molecules has become possible.[14] Early atomic force microscopy (AFM) work was focused on DNA-DNA interactions[15] and the streptavidin-biotin system.[16] Following the initial reports many other systems were described.[17,18,19,20] The interpretation of the corresponding data and the relation to known thermodynamic data remained inconclusive since Evans and co-workers have only later shown that single molecule rupture forces for systems in far-from-equilibrium situations are highly unloading rate-dependent.[21] Under these conditions, the theoretically predicted and experimentally observed rupture forces increase with increasing unloading rate.[22] In the meantime many groups have independently validated this rate dependence.[23]

Expanding on the theory of Kramers,[24] Evans *et al.* developed a theoretical framework for forced unbinding of host-guest complexes.[21,22,25,26] When a force is exerted on a "weak" bond, the lifetime of this bond is reduced. This reduction of the lifetime is directly related to the unloading rate. Owing to the reciprocal relationship of bond

lifetime and bond strength (under the applied force), "weak" bonds of host-guest complexes, such as biotin-streptavidin complexes, increase in measured rupture force and decrease in lifetime with increasing unloading rate. In single-molecule force spectroscopy experiments, the strength of the bond can be obtained by determining the most probable rupture force F*. From the dependence of the most probable rupture force on the logarithm of the unloading rate r, the barriers of the unbinding pathway can be determined. [21,22] F* can be expressed as a function of the rate constant for thermal decomplexation k_{off} and the force F_0, which defines the slope of the unloading rate dependent regime, as:[21,22]

Equation 6.1 $$F^* = F_0 \ln(r/F_0 k_{off})$$

This theory only takes dissociation into account, and is therefore especially suited for systems where spontaneous dissociation is negligible. Host-guest complexes of small molecules with reversible supramolecular interactions are in sharp contrast to these above systems,[5,27] since their association and dissociation are, at the same temperature, faster than the timescale of the experimental technique (for AFM ~ 10^{-3} - 10^{-4} s).[25] For example in hydrogen-bonded systems with a variable number of donors and acceptors, the range of association constants (k_a) measured for various pairs ranges from ≤ 10^2 M^{-1} to 10^5 M^{-1}.[28] Assuming a diffusion-limited complexation with rate constants (k_c) of ~ 10^8 M^{-1} s^{-1}, typical lifetimes on the order of 1 μs to 1 ms are obtained.

Experimental studies of single molecule force spectroscopy on systems that are in thermodynamic equilibrium have been reported. For instance, polymers and biopolymers have been stretched to non-equilibrium conformations under near-equilibrium conditions.[29] However, studies on molecular unbinding events and host-guest complex rupture forces under these conditions are scarce.[30,31]

Previous studies in our group have been carried out on the complexation behavior of ferrocene moieties, attached to a $(CH_2)_6$ spacer, with a β-cyclodextrin host immobilized in SAMs as determined by dynamic molecule force spectroscopy measurements using AFM (Scheme 6.1).[27] The observed unloading rate[32] independence of the quantized host-guest complex rupture force of 56 ± 10 pN was attributed to thermodynamic equilibrium at all data points measured during the experiment. For this particular β-CD system, the complexation constant (k_a) measured for the model compound ferrocenecarboxylic acid is 2400 M^{-1}.[33,34] Hence the unbinding occurs on a timescale of 1 μs, while the AFM timescale can be estimated to be 100 - 1000 μs.[25,27] Consequently, the ferrocene moieties can decomplex and rebind spontaneously many times on the AFM timescale as long as

the strain energy in the bound state is overcome by the free energy gain upon complexation. This strain energy may in part be attributed to a stretching of the $(CH_2)_6$ spacer of the ferrocene thiol molecule.

The work presented in this chapter is a systematic study of the concentration, unloading rate dependence, and spacer length of single host-guest complex rupture forces between a new β-cyclodextrin adsorbate[35] and several surface-confined guest molecules adsorbed in mixed SAMs onto AFM gold-coated tips, as depicted in Scheme 6.1. Correlation with thermodynamic data obtained with model guests in solution will be discussed as well.

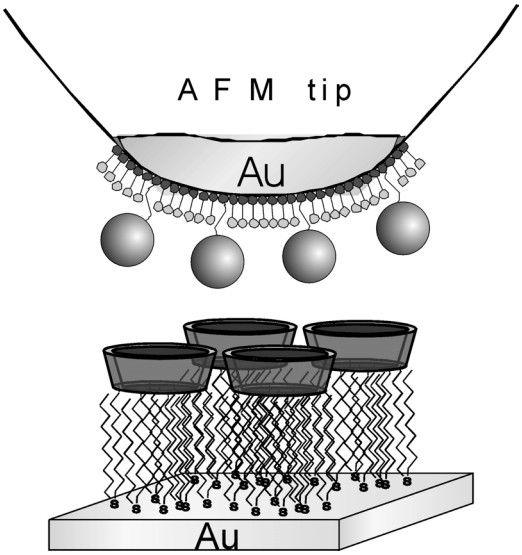

Scheme 6.1 Schematic representation (not to scale) of AFM-based single molecule force spectroscopy of guests immobilized in a hydroxyl-terminated SAM on an AFM tip and a SAM of a β-cyclodextrin heptathioether adsorbate on Au(111).

6.2 Determination of the dissociation force of individual host-guest complexes and their dependence on guest adsorbate chain length

6.2.1 General

All adsorbates **1**-**7** (Chart 6.1 and Chart 6.2) have been synthesized according to literature procedures.[34,36,44,45] Self-assembled monolayers of **1** on gold surfaces have been prepared from 0.1 mM solutions in $CHCl_2$/EtOH (3/1), for 16 h at 60º C.[34,36]

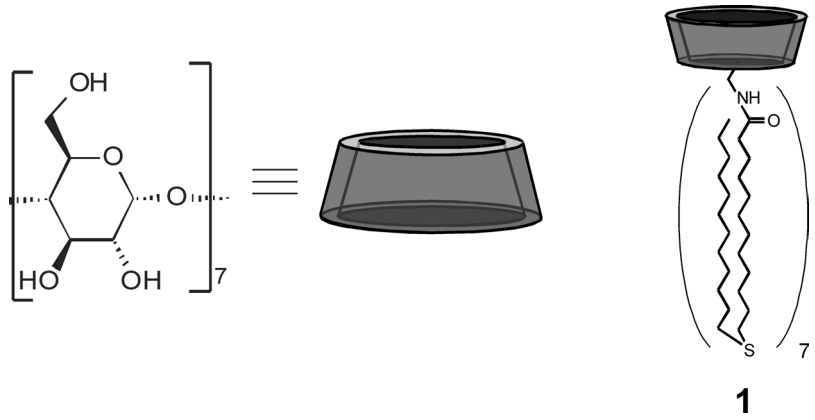

Chart 6.1 Chemical structure of the β-cyclodextrin and of adsorbate **1**.

Mixed SAMs on gold-modified AFM tips of adsorbates **2**-**7** (0.2% and 1%) and 2-mercaptoethanol have been prepared from 1 mM (total thiol concentration) solutions in ethanol, for 16 h at r.t. Adsorbate **3** has also been coadsorbed onto AFM gold-coated tips with 11-mercapto-1-undecanol, following the same experimental procedure. Characterization of mixed SAMs of adsorbates **2**-**7** on flat gold has been reported previously (for adsorbates **2** and **3** see also Chapter 5).[36,45]

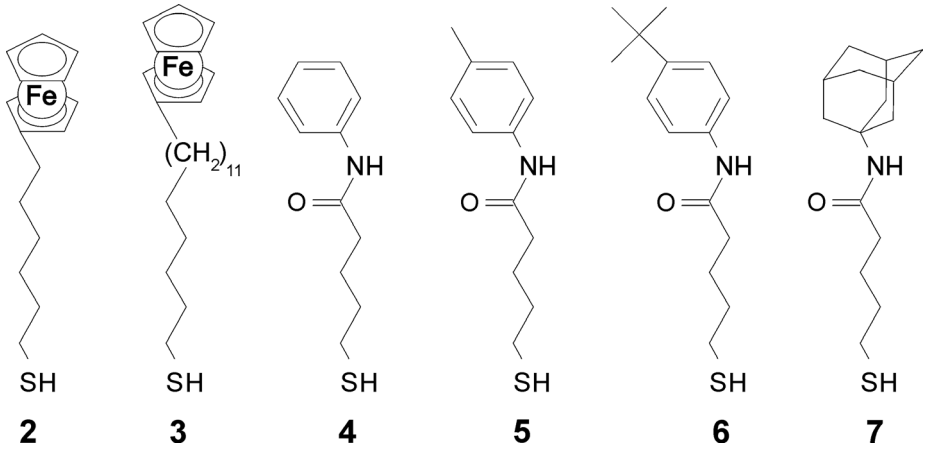

Chart 6.2 Structure of the adsorbates **2**-**7**.

6.2.2 Force-displacement (f-d) curves

In force-displacement (f-d) measurements between AFM tips functionalized with ferrocenylthiols **2** or **3** and SAMs of the β-CD receptor **1**, rupture events were detected as

shown in Figure 6.1. The f-d curves obtained using tips with 1% of **2** showed *multiple* pull-off events upon retraction of the sample from the tip, while a dilution of the guest molecule in the 2-mercaptoethanol SAM down to 0.2% led to a significant reduction of the number of pull-off events. In several cases, single pull-off events were observed using very sharp tips (Figure 6.1b).

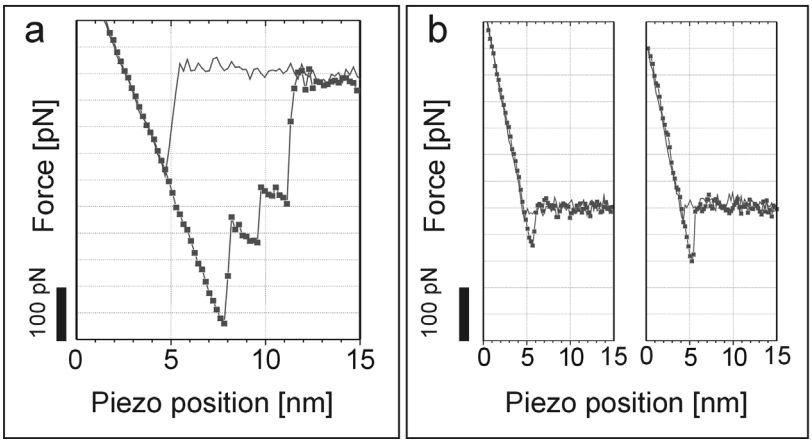

Figure 6.1 Force-displacement curves recorded in Milli-Q water between SAMs of **1** on Au(111) and ferrocene modified tips: (a) 1% of **2** in 2-mercaptoethanol, (b) 0.2% of **2** in 2-mercaptoethanol.

The interpretation of the experiments is based on the assumption that the individually resolved pull-off events can be attributed to specific host-guest complex rupture events (see Sections 6.2.3 and 6.2.4). More than 15 independent data sets were analyzed and the measured tip displacements corresponding to the pull-off events were translated into forces, using independently determined AFM cantilever spring constants. All pull-off forces determined from individually resolved events were collected in bins with a bin size of 8 pN, corresponding to the experimental error of the force values, and presented in histograms. Fast Fourier transform (FFT) smoothing of the histograms shows a periodic distribution of forces, as shown in Figure 6.2 and 6.3 and summarized in Table 6.1.

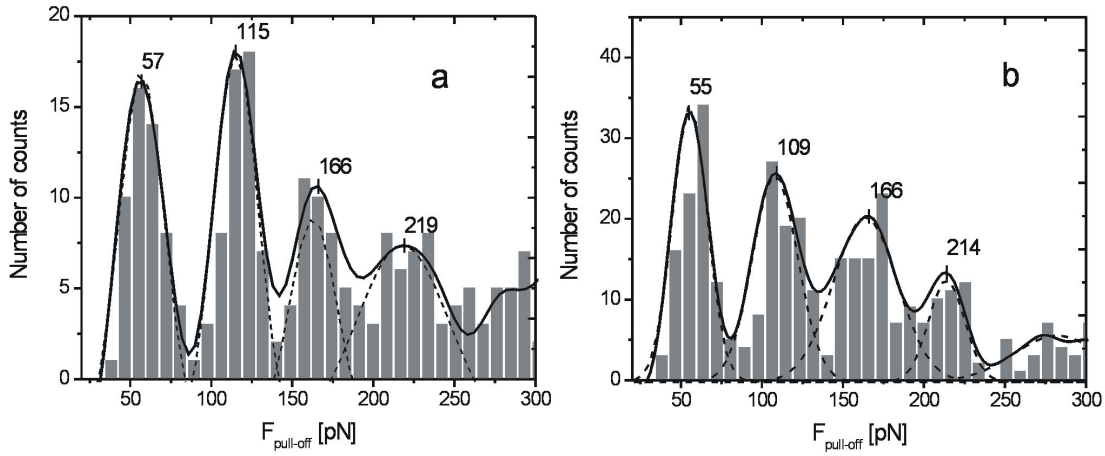

Figure 6.2 Histograms of pull-off forces for the systems containing on the tip: (a) 1% of **2** in 2-mercaptoethanol, (b) 0.2% of **2** in 2-mercaptoethanol. The solid lines represent the FFT-smoothed histograms; Gaussian curves fitted to the smoothed histograms are drawn as dashed lines.

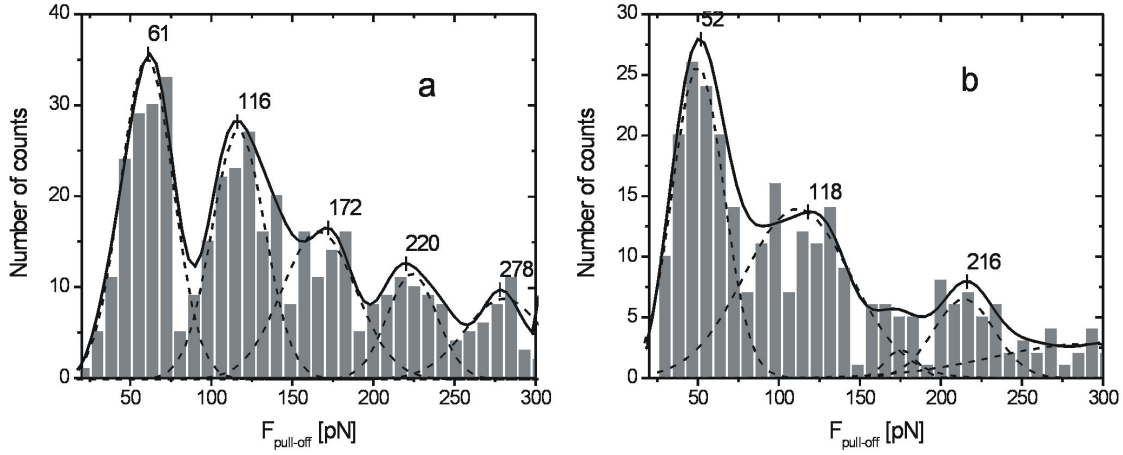

Figure 6.3 Histograms of pull-off forces for the systems containing on the tip: (a) 0.2% of **3** in 2-mercaptoethanol, (b) 0.2% of **3** in 11-mercapto-1-undecanol. The solid lines represent the FFT-smoothed histograms; Gaussian curves fitted to the smoothed histograms are drawn as dashed lines.

Table 6.1 The single host-guest complex rupture forces determined from the histograms of the different systems studied and widths of the Gaussian peaks fitted to the FFT-smoothed histograms.

System	Quantized force $F_{pull\text{-}off}$ [pN]	Peak width (Gaussian) [pN] σ_1	σ_2	σ_3
2 (1.0%) – 2-mercaptoethanol	**56** ± 10[1)]	27	27	31
2 (0.5%) – 2-mercaptoethanol	**56** ± 10[1)]	26	28	33
2 (0.2%) – 2-mercaptoethanol	**55** ± 10[1)]	21	28	39
3 (0.2%) - 2-mercaptoethanol	**59** ± 10[1)]	32	33	45
3 (0.2%) – 11-mercapto-1-undecanol	**55** ± 15[2)]	34	68	-[2)]

[1)] The mean value was determined based on the first three maxima in the histogram. The error was estimated taking into account the uncertainty of the determination of the spring constant (15%) and the sensitivity of the photodetector (3%).
[2)] The value was determined based on the first two maxima in the histogram since there was no well-pronounced third peak present. In this case the estimated error was increased due to the poorer statistics of the histogram.

The first peak represents the force associated with the rupture of a single host-guest complex between the tip-immobilized guest and the β-CD SAM. Other peaks are attributed to the simultaneous decomplexation of several host-guest complexes and, since no other maxima were observed, these peaks are integer multiples of the rupture force "quantum", here $F_{pull\text{-}off}$ = 55 ± 10 pN. The value of the force quantum is identical to the single host-guest rupture force of 56 ± 10 pN found previously for a very similar β-CD adsorbate.[27,37] The presence of multiple peaks in the histograms is observed for both concentrations (0.2% and 1%) of **2** on the tip. The peak positions indicated in Figure 6.2 are the same for both concentrations of ferrocene on the tip within the experimental error.
In Figure 6.2 it can be observed that the height of the peak attributed to two unbinding events is larger than the peak attributed to single events for 1% ferrocene, while for 0.2% ferrocene the peak for single unbinding events is the predominant peak. Thus, the number of resolved pull-off events and hence interacting β-CD and ferrocene moieties qualitatively correlates with the composition of the SAM on the functionalized AFM tip.[38,45]
The force quantum did not depend on the unloading rate over the experimentally accessible range of nearly 3 decades (Figure 6.4) for the system **2** coadsorbed with 2-mercaptoethanol.[32] Based on Equation 6.1 the unloading rate-dependent regime, calculated assuming $k_{off} = 10^5\ s^{-1}$ and $F_0 = F_{pull\text{-}off}$, starts only at rates > 10^7 pN/s, as

shown in Figure 6.4. Linear regression analysis yields a negligible slope. This result agrees very well with the previously reported unloadingrate independence for a similar β-CD-ferrocene system.[27]

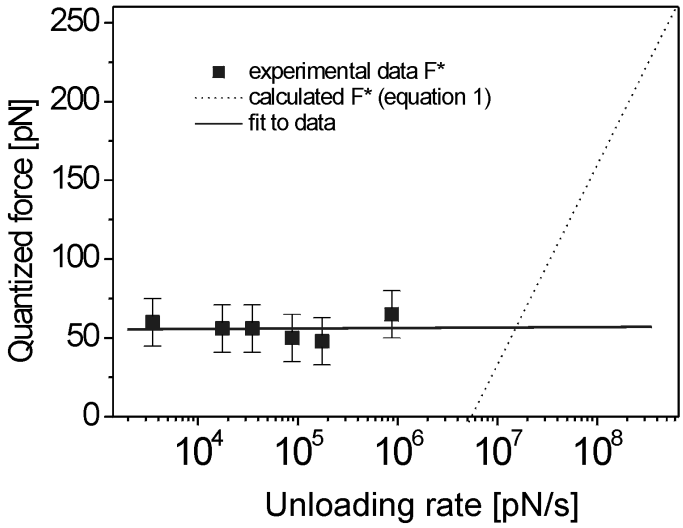

Figure 6.4 Unloading rate dependence of the quantized rupture force for **2** (0.2%) in 2-mercaptoethanol, linear regression analysis,[32] and anticipated unloading rate dependence calculated based on Equation 6.1.

6.2.3 Specific vs. non-specific interactions

The presence of multiple pull-off events in the f-d curves and the quantized force obtained in the histograms contrasts with the results obtained using AFM tips functionalized with *pure* 2-mercaptoethanol SAMs and β-CD SAMs, which show exclusively single pull-off events. Their histograms show a single broad distribution of pull-off forces with a mean force value F_{mean} = 230 pN (Figure 6.5). The absence of multiple pull-off events in the blank experiments without guest molecules and without host molecules (data not shown) proofs that the presence of both (diluted) guest *and* β-CD host is necessary to observe multiple pull-off events.

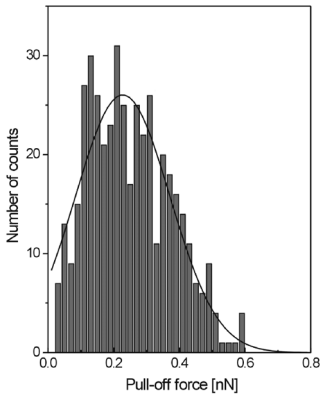

Figure 6.5 Histogram of the pull-off forces between a β-CD SAM and a neat 2-mercaptoethanol-modified tip.

In the case of multiple pull-off events in AFM-based force spectroscopy experiments, it has been argued previously that the early events are likely convoluted by the presence of non-specific adhesion forces.[16] However, in our experiments, a clear trend in the histograms that could be related to significant non-specific adhesion forces has not been observed. As shown in Figure 6.6, the *same* quantized rupture force $F_{pull\text{-}off}$ is observed when exclusively the last pull-off event for each f-d curve is analyzed. The same holds when exclusively the early pull-off events are taken. Thus, we conclude that possible non-specific adhesion forces, which may convolute the individually resolved pull-off events, must be negligible.

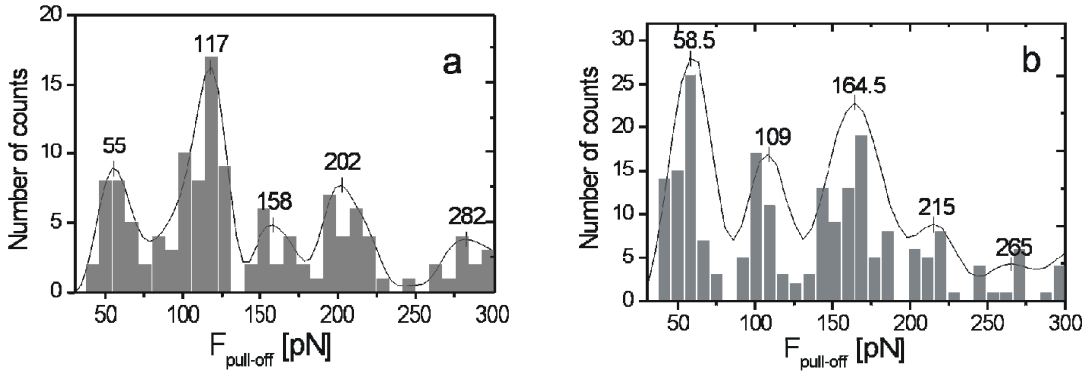

Figure 6.6 Histograms of pull-off forces for the systems containing 0.2% of **2** in 2-mercaptoethanol. Histograms are based on: (a) the last pull-off events, (b) all but the last pull-off events. The solid lines represent the FFT-smoothed histograms.

This above result seems to conflict with the pull-off forces measured between 2-mercaptoethanol-functionalized tips and SAMs of β-CD. This may be attributed to a difference of the solvent exclusion.[39] For the neat 2-mercaptoethanol SAM, the surfaces can be assumed to be in intimate contact during the repulsive part of the force-displacement curve, while the ferrocene molecules may support the load partially and may result in solvated surfaces of the contacting SAMs. Recent simulation results imply that loads, which are typical for our experiments, may indeed be supported by similar molecules.[40]

When a 100 μM aqueous solution of the more strongly binding guest 1-anilino-naphthalene-8-sulfonate (1,8-ANS) was injected into the cell, the number of pull-off events decreased markedly as observed previously.[27] This reversible effect can be attributed to the partial blocking of the β-CD cavities due to the competition between the tip-immobilized ferrocene moieties and 1,8-ANS in solution for binding in the β-CD host sites.[27,41] 1,8-ANS is known to bind strongly to SAMs of β-CD derivatives[46] and since the process is reversible, this indicates that the receptor sites are blocked to a large extent by 1,8-ANS.[27,46] Moreover, the pull-off forces (single and multiple events) measured in the presence of 1,8-ANS showed the same force quantum.

From the above reported results it can be concluded that the characteristic f-d curves observed between a guest-functionalized AFM tip, independent of the concentration, and β-CD SAMs is related to the dissociation of host-guest complexes. Moreover the pull-off force distribution with quantized maxima and a well distinct force quantum is *directly* linked to the presence of the interacting molecular pairs.

6.2.4 Chain length effect

The effect of the spacer length of the ferrocene guest molecule was addressed in a separate set of force spectroscopy experiments. As shown in the corresponding histograms (Figure 6.3), the force quantum remains unchanged for different spacer lengths and spacer length differences between ferrocene and hydroxyl-terminated thiol adsorbates. However, the peaks for **3** show significant broadening compared to the experiments with shorter spacers (see also Table 6.1). This phenomenon can be attributed to a differentiation of the decomplexation pathways compared to the case of **2**, related to the presence of a longer spacer, which increases the number of accessible host cavities in the β-CD SAM. In addition, partial stretching of the alkyl spacer itself, with subsequent conformational changes, cannot be excluded a priori.

In accordance with the results obtained for adsorbate **2**, in the case of AFM tips modified with mixed SAMs of **3** no unloading rate dependence was observed, indicating a situation of thermodynamic equilibrium, where the most probable rupture force and the lifetime of the bond do *not* depend on the unloading rate.

The above analysis leads to the conclusion that the quantized rupture forces between β-CD and SAMs of **3** can be once more attributed to specific host-guest complexes, as shown in Table 6.1 and Figure 6.3. The characteristics of length and stiffness of the spacer neither lead to any change in the intrinsic force quantum nor influence the unloading rate independence, as described in Section 6.3.2 and in the Appendix.

6.3 Relation between pull-off forces and thermodynamics for different host-guest motifs

6.3.1 Experimental comparison of pull-off forces with thermodynamic data

As shown above, the force values obtained by force spectroscopy experiments are related exclusively to specific host-guest interactions and do not depend on spacer length, structure, and concentration on the tip. Four different thiol-modified guests, **4**, **5**, **6**, and **7** (Chart 6.2) were synthesized in order to investigate how changes in the host-guest motif would affect the rupture force. Force displacement curves for guest concentrations of 0.2% and 1% on the tip showed in all cases the characteristic multiple pull-off events (Figure 6.7 left).

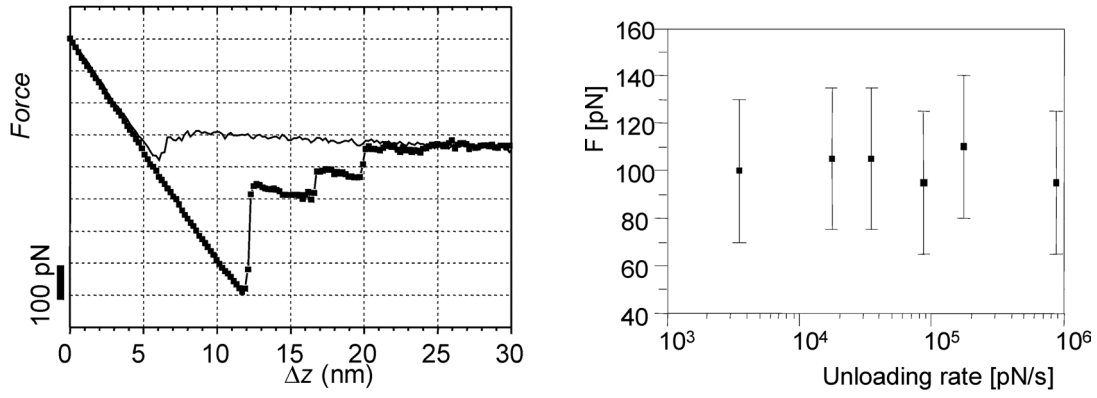

Figure 6.7 Representative force-distance curve for the interaction of a tip covered with a mixed SAM of 1% of **7** and 2-mercaptoethanol with a SAM of **1** (left), and unloading rate dependence (right).

The histograms of the pull-off forces between tips functionalized with **4**, **5, 6** or **7**, were obtained as described above for **2** and **3**, and the force quanta values are 39 ± 15, 45 ± 15, 89 ± 19, and 102 ± 25 pN, respectively (Figure 6.8). As seen for **2** and **3,** the quantized pull-off force appears to be independent of the guest concentration on the tip.

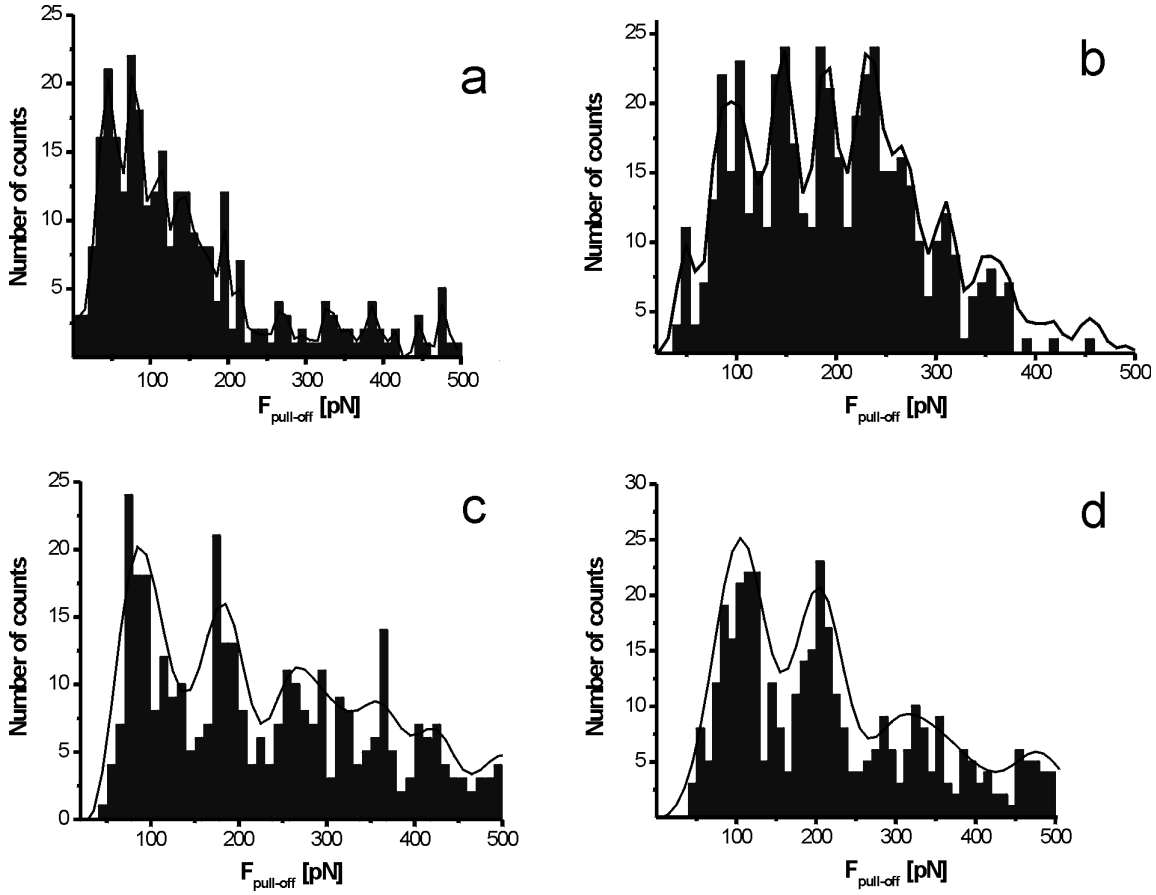

Figure 6.8 Histograms of pull-off forces for the systems containing 1% of **4** (a), 1% of **5** (b), 1% of **6** (c), and 1% of **7** (d) and 2-mercaptoethanol with SAMs of **1**. The solid line represents the FFT-smoothed histograms.

As shown above for **2** and **3**, the unloading rate was changed over several orders of magnitude for tips covered with monolayers with 1% of guest. Again the quantized force was unaffected by the unloading rate for any of the guests, even for the strongest guest **7**, as shown in Figure 6.7 right.

The initially attempted correlation of rupture forces and thermodynamic quantities[16] must be regarded with reservation due to the pronounced dependence of the rupture forces on the unloading rate because those systems were studied under far-from-equilibrium

conditions.[22] In contrast, the results reported here, which show no dependence on the unloading rate, open the possibility to investigate the relation between rupture forces and thermodynamic quantities, such as the Gibbs free energy of binding.

Isothermal titration calorimetry (ITC) and surface plasmon resonance (SPR) spectroscopy have been employed to evaluate the thermodynamics of complex formation between compounds **8-12** (Chart 6.3), model systems for **2-7**, and β-cyclodextrin derivatives in solution and on surfaces. The experimental data obtained by these two independent techniques show excellent agreement, as shown in Table 6.2. This allows us to extrapolate from the ITC results the binding parameters on surfaces for compounds **9** and **10** for which SPR experiments did not allow direct evaluation of the complexation constants on SAMs of **1**, due to the poor solubilities and weak interactions.

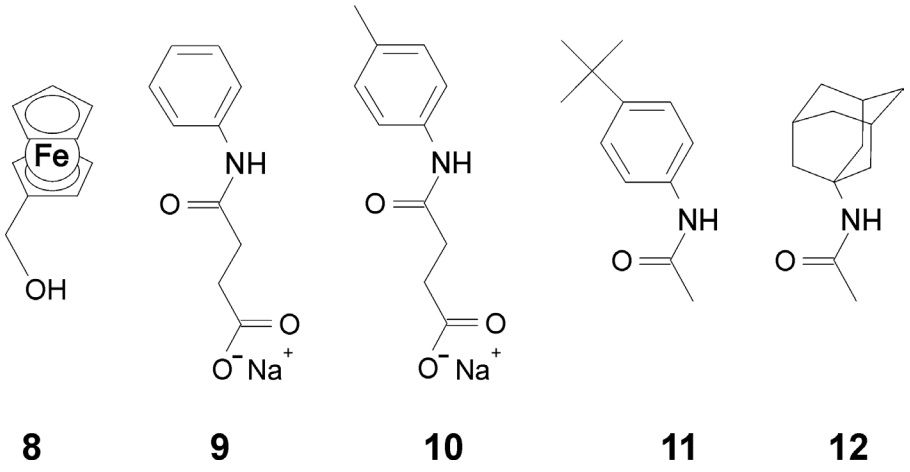

Chart 6.3 Model compounds **8-12** for adsorbates **2-7** employed in ITC and SPR experiments.

In Table 6.2 are summarized the pull-off force values for adsorbates **2-7** with the thermodynamic parameters for host-guest complexes of compounds **8-12**.[34] The data clearly show that guests that bind more strongly to the SAM of **1** give a higher unbinding force, while there seems to be no direct correlation with the binding enthalpy to β-CD in solution.

Table 6.2. Force values, $F_{pull\text{-}off}$, for guests **2-7** measured by force spectroscopy; thermodynamic data at SAMs of **1** for model compounds **8**, **11** and **12**, measured by SPR, and solution data for model compounds **8-12** with native β-CD measured by ITC.[34]

Guest	AFM	Model guest	SPR	ITC		
	$F_{pull\text{-}off}$ pN		ΔG^o kcal mol^{-1}	ΔG^o kcal mol^{-1}	ΔH^o kcal mol^{-1}	$T\Delta S^o$ kcal mol^{-1}
2, 3	56 ± 10	**8**	-5.4	-5.4	-6.1	-0.7
4	39 ± 15	**9**	---[a]	-2.3	-2.3	0
5	45 ± 15	**10**	---[a]	-3.0	-2.7	0.37
6	89 ± 19	**11**	-6.0	-6.1	-5.2	0.9
7	102 ± 25	**12**	-6.5	-6.6	-5.9	0.7

[a] Low solubility and weak interactions with the CD SAM do not allow accurate measurements of the thermodynamic parameters for this guest**.**

6.3.2 Theoretical model for the correlation of pull-off forces with thermodynamic data

Willemsen *et al.* demonstrated[42] that by monitoring the Brownian movement of an AFM tip in a potential well the total potential can be derived from the probability distribution of the tip position. The total potential consists of the sum of the harmonic cantilever potential and of the tip-surface interaction potential.

For our system the experimental data indicate no contribution from non-specific interactions to the pull-off force, thus the tip-surface interactions can be attributed exclusively to the host-guest complex (HG). The potential energy curve is approximated by a Lennard-Jones potential (U_{LJP}) with a characteristic well depth ε as derived from a molecular dynamics (MD) simulation. The LJP has been modified to take into account the presence of the alkyl spacer with length *L* (see Section 6.6). The alkyl chain is treated as an infinitely flexible linker until the maximum elongation is reached, while it can not be stretched beyond its fully elongated conformation. These considerations result in a total potential energy of the complex $U_{complex} = -\varepsilon$ for $-L < z < 0$, and $U_{complex} = U_{LJP}$ for $z < -L$ and $z > 0$. To correlate U_{LJP} to ΔG^o of the complex via the complexation constant *K* two different space integrations (either spherical or cylindrical) over a properly defined volume have been applied (see Section 6.6). The former, derived from a descriptive model for point charge electrostatic interactions,[43] can be envisioned only as a rough approximation due to the geometrical constraints imposed by the cavity wall on the

complexed guest. The second integration is, in that respect, a better approximation because it incorporates a preferential dissociation pathway. The cantilever potential is described by a harmonic function, determined by the stiffness of the cantilever. The total potential energy can thus be calculated as the sum of the two potentials. The total potential energy curve is affected by changes in the position of the cantilever minimum, occurring upon retraction of the tip. Up to a certain point, only one minimum ("bound" state), mainly governed by the interaction potential, exists. Near the point where a pull-off event takes place, a second minimum ("unbound" state), largely governed by the tip, appears and quickly becomes the predominant one. A full description is given in the Section 6.6.

In the situation where two minima are present the probability of the system to be in the "bound" or "unbound" state can be calculated by a Boltzmann distribution, taking into account the widths of the minima w_{bound} and $w_{unbound}$ (Equation 6.2), which are inversely related to the stiffness, *i.e.* the spring constants of the complex ($k_{complex}$) and of the cantilever (k_{tip}).

Equation 6.2

$$\frac{p_{bound}}{p_{unbound}} = \frac{w_{bound}}{w_{unbound}} e^{-(U_{bound} - U_{unbound})/RT} = \frac{k_{tip}}{k_{complex}} e^{-\Delta U/RT}$$

To approximate the stiffness of the HG system, a parabola ($U = a \times (z - b)^2 + c$) can be used to fit U_{tot} in proximity of the "bound" minimum. This approach evidences as well that a 5 Å linker is already long enough to avoid any linker chain length dependence of the stiffness of the complex. For the two ferrocenyl terminated guests **2** and **3**, with chain length spacers of respectively 6 and 16 carbon atoms, no detectable difference in the $F_{pull\text{-}off}$ could be observed, thus such a theoretical derivation is strongly supported by the experimental data.

Knowing $k_{complex}$ and k_{tip} allows one to describe, for different piezo positions (leading to different positions z_1, of the tip potential minimum), the probability distribution for the system to be in the "bound" or "unbound" states, with identification of the last bound and first unbound datapoint corresponding, macroscopically, to the pull-off event of the tip. The chance to observe such a pull-off event can be thus defined as in Equation 6.3 (cfr. Section 6.6):

Equation 6.3

$$p_{pull\text{-}off} = p_{bound,\, z1} \times (1 - p_{bound,\, z1+2})$$

The corresponding graphs for p_{bound} and $p_{pull\text{-}off}$ are shown in Figure 6.9. The curve also shows that for a certain HG complex probed under identical conditions, z_1 at which the

pull-off is observed has a certain distribution of approx. ± 1.5 Å, which corresponds to an intrinsic variability of $F_{pull\text{-}off}$ of ± 10 pN.

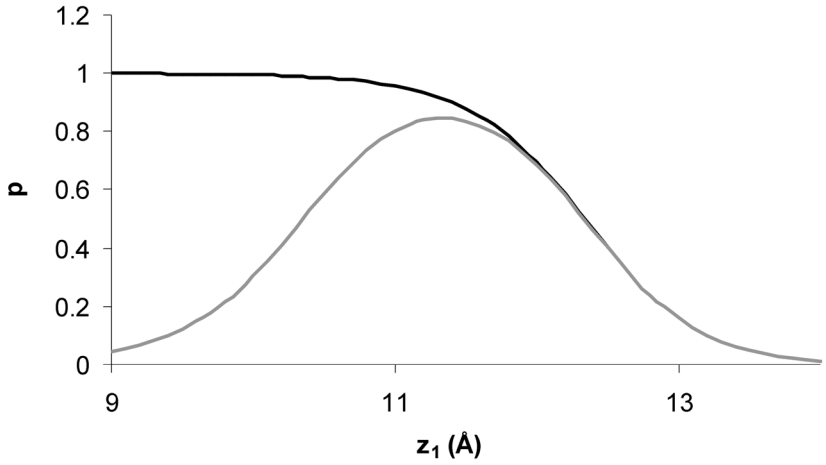

Figure 6.9 Plot of p_{bound} (black line) and $p_{pull\text{-}off}$ (gray line) as a function of z_1 (ε = 10 kcal mol^{-1}).

Once the maximum pull-off force probability is determined, the corresponding tip deflection Δz_{max} is converted into the force exerted by the cantilever according to Equation 6.4, determining the pull-off force value.

Equation 6.4 $$F_{pull\text{-}off} = k_{tip} \times \Delta z_{max}$$

From this model follows a square root dependence of the pull-off force value on ΔGº. Figure 6.10 shows a plot of the force quantum values for guests **2-7** and SAMs of **1** measured via force spectroscopy and the ΔGº of the HG complexes as in Table 6.2. On the same graph the two square root dependence fittings, corresponding to the two space integrations of the potential energy, are reported. It can be seen that the cylindrical integration fits the experimental data better, supporting the model adopted to describe the dissociation of the HG complex under the influence of the AFM tip, with the guest dissociating preferentially perpendicular to the plane of the β-CD cavity (see Section 6.6).

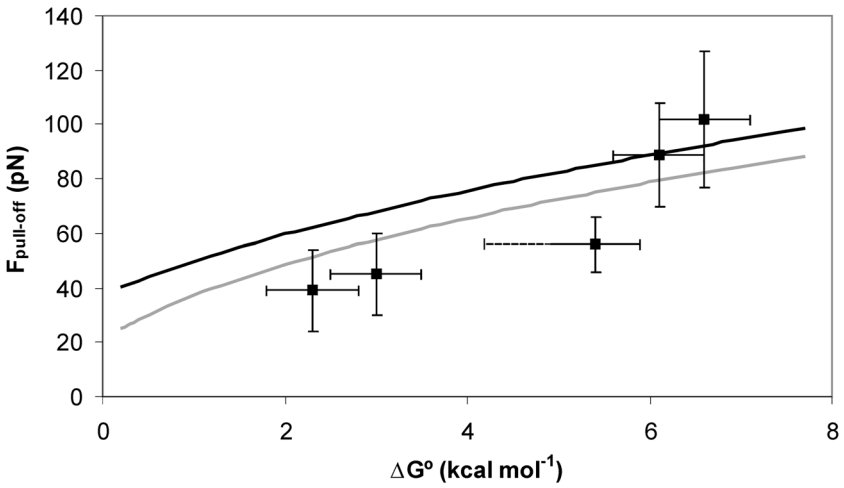

Figure 6.10 Experimental pull-off forces vs. ΔG^o (■), and calculated square root functions for spherical (Equation 6.6) (black solid line) and cylindrical integration (Equation 6.7) (gray solid line). Horizontal error bar for the 3rd point (ferrocene) is related to the ΔG^o range stemming from different model compounds measured by isothermal titration calorimetry.

The theoretically derived square root dependence of $F_{pull\text{-}off}$ with ΔG^o can intuitively be understood from the fact that a deeper well ε (and thus a linear change in ΔG^o) can be compensated by a square root change in z_1 and thus in force, since the potential energy of the cantilever depends quadratically on deflection.

It is necessary, at this point, to address a certain number of factors that could affect the value of $F_{pull\text{-}off}$. As already stated above an intrinsic variability of $F_{pull\text{-}off}$ follows from the probability distribution of $p_{pull\text{-}off}$. Other sources of deviation can be related to differences in the dissociation trajectories of the HG system. Different HG complex geometries could originate from different orientations of the molecular pairs on the two surfaces (tip and substrate), as well as being related to the granular structure of the gold layer on the AFM tip. However, different dissociation pathways should play a marginal role in determining the $F_{pull\text{-}off}$ as observed for the theoretical curves reported in Figure 6.10, for which a change in the integration volume from a sphere to a cylinder does not severely affect the corresponding force value.

The model described here does strictly apply to the interactions between one single guest on the tip and one β-CD cavity on the surface. Multiple, simultaneous pull-off events are not taken into consideration.[36]

Because of the thermodynamic equilibrium condition of the experiments, our results complement the theoretical work of Evans *et al.* and recent experimental work by various

groups for systems under far-from-equilibrium conditions. Furthermore, the complexation constants, and hence host-guest complex lifetimes, in thermodynamic equilibrium of various supramolecular systems, *e.g.* in hydrogen-bonded systems,[5] can be designed and controlled. Thus, it can be anticipated that a large spectrum of host-guest complex lifetimes and rupture forces can be explored using rather simple and well-defined systems. The advantage of simplicity and high definition in our supramolecular systems is expressed in the potential energy landscapes of the unbinding pathways, which should help in the development of advanced models and theories for both equilibrium and non-equilibrium conditions.

6.4 Conclusions

Using an atomic force microscope the rupture forces of individual β-cyclodextrin-ferrocene host-guest complexes in aqueous medium have been determined. The observed force quantum of 55 ± 10 pN, which is attributed to the rupture of a single host-guest complex, is in quantitative agreement with a previous report on the interactions between ferrocene and a very similar cyclodextrin adsorbate.[27] Depending on the concentration of ferrocene moieties on the AFM tip, multiple or predominantly single pull-off events were observed. The effects of the alkyl spacer length of the ferrocene adsorbates, the relative concentration of ferrocene in the mixed monolayer on the AFM tip, and the unloading rate were found to have a negligible effect on the observed pull-off force. Furthermore, by employing different types of guests immobilized on the AFM tips, force displacement curves show the characteristics multiple pull-off events in all cases. Modeling of the histograms led to periodic distribution of forces with maxima at integer values of a certain force quantum characteristic of the guest. The force quanta values are 39 ± 15, 45 ± 15, 89 ± 19, and 102 ± 25 pN, respectively. The force values follow the same trend as the complexation constants measured for model compounds on β-CD monolayers. All observations reported are thus consistent with the view that the fast complexation and decomplexation events are probed under thermodynamic equilibrium conditions. A model has been developed that correlates the force quanta with the ΔG^{o} of the host-guest complexes for model compounds.

6.5 Experimental

Materials. 2-Mercaptoethanol and 11-mercapto-1-undecanol were purchased from Aldrich and used without any further purification. Adsorbates **2**, **3**, **4**, **5**, **6**, and **7** were synthesized according to literature procedures.[36,44,45] The β-cyclodextrin adsorbate **1** was synthesized and SAMs on Au(111) were prepared as reported previously.[34,46] All solvents used in monolayer preparation were of p.a. grade.

AFM Tip Modification. V-shaped silicon nitride cantilevers with pyramidal tips (purchased from Digital Instruments (DI), Santa Barbara, CA) were coated with ca. 2 nm Ti and ca. 75 nm Au by evaporation in high vacuum (Balzers). The tips were functionalized as described previously[47] in 1 mM ethanolic solutions containing mixtures of a hydroxyl-terminated thiol (2-mercaptoethanol or 11-mercapto-1-undecanol) and a guest adsorbate (**2**, **3**, **4**, **5, 6,** or **7**) in different ratios. For **2** and **3,** the composition of the mixed SAMs was determined by extrapolation of cyclic voltammetry measurements on SAMs prepared from solutions with χ_{Fc} = 0.05 - 0.90 to lower concentrations. From the electrochemical data a linear correlation between the mol fraction of the adsorbates in solution and in the mixed monolayer was found, which can be extrapolated to the low mol fractions used in the experiments (see Chapter 5). The estimated error for the solution composition is on the order of 10% for the minority component. Mixed SAMs of 2-mercaptoethanol and **4**, **6**, and **7** in different ratios were analyzed by X-ray Photoelectron Spectroscopy (XPS), and the results were assumed to hold also for adsorbate **5**.[36]

AFM Measurements and Analysis. The AFM measurements were carried out with a NanoScope III multimode AFM (DI) utilizing a 10 μm (E) scanner and a DI liquid cell on SAMs of **1** on atomically smooth Au(111).[27] The calibration of the AFM scanner in the z-direction was carried out using a set of three vertical calibration standards (TGZ 01 - 03) with step heights of 25, 104, and 515 nm, respectively (Silicon-MDT, Moscow, Russia). The cantilever spring constants (in the range of 0.05 - 0.12 N/m) were calibrated using the reference method described by Tortonese and Kirk[48] and by the thermal noise method.[49] The shape of the gold-modified tips was determined by imaging an array of sharp tips (Silicon-MDT, Moscow, Russia). A granular morphology with grain sizes between ~20 and ~40 nm was found, in agreement with previous high resolution SEM experiments.[27,50] Force-displacement (f-d) curves were recorded in Milli-Q water at different positions on the sample surface. The loading force was limited to < 500 pN. By varying the vertical scan rate and scan size, as well as the cantilever spring constant, the unloading rate was varied between 3.5×10^3 pN/s and 8.8×10^5 pN/s.[32] The quantitative

analysis of the observed individual pull-off events was performed for several hundred force-displacement curves for a given data set. Each individually resolved pull-off event with a rupture force above the noise level of the freely vibrating cantilever (ca. 15 pN) was included in the analysis. These data were contrasted with rupture forces of the very last pull-off event of each f-d curve. The data were plotted in histograms, which were subsequently subjected to FFT filtering in order to determine the center position of the local maxima observed. It should be mentioned that the procedure results in local maxima positions, which are independent of the bin size of the histogram. Following this procedure the smoothed functions were deconvoluted by fitting up to 5 Gaussian peaks using the Levenberg-Marquardt algorithm.

Isothermal Titration Calorimetry. Titrations were performed at 25 °C using a Microcal VP-ITC titration microcalorimeter. Sample solutions were prepared using Milli-Q water. Titrations of guests **8**, **11**, and **12** were performed by adding aliquots of a 1 mM β-CD solution to a 0.1 mM guest solution, while 50 mM solutions of compounds **9** and **10** were titrated to β-CD solution 5 mM. The titrations were analyzed using a least squares curve fitting procedure. Control experiments involved addition of β-cyclodextrin to water and addition of water to a guest solution.[36]

Surface Plasmon Resonance. SPR measurements were performed in a two-channel vibrating mirror angle scan set-up based on the Kretschmann configuration, described by Lenferink *et al.*[51] Light from a 2 mW HeNe laser is directed onto a prism surface by means of a vibrating mirror. The intensity of the light is measured by means of a large-area photodiode. This set-up allows determination of changes in plasmon angle with an accuracy of 0.002°. The gold substrate with the monolayer was optically matched to the prism using an index matching oil. A teflon cell was placed on the monolayer via an O-ring, to avoid leakage, and filled with 800 μl of Milli-Q water. After stabilization of the SPR signal, titrations were performed by removing an amount of water and adding the same amount of 0.1 mM stock solution of the guest **8**, **11**, or **12**. Between each addition the cell was thoroughly washed with Milli-Q water (700 μl of water 5 times). SPR measurements were repeated 3 times for each monolayer guest system.[34]

Molecular Dynamics. Coordinates for the native β-cyclodextrin were derived from an X-ray structure and the water molecules were removed. All calculations were done with Quanta/CHARMm 24.0 and refer to an unsubstitued ferrocene molecule. The cyclodextrin was charged with the charge template method and excess charge was smoothed over non-polar carbons and hydrogens. The ferrocene was treated as a rigid body by applying large harmonic potentials between all carbon-iron pairs. The iron atom

was charge +2 and the two cyclopentadenyl ligands -1. The ferrocene was placed "manually" in the cavity of the cyclodextrin, followed by ABNR minimization until the root-mean square of the energy gradient was ≤ 0.001 kcal mol^{-1} $Å^{-1}$. This complex was placed in the center of a cubic box of TIP3P water of 30 Å,[52] as implemented in CHARMm). The ferrocene was translated along the quasi seven-fold axis of the cyclodextrin in steps of 0.5 Å. Overlapping waters were removed (on the basis of heavy-atom interatomic distances of $\leq$ 2.3 Å). The positions of the carbon atoms of the cyclodextrin bearing the CH_2OH groups and the Fe were constraint. Before the MD simulations were run the system was minimized by steepest descent for a maximum of 1000 steps or until a root-mean square of the energy gradient of ≤ 1 kcal mol^{-1} $Å^{-1}$ was reached. The system was heated to 300 K in 5 ps, followed by equilibration of 10 ps, after which the MD (NVE ensemble, no systematic deviation from 300 K) was run for 100 ps. During the simulation the non-bonded list was updated every 20 time steps with a cutoff of 14 Å. The Van der Waals interactions were treated with a switch function between 10 and 13 Å, whereas the shift function was applied to the electrostatic interactions (cutoff 13 Å. The time step was 1 fs, with the SHAKE algorithm placed on the hydrogens.[53] Coordinate sets were saved regularly and used for subsequent data analysis. The interaction energy between the cyclodextrin and ferrocene were averaged over all data sets.

6.6 Appendix: a theoretical model relating host-guest ΔG^o to pull-off force

The following section is devoted to present a descriptive model to correlate the experimental rupture forces measured for different host-guest (HG) complexes with the corresponding thermodynamic parameters. The model refers to the interactions existing between one single guest on the tip and one β-CD cavity on the surface.

6.6.1 Relationship between host-guest ΔG^o and a potential energy description

A potential energy description is used to model the HG system. Molecular dynamics (MD) calculations (Figure 6.11 left) have been employed to describe the potential energy of the HG complex for a linear dissociation pathway, *i.e.* the guest is pulled out of the cavity, driven by the tip, under a predefined trajectory orthogonal to the CD plane (Figure 6.11 right).

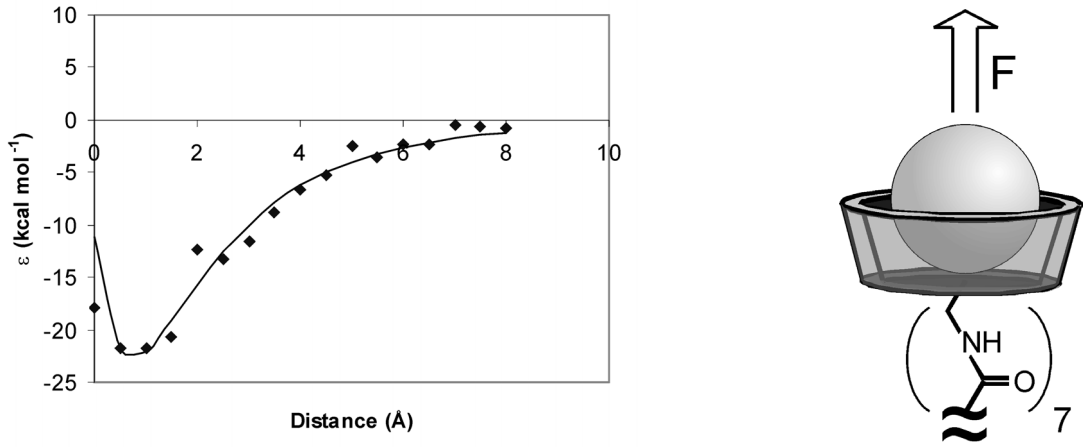

Figure 6.11 Molecular dynamics simulation of the potential energy for the HG complex and Lennard-Jones potential fitting (solid line) (left). Distance of 0 Å is the position of the ferrocene in the minimized complex. Schematic representation of a guest molecule pulled out of the surface confined β-CD cavity, driven by the AFM tip (right).

The interactions of a cyclodextrin cavity with a guest can be described by a potential energy well, the shape of which is approximated by a Lennard-Jones potential (LJP) (Equation 6.5).

Equation 6.5

$$U_{LJP} = 4\varepsilon\left(\left(\frac{s}{z+z_0}\right)^{12} - \left(\frac{s}{z+z_0}\right)^{6}\right)$$

Here z represents the distance from the LJP minimum along the dissociation axis, z_0 is an offset parameter with a value of $\sqrt[6]{2}s$ (assuring that the well minimum occurs at z = 0: U_{LJP} = -ε and $\frac{dU_{LJP}}{dz} = 0$), ε is the well depth, and s determines the width of the well. The width of the well (s = 7.78 Å), which corresponds to the depth of the cyclodextrin cavity, is obtained from the MD simulation as well.

A space integration of U_{LJP} allows one to correlate the depth of the well ε associated with each HG complex to the corresponding ΔG^o value, via the complexation constant K. In a first attempt, a relationship between the HG equilibrium constant K and the potential energy has been derived from a model describing electrostatic interactions in a point charge system.[43] This is based on the space integration of U_{LJP} with a radial dependence according to Equation 6.6, where N_{av} is Avogadro's number. In our case the space

integration over $z \geq 0$ represents a hemisphere above the β-CD cavity, while $z \leq 0$ represents the cavity interior (repulsive LJP interactions). This integration may not be entirely correct since, as stated above, the pull-off trajectory of the guest out of the cavity can better be assumed to be linear. Therefore in an alternative, second integration approach, the sampled volume has been restricted to a cylinder defined by the area available for in-plane movement of the guest in the cavity ($A_{CD} = \pi r^2$ with r = 2 Å) and the linear trajectory perpendicular to this area along which the guest is dissociated (Equation 6.7).

Equation 6.6

$$K = 2\pi N_{av} \int_{-\infty}^{+\infty} z^2 e^{-U_{LJP}/RT} dz$$

Equation 6.7

$$K = N_{av} A_{CD} \int_{-\infty}^{+\infty} e^{-U_{LJP}/RT} dz$$

Employing $\Delta G^o = -RT \ln K$ led to the following linear relationships: $\Delta G^o = 0.85\varepsilon - 3.32$ and $\Delta G^o = 0.96\varepsilon - 2.76$ for the spherical and the cylindrical integrations, respectively, with ΔG^o and ε in kcal mol^{-1}. For our HG systems the ΔG^o values vary between 2.3 and 6.4 kcal mol^{-1}, as determined from ITC and SPR measurements, and thus ε ranges from 6.6 – 11.4 kcal mol^{-1} or 5.3 – 9.5 kcal mol^{-1}, respectively.

6.6.2 Potential energy description of the cantilever/host-guest system

In our model setup, the tip-surface interactions are attributed exclusively to the formation of the host-guest complex, because non-specific interactions are considered negligible, which has been confirmed experimentally as discussed above.

In order to link tip and HG potential, the Lennard-Jones potential needs to be modified to include the presence of the alkyl chain with length L between the guest moiety and the AFM tip. The alkyl chain is treated as an infinitely flexible linker until the maximum elongation is reached, while it cannot be stretched beyond its fully elongated conformation. These considerations result in a total potential energy of the complex $U_{complex} = -\varepsilon$ for $-L < z < 0$, and $U_{complex} = U_{LJP}$ for $z < -L$ and $z > 0$, as shown in Figure 6.12.

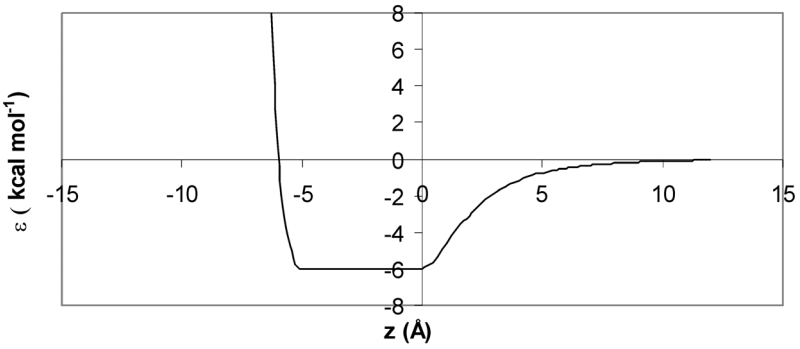

Figure 6.12 Potential energy description for a host-guest complex with ε = 6 kcal mol^{-1}, including the presence of an alkyl spacer with L = 5 Å.

The cantilever potential U_{tip} is described by a harmonic potential (Equation 6.8)

Equation 6.8 $$U_{tip} = \tfrac{1}{2} k \Delta z^2$$

where Δz is the cantilever deflection. When the tip is in contact with the sample, Δz is assumed equal to the height difference between the LJP minimum (at z = 0) and tip minimum (at z = z_1) (see below), where z_1 represents the height of the minimum of the cantilever parabola potential and is controlled by the piezo movement.
The total potential energy of the system can now be derived as the sum of the modified Lennard-Jones potential, describing the host-guest complex, and the harmonic potential describing the cantilever potential (Equation 6.9).

Equation 6.9 $$U_{tot} = U_{complex} + U_{tip}$$

Changes in the piezo position are reflected in the total potential energy curve. Initially, when the piezo has not yet been moved (Δz = 0), the position of the minima of $U_{complex}$ and U_{tip} coincide and only one minimum for U_{tot} is observed (Figure 6.13A). Retraction of the piezo (in our setup z_1 is changed in 2 Å steps) is translated into a cantilever deflection (Δz > 0) with a shift of the parabola potential minimum z_1 to the right, thus raising the minimum observed at z = 0 for the total potential energy curve (Figure 6.13B). Up to a certain point, only one minimum exists, called “bound” in which the tip stays in contact with the sample while the HG complex may rapidly dissociate and reassociate. In Figure 6.13 it can also be seen that this “bound” minimum stays at the same position, owing to the larger stiffness of the complex (see below), so that the observed deflection

Δz is equal to z_1. Near the point where a pull-off event takes place, a second minimum, called "unbound", appears and quickly becomes the predominant one (Figure 6.13D). Here the tip is not in contact with the surface, and the HG complex is dissociated. In Figure 6.13B to E the tip movement is simulated by four sequential energy potential curves, with z_1 = 6, 8, 10, and 12 Å respectively, showing the corresponding changes in U_{tot}, and describing the transition from the "bound" to the "unbound" state as the most energetically favorable situation.

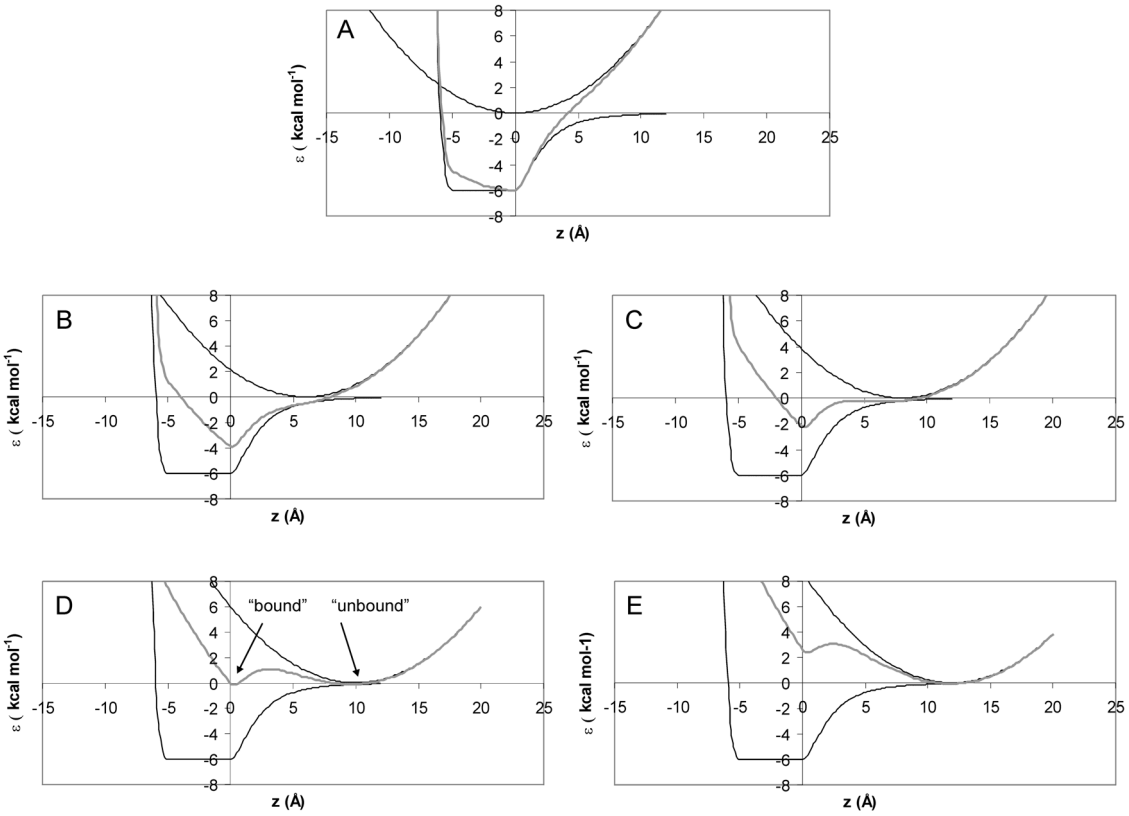

Figure 6.13 Total energy description: U_{tip} (parabola), $U_{complex}$ (black line), and U_{tot} (gray line). The piezo displacement z_1 from A to E is respectively 0, 6, 8, 10, and 12 Å.

6.6.3 The Boltzmann distribution

In the situation where two minima are present, the chance of being in either minimum, describing the "bound" and the "unbound" states, is governed by the Boltzmann distribution where w_{bound} and $w_{unbound}$ are the widths of the minima, which are inversely

related to the stiffness, *i.e.* the spring constants of the complex ($k_{complex}$) and the cantilever (k_{tip}) (Equation 6.10).

Equation 6.10

$$\frac{p_{bound}}{p_{unbound}} = \frac{w_{bound}}{w_{unbound}} e^{-(U_{bound} - U_{unbound})/RT}$$

where $w_{bound} = \frac{1}{k_{complex}}$ and $w_{unbound} = \frac{1}{k_{tip}}$, from which follows:

$$p_{bound} = \frac{1}{1 + \frac{k_{complex}}{k_{tip}} e^{\Delta U/RT}} \qquad \text{where } \Delta U = U_{bound} - U_{unbound} \qquad \text{with}$$

$$U_{bound} \approx U_{tot,z=0} = -\varepsilon + \tfrac{1}{2} k_{tip} (\Delta z)^2 \text{ and } U_{unbound} \approx U_{tot,z=z_1} = 4\varepsilon \left(\left(\frac{s}{z_1 + z_0} \right)^{12} - \left(\frac{s}{z_1 + z_0} \right)^{6} \right)$$

To approximate the stiffness of the HG system, a parabola ($U = a \times (z - b)^2 + c$) can be used to fit U_{tot} in proximity of the "bound" minimum (Figure 6.14A), so that $k_{complex} = 2a$. The plot of the stiffness of the complex as a function of ε shows a linear correlation leading to $k_{complex}$ = 23.81ε pN Å^{-1}, with ε in kcal mol^{-1}, while k_{tip} = 8 pN Å^{-1}, as determined experimentally. Since for our systems ε ranges roughly from 5 to 12 kcal mol^{-1}, $k_{complex}$ may range from 125-300 pN Å^{-1}, which is in all cases much higher than the stiffness of the cantilever. It is also seen that a 5 Å linker is already long enough to avoid any linker chain length dependence on the stiffness of the complex.

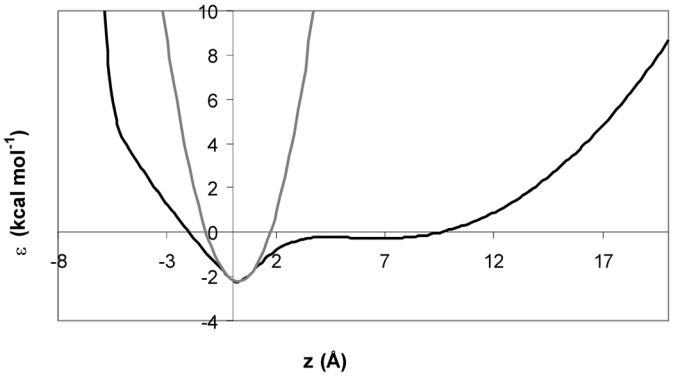

Figure 6.14 Parabola fitting (gray line) of the "bound" minimum U_{tot} as given in Figure 6.13C (black line).

Knowing $k_{complex}$ and k_{tip} allows one to describe the probability distribution for a certain host-guest pair to be in the "bound" or "unbound" state for each piezo position. Figure 6.15 shows p_{bound} as a function of z_1 for ε = 10 kcal mol^{-1}. Here it is seen that p_{bound} drops from 1 to 0 in about 4 Å piezo change, *i.e.* within only 2 datapoints. The specific z_1 at which this occurs obviously depends on ε, but the shape of the curve hardly changes. A macroscopic pull-off event thus corresponds to one datapoint being in the "bound" state while for the next datapoint the "unbound" state is observed, thus the chance to observe such a pull-off event, $p_{pull\text{-}off}$, can be defined as in Equation 6.11:

Equation 6.11

$$p_{pull\text{-}off} = p_{bound,\,z1} \times p_{unbound,\,z1+2}$$
$$= p_{bound,\,z1} \times (1 - p_{bound,\,z1+2})$$

where p_{bound} is given in Equation 6.10. The dependence of $p_{pull\text{-}off}$ on z_1 is also shown in Figure 6.15. Again, the steep dependence of $p_{pull\text{-}off}$ on z_1 ensures that the pull-off event occurs at a specific datapoint and that no switching back and forth between the "bound" and the "unbound" states will occur in the experimental setup used here, unless one were to detect datapoints for relatively long periods of time at all z_1 of a pull-off experiment. The curve also shows that for an identical HG complex probed under identical conditions, z_1 where the pull-off is observed has a certain distribution (approx. ± 1.5 Å, corresponding to ± 10 pN).

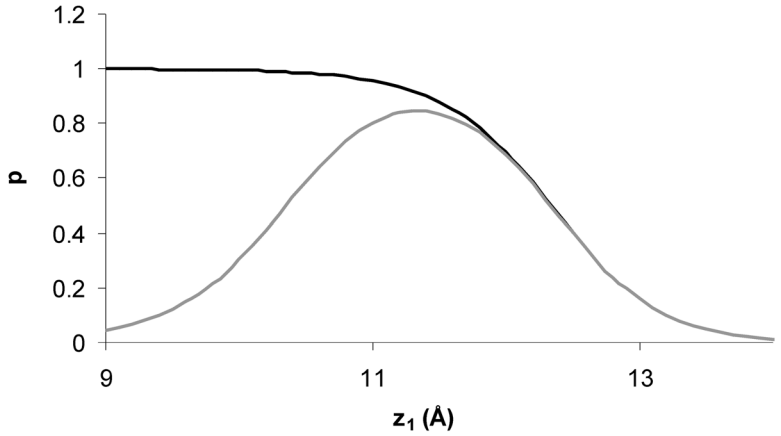

Figure 6.15 Plot of p_{bound} (black line) and $p_{pull\text{-}off}$ (gray line) as a function of z_1 (ε = 10 kcal mol^{-1}).

6.6.4 From energy domain to force

Once the maximum pull-off probability is determined, the corresponding tip deflection Δz_{max} is converted into the force exerted by the cantilever according to Equation 6.12, thus determining the pull-off force value.

Equation 6.12 $$F_{pull\text{-}off} = k_{tip} \times \Delta z_{max}$$

From the above described model it is possible to derive the dependence of $p_{pull\text{-}off}$, and thus of the pull-off force with ε. Figure 6.16 shows the pull-off force $F_{pull\text{-}off}$ as a function of ε, and this appears to be a square root dependence.

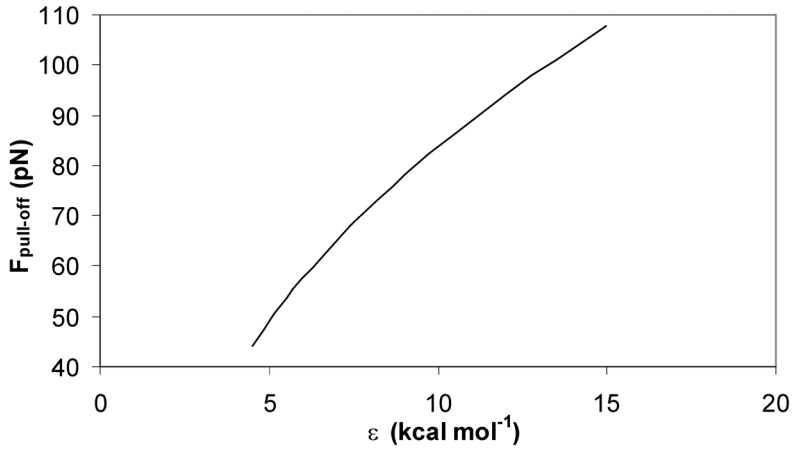

Figure 6.16. Square root dependence of the pull-off force as a function of ε.

The relationship between ε and ΔGº described in Section 6.6.1 allows one to extend the correlation between energy and force to the thermodynamics of the HG complex. Figure 6.17 reports the derived dependence of pull-off force vs. ΔGº for the spherical and cylindrical integration approaches, $F = 32.85 \times \sqrt{\Delta G^{o} + 1.29}$ and $F = 30.97 \times \sqrt{\Delta G^{o} + 0.45}$ respectively (with ΔGº in kcal mol^{-1} and F in pN), while the experimental values for the five host-guest complexes investigated are shown as well.

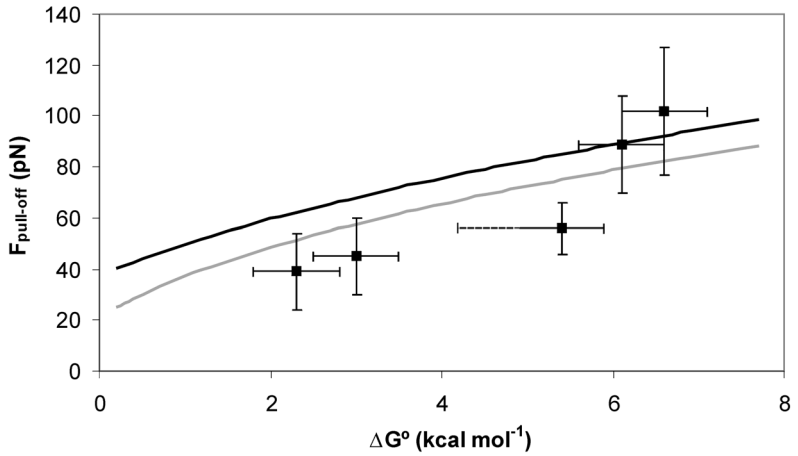

Figure 6.17 Experimental pull-off forces vs. ΔG^{o} (■), and calculated square root functions for spherical (Equation 6.6) (black solid line) and cylindrical integration (Equation 6.7) (gray solid line). Horizontal error bar for the 3rd point (ferrocene) is related to the ΔG^{o} range stemming from different model compounds measured by isothermal titration calorimetry.

6.7 References and notes

[1] Behr, J.-P. *The Lock and Key Principle: The State of the Art*; Wiley: Chichester, 1994.

[2] Buckingham, A. D.; Legon, A. C.; Roberts, S. M. *Principles of Molecular Recognition*; Blackie: London, 1993.

[3] *Biochemistry 4th ed*.; Freeman: New York, 1995.

[4] Cram, D. J.; Karbach, S.; Kim, Y. H.; Baczynskyj, L.; Kalleymeyn, G. W. *J. Am. Chem. Soc.* **1985**, *107*, 2575-2576.

[5] For a recent review see: Prins, L. J.; Reinhoudt, D. N.; Timmerman, P. *Angew. Chem. Int. Ed.* **2001**, *40*, 2382-2426.

[6] a) For a review see: Whitesides, G. M.; Simanek, E. E.; Mathias, J. P.; Seto, C. T.; Chin, D. N.; Mammen, M.; Gordon, D. M. *Acc. Chem. Res.* **1995**, *28*, 37-44. b) Timmerman, P.; Vreekamp, R. H.; Hulst, R.; Verboom, W.; Reinhoudt, D. N.; Rissanen, K.; Udachin, K. A.; Ripmeester, J. *Chem. Eur. J.* **1997**, *3*, 1823-1832.

[7] a) Lehn, J.-M. *Macrom. Chem. Macrom. Symp.* **1993**, *69*, 1. b) Sijbesma, R. P.; Beijer, F. H.; Brunsveld, L.; Folmer, B. J. B.; Hirschberg, J. H. K. K.; Lange, R. F. M.; Lowe, J. K. L.; Meijer, E. W. *Science* **1997**, *278*, 1601-1604. c) Sherrington, D. C.; Taskinen, K.

A. *Chem. Soc. Rev.* **2001**, *30*, 83-93. d) Brunsveld, L.; Folmer, B. J. B.; Meijer, E. W.; Sijbesma, R. P. *Chem. Rev.* **2001**, *101*, 4071-4098.

[8] a) Wenz, G. *Angew. Chem. Int. Ed.* **1994**, *33*, 803-822. b) *Chem. Rev.* **1998**, *98*, Issue 5. c) *Comprehensive Supramolecular Chemistry*; Pergamon Press: Oxford, 1996, vol. 3.

[9] Rekharsky, M.V.; Inoue, Y. *Chem. Rev.* **1998**, *98*, 1875-1917.

[10] Folmer, B. J. B.; Sijbesma, R. P.; Versteegen, R. M.; Van der Rijt, J. A. J.; Meijer, E. W. *Adv. Mater.* **2000**, *12*, 874-878.

[11] Binnig, G.; Quate, C. F.; Gerber, Ch. *Phys. Rev. Lett.* **1986**, *56*, 930-933.

[12] Evans, E.; Ritchie, K.; Merkel, R. *Biophys. J.* **1995**, *68*, 2580-2587.

[13] Kuo, S. C.; Sheetz, M. P. *Science* **1993**, *260*, 232-234 and references cited herein.

[14] For recent reviews see: Hugel, T.; Seitz, M. *Macromol. Rapid Commun.* **2001**, *22*, 989-1016.

[15] Lee, G. U.; Chrisey, L. A.; Colton, R. J. *Science* **1994**, *266*, 771-773.

[16] a) Florin, E.-L.; Moy, V. T.; Gaub, H. E. *Science* **1994**, *264*, 415-417; b) Moy, V. T.; Florin, E.-L.; Gaub, H. E. *Science* **1994**, *266*, 257-259.

[17] Ros, R.; Schwesinger, F.; Anselmetti, D.; Kubon, M.; Schäfer, R.; Plückthun, A.; Tiefenauer, L. *Proc. Natl. Acad. Sci. USA* **1998**, *95*, 7402-7405 and references cited herein.

[18] For a recent review, see: Janshoff, A.; Neitzert, M.; Oberdörfer, Y.; Fuchs, H. *Angew. Chem. Int. Ed.* **2000**, *39*, 3212-3237.

[19] Zlatanova, J.; Lindsay, S. M.; Leuba, S. H. *Prog. Biophys. Molec. Biol.* **2000**, *74*, 37-61.

[20] Samorì, B. *Chem. Eur. J.* **2000**, *6*, 4249-4255.

[21] Evans, E.; Ritchie, K. *Biophys. J.* **1997**, *72*, 1541-1555.

[22] Merkel, R.; Nassoy, P.; Leung, A.; Ritchie, K.; Evans, E. *Nature* **1999**, *397*, 50-53.

[23] a) Rief, M.; Gautel, M.; Osterhelt, F.; Fernandez, J. M.; Gaub, H. E. *Science* **1997**, *276*, 1109-1112. b) Fritz, J.; Katopodis, A. G.; Kolbinger, F.; Anselmetti, D. *Proc. Natl. Acad. Sci. USA* **1998**, *95*, 12283-12288. c) Marszalek, P. E.; Lu, H.; Li, H.; Carrion-Vazquez, M.; Oberhauser, A. F. *Nature* **1999**, *402*, 100-103. d) Strunz, T.; Oroszlan, K.; Shafer, R.; Güntherodt, H.-J. *Proc. Natl. Acad. Sci. USA* **1999**, *96*, 11277-11282. e) Evans E.; Ludwig, F. *J. Phys. Condens. Matter* **2000**, *12*, 315-320. f) Baumgartner, W.; Hinterdorfer, P.; Ness, W.; Raab, A.; Vestweber, D. *Proc. Natl. Acad. Sci. USA* **2000**, *97*, 4005-4010. g) Lee, I.; Marchant. R. E. *Surf. Sci.* **2001**, *491*, 433-443.

[24] a) Kramers, H. A. *Physica* **1940**, *7*, 284-312. b) Hanggi, P.; Talkner, P.; Borkovec, M. *Rev. Mod. Phys.* **1990**, *62*, 251-341.

[25] Evans, E. *Annu. Rev. Biophys. Biomol. Struct.* **2001**, *30*, 105-128.

[26] Merkel, R. *Phys. Reports* **2001**, *346*, 343-385.

[27] a) Schönherr, H.; Beulen, M. W. J.; Bügler, J.; Huskens, J.; Van Veggel, F. C. J. M.; Reinhoudt, D. N.; Vancso, G. J. *J. Am. Chem. Soc.* **2000**, *122*, 4963-4967. b) Schönherr, H.; Beulen, M. W. J.; Van Veggel, F. C. J. M.; Bügler, J.; Huskens, J.; Reinhoudt, D. N.; Vancso, G. J. in *Interfacial Properties on the Submicron Scale*; ACS Symposium Series 781, 2001, Chapter 7, pp. 113-128.

[28] Beijer, F. H.; Kooijman, H.; Spek, A. L.; Sijbesma, R. P.; Meijer, E. W. *Angew. Chem. Int. Ed.* **1998**, *37*, 75-78.

[29] a) Marszalek, P. E.; Oberhauser, A. F.; Pang, Y.-P.; Fernandez, J. M. *Nature* **1998**, *396*, 661-664. b) Cluzel, P.; Lebrun, A.; Heller, C.; Lavery, R.; Viovy J.-L. *Science* **1996**, *271*, 792-794.

[30] a) Rief, M.; Clausen-Schaumann, H.; Gaub, H. E. *Nat. Struct. Biol.* **1999**, *6*, 346-349. b) Essevaz-Roulez, B.; Bockelmann, U.; Heslot, F. *Proc. Natl. Acad. Sci. USA* **1997**, *94*, 11935-11940.

[31] The complexation constant for carbohydrate interactions of Lewis^X antigen of 10 M^{-1} reported by Tromas *et al.* implies near-equilibrium conditions similar to our experiments: Tromas, C.; Rojo, J.; de la Fuente, J. M.; Barrientos, A. G.; García, R.; Penadés, S. *Angew. Chem. Int. Ed.* **2001**, *40*, 3052-3055.

[32] In our work we state the nominal unloading rate considering only the velocity of the piezo actuator and the spring constant of the cantilever. While the true unloading rate may deviate from this value due to cantilever acceleration or retardation, these changes are expected to be small. The range of unloading rates and the order of magnitude of these rates are certainly correct.

[33] Godinez, L. A.; Schwartz, L.; Criss, C. M.; Kaifer, A. E. *J. Phys. Chem. B* **1997**, *101*, 3376-3380.

[34] De Jong, M. R.; Huskens, J.; Reinhoudt, D. N. *Chem. Eur. J.* **2001**, *7*, 4164-4170.

[35] This adsorbate differs from the previously reported one (ref. 27a) having an additional CH_2 group in the anchoring thioether substituents (cfr. also ref. 37).

[36] De Jong, M. R. *Ph.D. Thesis*, University of Twente, the Netherlands, 2001.

[37] The structural difference, i.e. a single methylene group in the anchoring dialkylsulfide substituents, is located outside the β-CD cavity, which is responsible for the complexation behavior. Hence the results are consistent with the interpretation of the observed multiple pull-off events as unbinding events of the β-CD - ferrocene host -guest complex.

[38] An estimate of the number of molecules present in the contact area between tip and sample at maximum loading roughly agrees with the number of host-guest complex rupture events calculated from the corresponding histograms.[27] For χ_{Fc} = 0.01 we observed on average 11 host-guest complex rupture events per f-d curve, whereas for χ_{Fc} = 0.002 we detected 5 rupture events, and in some cases as few as one or two events.

[39] Sinniah, S. K.; Steel, A. B.; Miller, C. J.; Reutt-Robey, J. E. *J. Am. Chem. Soc.* **1996**, *118*, 8925-8931.

[40] Kreuzer, H. J.; Payne, S. H.; Livadaru, L. *Biophys. J.* **2001**, *80*, 2505-2514.

[41] The number of pull-off events decreased with each cycle as reported in our previous paper (ref. 27). This observation may be related to damage of the functionalized tip.

[42] Willemsen, O. H.; Kuipers, L.; Van der Werf, K. O.; De Grooth, B.; Greve, J. *Langmuir* **2000**, *16*, 4339-4347.

[43] Ermolaev, V. L.; Sveshnikova, E. B. *Russ. Chem. Rev.* **1994**, *63*, 905-922 and references therein.

[44] a) Chidsey, E. D.; Bertozzi, C. R.; Putwinski, T. M.; Mujsce, A. M. *J. Am. Chem. Soc.* **1990**, *112*, 4301-4306. b) Creager, S. E.; Rowe, G. K. *J. Electroanal. Chem.* **1994**, *370*, 203-211.

[45] For details on the characterization of mixed SAMs of **2** and **3** see: Auletta, T.; Van Veggel, F. C. J. M.; Reinhoudt, D. N. *Langmuir* **2002**, *18*, 1288-1293.

[46] Beulen, M. W. J.; Bügler, J.; De Jong, M. R.; Lammerink, B.; Huskens, J.; Schönherr, H.; Vancso, G. J.; Boukamp, B. A.; Wieder, H.; Offenhäuser, A.; Knoll, W.; Van Veggel, F. C. J. M.; Reinhoudt D. N. *Chem. Eur. J.* **2000**, *6*, 1176-1183.

[47] Schönherr, H.; Hruska, Z.; Vancso, G. J. *Macromolecules* **1998**, *31*, 3679-3685.

[48] Tortonese, M.; Kirk, M. *Proc. SPIE* **1997**, 3009, 53-60.

[49] a) Hutter, J. L.; Bechhoefer, J. *Rev. Sci. Instr.* **1993**, *64*, 1868-1873. b) Sader, J. E. *J. Appl. Phys.* **1998**, *84*, 64-76.

[50] Schönherr, H. *Ph.D. Thesis* University of Twente, the Netherlands, 1999.

[51] Lenferink, A. T. M.; Kooyman, R. P. H.; Greve, J. *Sens. Act. B* **1991**, *3*, 261-265.

[52] Jorgensen, W. L.; Chandrasekhar, J.; Madura, J. D.; Impey, R. W.; Klein, M. L. *J. Chem. Phys.* **1983,** *79*, 926-935.

[53] Berendsen, H. J. C.; Postma, J. P. M.; Dinola, A.; Van Gunsteren, W. F.; Haak, J. R. *J. Chem. Phys.* **1984**, *81*, 3684-3690.

Chapter 7

Host-Guest Complexes on β-Cyclodextrin Self-Assembled Monolayers: Surface Patterning via Multiple Non-Covalent Interactions

In this chapter multiple host-guest interactions between β-cyclodextrin self-assembled monolayers and a novel water-soluble calix[4]arene derivative bearing two adamantyl moieties on the lower rim are described. The thermodynamics of the process has been investigated by means of surface plasmon resonance spectroscopy and the complexation constant is on the order of 1×10^{10} M^{-1}. Selective transfer of guest molecules onto such surfaces has been achieved via soft lithographic techniques such as microcontact printing and dip-pen nanolithography, with sub-100 nm lateral resolution. The patterns created on the β–cyclodextrin layers proved to be stable under the same experimental conditions that allow complete removal of the adsorbed material from hydroxyl-terminated reference layers. Multiple host-guest interactions therefore provide a viable approach to form kinetically stable patterns, and allow to exploit the β–cyclodextrin monolayers as molecular printboards on which guest molecules can be immobilized selectively via non-covalent interactions.

7.1 Introduction

To solve the increasing request for miniaturization of devices, alternative methods to the traditional photolithographic[1] ones are currently investigated, with particular efforts in soft-lithography.[2] Microcontact printing (μCP)[3] and dip pen nanolithography (DPN)[4] are maskless patterning techniques able to transfer molecular inks onto a substrate from an elastomeric stamp and an atomic force microscopy (AFM) tip, respectively. Chemical affinity between the ink and the substrate should provide stability to the pattern in the so-called top-down/bottom-up combination.

Recognition events such as protein expression or enzymatic activity based on structural complementarity, mediated by weak interactions such as electrostatic, hydrogen bonds, and hydrophobic interactions are very common in biological processes.[5] Supramolecular chemistry relies on the formation of stable aggregates, which are generally at or very close to thermodynamic equilibrium, by spontaneous assembly of simpler molecular

building blocks. The structure of the final assembly is already encoded into the functional groups of these building blocks and their spatial arrangement.[6]

As already shown in Chapter 6, well ordered β-cyclodextrin self-assembled monolayers (β-CD SAMs) on gold have been prepared and characterized.[7] In this molecular printboard the surface-confined cavities retain their ability to form host-guest complexes with different molecules in solution or immobilized on an AFM tip, while the thermodynamic parameters of the process for these small guest motifs remain as observed in solution.[7c-e]

Surface plasmon resonance (SPR) spectroscopy is an optical technique based on the measurement of the angle at which resonance occurs between an incident light beam and the evanescent field created by the oscillation of the conducting electrons at a metal surface.[8] The SPR angle is a function of the optical properties and, more specifically, depends on the refractive index of the material in close proximity to the surface (a few nm). Upon absorption of a certain amount of material onto a substrate a change in the refractive index occurs, causing a change in the SPR angle. This technique has been employed successfully to detect adsorption from solution of several molecules on (modified) thin metal surfaces.[7d,9]

In this chapter, SPR results are presented for multiple host-guest interactions between a novel water-soluble calix[4]arene modified with two adamantyl units and β-CD SAMs. Subsequently, surface patterning results are shown employing the calix[4]arene derivative as an ink in μCP and DPN. The stability of the patterns has been probed and compared to results obtained with OH terminated reference layers. Resolution issues are discussed along with submicrometer patterns prepared by DPN.

7.2 Surface plasmon resonance

The synthesis of the bis-adamantyl-calix[4]arene derivative **1** was performed by Andrea Sartori.

SAMs of β-cyclodextrin heptathioether were prepared, as described previously (see also Chapter 6),[7] on gold-covered glass substrates with a metal thickness of 47.5 nm. The adsorption process of **1** onto these surfaces (Scheme 7.1) was investigated by SPR. Titrations were carried out in an 800 μl cell in the presence of native β-cyclodextrin as competitor, with concentrations ranging between 0.1 and 5 mM. Increasing amounts of a 1 μM solution of **1** (with 0 to 5 mM β-CD in solution) were added and the corresponding SPR angle shifts were recorded. The β-CD in solution is required to compete with the

binding sites on the SAM so that higher guest concentrations can be employed and depletion of the guest in solution can be avoided.

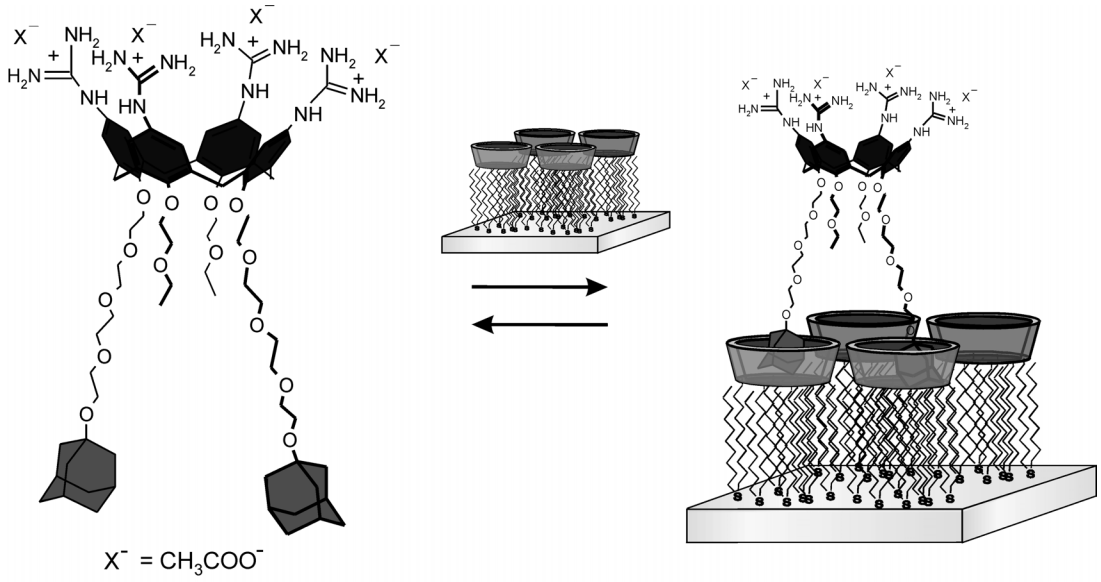

1

Scheme 7.1 Schematic representation of the adsorption of **1** on a β-CD SAM via multiple host-guest interactions.

After each addition it was necessary to repeatedly rinse the cell with a 10 mM solution of native β-cyclodextrin. After rinsing, the SPR baseline was almost completely restored, confirming that it was possible to remove most of the adsorbed guest. In Figure 7.1 four different SPR titration curves, performed at different β-CD concentrations, are reported with the corresponding fitted curves (solid lines). Upon increasing the native β-CD concentration in solution the slope of the binding curve decreases, indicating a competitive process between the host in solution and the β-CD SAMs. A 1:1 model, in which it is assumed that both adamantyl units of the adsorbate interact with a β-CD cavity on the surface, was employed to fit the experimental data and a complexation constant on the order of 1×10^{10} M^{-1} was obtained.[10]

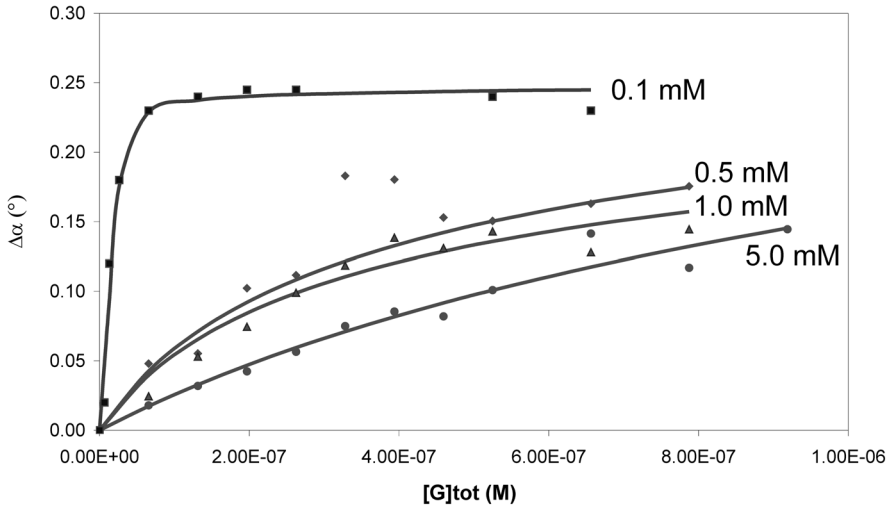

Figure 7.1 SPR titrations (data points) and corresponding fits (solid lines) for different titrations of **1** on β-CD SAMs at four different β-CD concentrations in solution.

SPR titrations were also performed in the presence of 0.1 M KCl as a background electrolyte to exclude possible structuring of the solution on top of the layers, arising from ionic interactions mediated by the cationic groups on the upper rim of **1**. Data fitting led to the same complexation constant, independent of the presence of the salt.
Experiments performed on 11-mercapto-1-undecanol reference SAMs (OH SAMs) only showed a concentration effect on the SPR angle, but no binding curve could be recorded (data not shown), indicating that there only non-specific interactions occur.

7.3 Supramolecular microcontact printing

Owing to the high complexation constant, multiple host-guest complexes provide stable interactions between adsorbate **1** and β-CD SAMs, allowing one to employ such a system in soft-lithographic techniques for surface patterning. We used microcontact printing $(\mu CP)^3$ to establish whether it was possible to transfer selectively molecules of **1** onto the molecular printboard and we investigated the stability of these structures (Scheme 7.2).
Due to the polar nature of the ink, hydrophilization of the stamps by mild oxidation in an ozone plasma reactor for 30 min was needed to transfer these water-soluble molecules.[11,12] After soaking the hydrophilic stamps in a 0.1 mM solution of **1** they were applied by hand onto the β-CD layers for 60 s (Scheme 7.2).

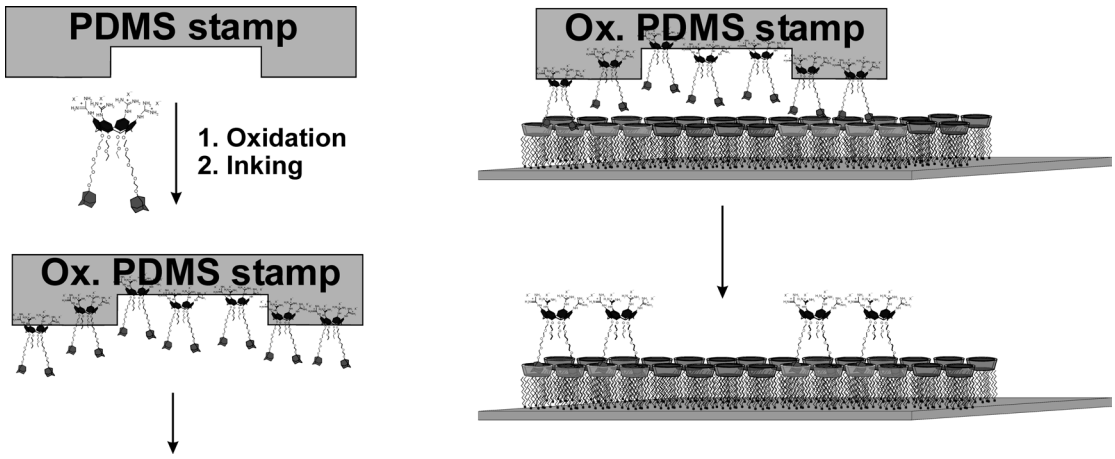

Scheme 7.2 Supramolecular microcontact printing.

A clear pattern could be observed in contact mode AFM imaging of the β-CD layer after the printing step, as shown in Figure 7.2, proving that material transfer between the stamp and the SAM had occurred. The master employed to prepare the PDMS stamp has 10 μm features with 5 μm gaps. However, ozone treatment of the stamp seems to modify the stamp features, leading to a pattern composed of features and gaps of comparable size (ca. 8.0 ± 1.0 μm). The darker lines represent the unmodified β-CD SAM areas, while the brighter ones are the areas printed with the calix[4]arene **1**.

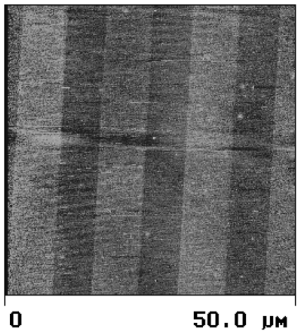

Figure 7.2 CM-AFM friction image in air (friction forces [a.u.] increase from dark to bright contrast) of a β-CD SAM (darker area) patterned with **1** (brighter areas) by microcontact printing.

In order to prove unequivocally that the patterns are stable and that the stability arises from the formation of supramolecular host-guest interactions between the CD cavities

and the adamantyl residues of the calix[4]arene **1**, several different rinsing procedures were applied. The printed substrates were thoroughly rinsed with copious amounts (200 ml) of either 10 mM β-CD in Milli-Q water, or 50 mM aq. NaCl, or Milli-Q water. CM-AFM friction imaging allowed clear identification of the transferred pattern (Figure 7.3), even when the competitive 10 mM native β-CD solution was used (Figure 7.3A), proving that strong interactions are established between the molecular ink and the surface.

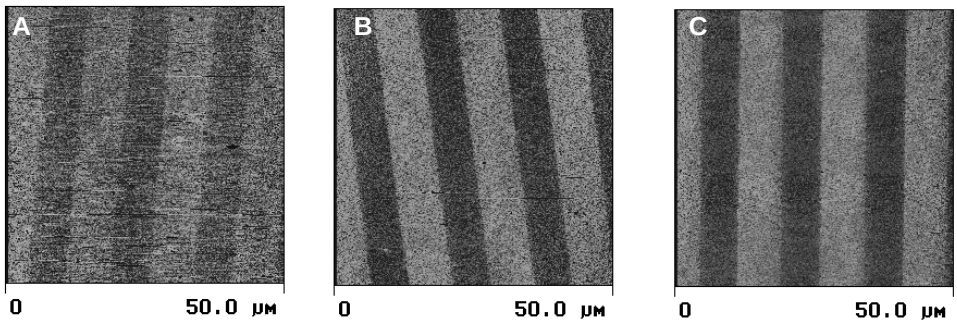

Figure 7.3 CM-AFM friction images in air of β-CD SAMs after μCP printing of **1** onto a β-CD SAM and rinsing with either 10 mM β-CD in water (A); or 50 mM aq. NaCl (B); or Milli-Q water (C) (friction forces [a.u.] increase from dark to bright contrast).

To rule out any interference from non-specific interactions, the same printing experiments were carried out on OH SAMs. These layers have surface groups comparable to the β-CD layers, but lack the possibility of forming inclusion complexes, and thus interactions with the ink are solely non-specific. In Figure 7.4 is reported a CM-AFM friction image after the printing of **1** on such an OH SAM.

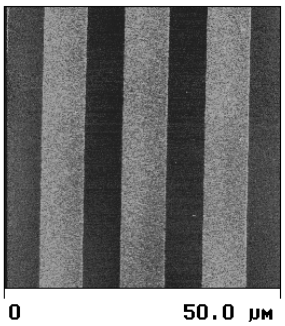

Figure 7.4 CM-AFM friction image in air (friction forces [a.u.] increase from dark to bright contrast) of an 11-mercapto-1-undecanol SAM (darker area) patterned with **1** (brighter areas) by microcontact printing.

A clear pattern is again observed, with the same lateral dimensions and friction scale as the one observed on the β-CD SAM. However, exposing the OH SAMs patterned with **1** to the same rinsing procedures described above led to complete removal of the adsorbed material, as shown in Figure 7.5.

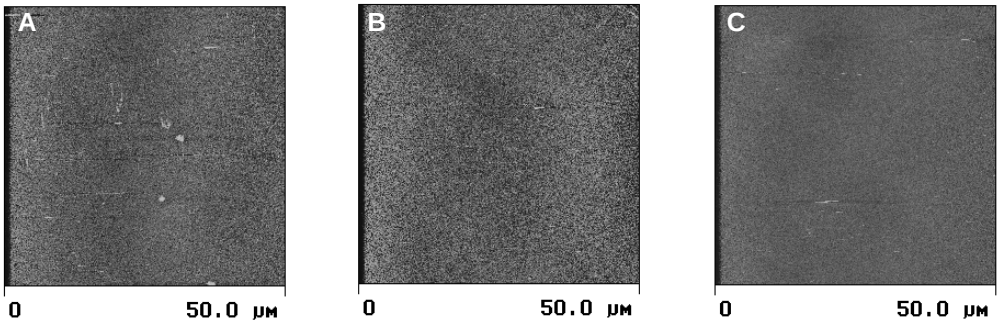

Figure 7.5 CM-AFM friction images in air of OH SAMs after μCP of **1** and rinsing with either 10 mM β-CD in water (A); or 50 mM aq. NaCl (B); or Milli-Q water (C) (friction forces [a.u.] increase from dark to bright contrast).

The μCP results show that the transfer process of material from the stamp onto the layer does not rely on specific interactions, but that physical contact is enough to produce a pattern. However, in case of the β-CD SAMs, a stable pattern is obtained, while onto the OH layers no firm anchoring of the ink is possible. Thus, the stability of the patterns on the former SAMs can be attributed exclusively to the presence of multiple host-guest interactions on the molecular printboard.

To quantify the amount of material transferred during the soft lithographic step, μCP with flat, featureless PDMS stamps was performed, either followed or not by rinsing with 50 mM aq. NaCl. XPS (Table 7.1), contact angle goniometry (Table 7.2), cyclic voltammetry (CV) and electrochemical impedance spectroscopy (EIS) (Table 7.3) were employed to characterize the substrates before and after the printing/rinsing process and results were compared to those obtained for samples prepared by absorbing the guest **1** from a 0.5 mM solution and to calculated theoretical values.

Table 7.1 XPS results obtained for μCP substrates in comparison with data for adsorption from solution and theoretical values (std. dev. in brackets).

SAM	C1s	N1s	O1s	S2p	C/N	C/O
β-CD calcd.	81.0	2.7	13.5	2.7	30.0	6.0
β-CD exp.	79.5 (0.9)	2.6 (0.5)	16.2 (0.4)	1.7 (0.1)	30.2	4.9
$(\beta\text{-CD})_2$/CalixAd$_2$ calcd.	79.2	4.1	14.4	2.2	19.4	5.5
Adsorption from solution	77.8 (0. 6)	3.9 (0.3)	17.1 (0.6)	1.1 (0.3)	19.7	4.5
Printing/rinsing	76.7 (0.7)	3.6 (0.2)	18.5 (1.0)	1.3 (0.2)	21.5	4.1
Printed/no rinsing	74.5 (0.5)	3.7 (0.4)	20.6 (0.9)	1.1 (0.1)	20.0	3.6
4 ML* calcd.	76.4	6.3	16.0	1.4	12.2	4.8
3 ML* calcd.	77.1	5.7	15.6	1.6	13.4	4.9
2.5 ML* calcd.	77.5	5.4	15.4	1.7	14.3	5.0
2 ML* calcd.	78.0	5.0	15.1	1.9	15.5	5.1

*One monolayer (ML) of guest is defined on a 1:2 ratio with the CD layer, thus 1 CD layer and 0.5 of **1** layer, reflecting the interaction of both adamantyl units with a CD cavity of the SAM.

From the XPS data (Table 7.1) it can be concluded that: (i) 3-5 monolayers of guest ink are transferred by μCP onto the SAMs; (ii) approximately one monolayer of guest is present after the rinsing step.

Table 7.2 Contact angle values obtained for μCP substrates in comparison with data for a β-CD SAM and adsorption from solution.

SAM	Advancing contact angle
β-CD	47.93 ± 4.57
Adsorption from solution	45.74 ± 2.87
Printed	58.74 ± 2.21

The advancing contact angle values do not show significant differences between the wettability of β-CD SAMs before and after adsorption of the guest from solution, indicating, in both cases, a pronounced polarity of the surface, in agreement with the nature of the outer most exposed functional groups. This suggests a well-ordered layer of the guest

in which the apolar adamantyl moieties are buried in proximity of the CD cavities and only the amidinium moieties or portions of the polyethylene glycol spacer are exposed. In contrast, the sample prepared by μ-CP shows a higher advancing contact angle, indicating a more disordered layer, with significant hydrophobic portions of the guest molecules exposed to the surface. This reflects the presence of multiple layers of ink, with uncomplexed, hydrophobic adamantyl groups exposed to the solution in this case.

Table 7.3 EIS results obtained for μCP substrates in comparison with data for β-CD SAM and adsorption from solution (std. dev. in brackets).

SAM	**Capacitance (μF/cm^2)**	**Thickness (Å)**	**Resistance (kΩ)**
β-CD	2.85 (0.15)	6.95 (0.36)	18.4
Adsorption from solution	2.11 (0.04)	9.37 (0.18)	257.2
Printed	2.51 (0.07)	7.90 (0.21)	91.0

Electrochemistry data suggest, in agreement with the other characterization techniques, that adsorption from solution leads to a highly organized layer of guest molecules on the β-CD surface. This is reflected in the higher resistance value, compared to the β-CD layer and, partially, in a thickness increase. The printed layer shows instead a less ordered structure compared to the solution-assembled case, as indicated by the lower resistance and thickness values. Comparison with the β-CD layer indicates, however, the presence of material on the surface. Quantitative evaluation of the thickness is difficult, due to the high capacitance value associated to the β-CD layer itself, and thus only relative evaluations can be carried out.

7.4 Supramolecular dip pen nanolithography

The other approach exploited to transfer the molecular ink **1** onto the β-CD monolayer has been dip pen nanolithography, again in a *supramolecular* fashion, as depicted schematically in Scheme 7.3.[4]

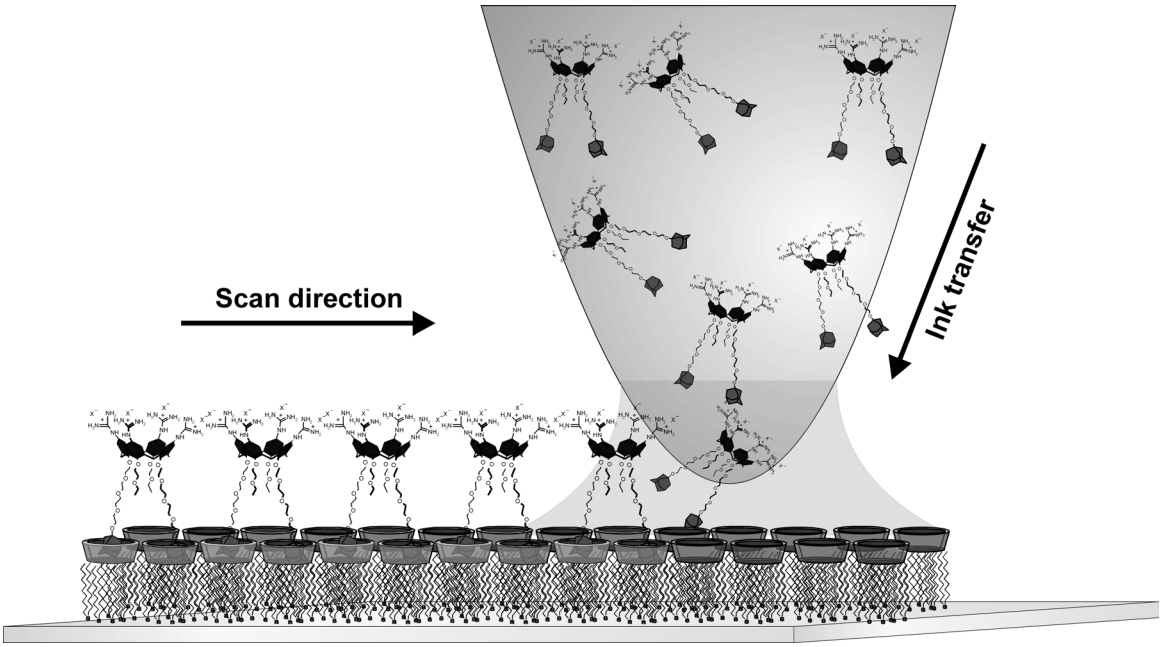

Scheme 7.3 Schematic representation of supramolecular DPN (adapted from ref. 4a).

Contact mode AFM tips have been soaked in a 0.5 mM solution of **1** and then scanned across the surface with a scan velocity of ~ 21 μm/s to produce a 7 × 7 μm^2 square. Upon increasing the scan velocity to 100 - 300 μm/s and the scan size to 30 × 30 μm^2 it was possible to visualize the produced structure (Figure 7.6). Friction inversion with respect to the μCP experiments is probably related to the AFM tip employed in the imaging step, which is the same as in the writing step and thus still covered with the molecular ink.

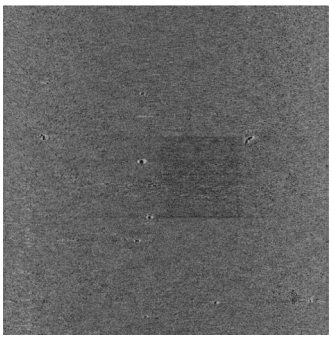

Figure 7.6 CM-AFM friction image in air of a 7 × 7 μm^2 square of **1** on a β-CD SAM produced by DPN (scan size 30 × 30 μm^2; friction forces [a.u.] increase from dark to bright contrast).

As a control experiment a β-CD SAM was scanned with a bare Si_3N_4 tip under the same experimental conditions reported above for the writing experiment and subsequent CM-AFM imaging did not show any visible pattern onto the surface. This proves that the structure of Figure 7.6 does not arise from mechanical forces applied by the tip to the SAM.

To test the stability of the pattern, the writing experiment was performed in a liquid cell setup, which, after ink deposition, was flushed first with 5 ml Milli-Q water and then with 5 ml of 50 mM aq. NaCl. This setup allows one to image immediately in liquid the patterned area, and after rinsing the square was still clearly visible, as shown in Figure 7.7, proving that the molecular ink can interact firmly with the surface.

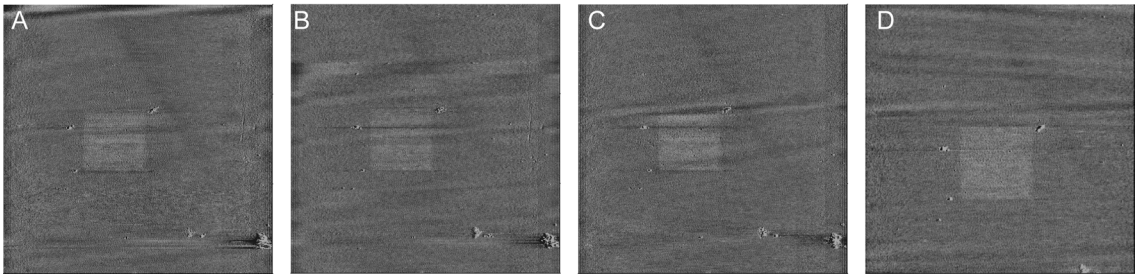

Figure 7.7 Sequence of CM-AFM friction images in liquid (scan size 30 × 30 μm^2; friction forces [a.u.] increase from dark to bright contrast) showing the stability of the structure produced by DPN on a β-CD SAM using **1** as the ink, upon rinsing *in situ* with Milli-Q water (A and B) and 50 mM aq. NaCl (C and D), using a liquid cell setup.

To unequivocally confirm that the stability of the structure is achieved via formation of host-guest complexes between the adamantyl moieties of the ink and the surface-confined β-CD cavities, DPN has been carried out on OH SAMs, drawing a 7 × 7 μm^2 square structure.

Figure 7.8A-D shows a series of in situ CM-AFM friction images of the square upon flushing the liquid cell with 5 ml water (Figure 7.8A-B) and 5 ml of 50 mM aq. NaCl (Figure 7.8C-D), *i.e.* the same rinsing procedure that does not affect the structure created on the β-CD SAM. It can be seen clearly that after flushing the liquid cell with Milli-Q water, the square is still visible, probably due to the small volume employed, while using the 50 mM aq. NaCl solution leads to complete removal of the pattern.

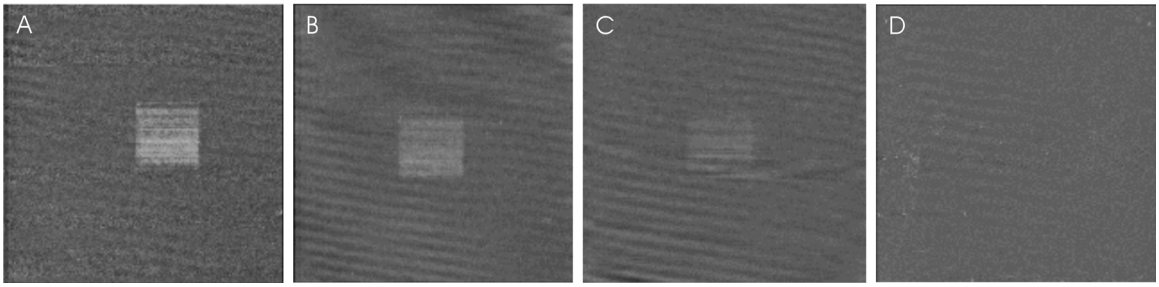

Figure 7.8 Sequence of CM-AFM friction images in liquid (scan size 30 × 30 μm^2; friction forces [a.u.] increase from dark to bright contrast) showing the progressive removal of the square deposited by DPN on an OH SAM using **1** as the ink, upon rinsing *in situ* with Milli-Q water (A-B) and 50 mM aq. NaCl (C-D), using a liquid cell setup.

As already observed in the μCP experiments, the material transferred during the lithographic step is simply physisorbed, and thus it can be removed in the washing step. On the OH SAM no stable supramolecular interactions can take place, which are instead present on the β-CD monolayer and are responsible for the anchoring of the molecular ink onto the surface.

DPN allows, in principle, the creation of submicrometer patterns. Therefore, the lateral resolution of supramolecular DPN was tested by drawing patterns with different length-to-width ratios. In Figure 7.9A is reported a CM-AFM friction image of a pattern consisting of three different rectangular structures, 7 μm long and with widths of 220, 440, and 880 nm, from top to bottom, respectively, each created by scanning an inked AFM tip over a β-CD SAM for 10 min. The measured widths are 290 ± 20 nm, 480 ± 30 nm and 885 ± 50 nm, respectively. The good agreement between the experimental and the theoretical widths indicates that lateral diffusion of the ink does not significantly affect the pattern resolution. Figure 7.9B and C show sub-100 nm writing and registry capability of supramolecular DPN for patterns of lines with lateral dimensions of respectively 50 ± 10 nm and 60 ± 20 nm.

As demonstrated above, in our supramolecular DPN approach transfer of ink occurs anyway, regardless of the type of substrate (printboard or OH SAM), and the resolution is a function of factors such as contact time, tip radius, ink concentration, and ink transfer mechanism, as in traditional DPN. Clearly, the novelty of the employed supramolecular printboard lies in the *stability* of the pattern, as probed under rinsing.

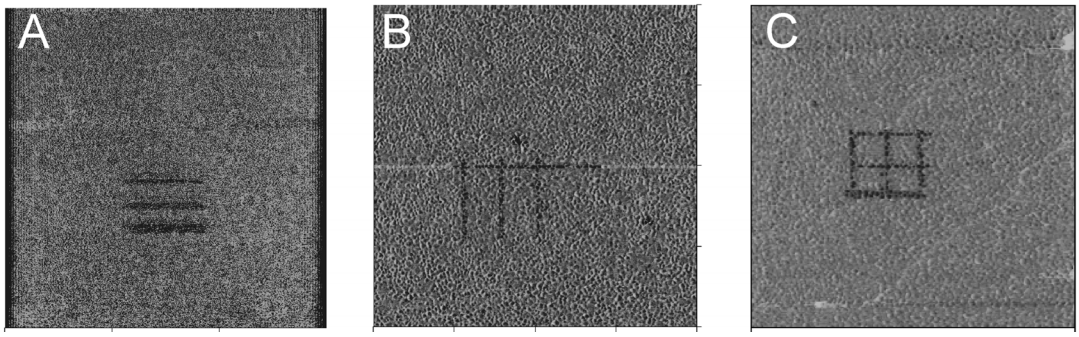

Figure 7.9 CM-AFM friction force images in air (friction forces [a.u.] increase from dark to bright contrast) of arrays of lines with mean widths of 290 ± 20 nm, 480 ± 30 nm, and 885 ± 50 nm (A; scan size 30 × 30 μm^2), and 50 ± 10 nm (B; scan size 1 × 1 μm^2), and 60 ± 20 nm (C; scan size 1 × 1 μm^2) produced by DPN.

7.5 Conclusions

In this chapter multiple host-guest interactions between guest **1** and β-CD monolayers have been investigated. The use of SPR allows evaluation of the adsorption of **1** onto the surface, and modeling of the experimental data provides a complexation constant value of 1×10^{10} M^{-1}. In combination with supramolecular microcontact printing and supramolecular dip pen nanolithography the guest molecules have been transferred selectively onto the β-CD monolayers, which can therefore act as a molecular printboard, creating patterns with sub-100 nm lateral resolution. Reference experiments proved that the stability of the patterned features is provided by the presence of the supramolecular host-guest interactions.

7.6 Experimental

General Procedures. All moisture sensitive reactions were carried out under nitrogen atmosphere. Reagents were commercial and used without further purification. All dry solvents were prepared according to standard procedures and stored over molecular sieves. ^{1}H NMR and ^{13}C NMR spectra were recorded on Bruker AC300 or Bruker AMX400 spectrometers. Spectra are reported in ppm downfield from TMS as an internal standard. Mass spectra by electrospray ionization (ESI) and chemical ionization (CI) methods were recorded on a Micromass ZMD and on a Finnigan Mat SSQ710 spectrometer, respectively. FAB-MS spectra were recorded with a Finnigan MAT 90

spectrometer using *m*-NBA as a matrix. Analytical TLC was performed using Merck prepared plates (silica gel 60 F-254 on aluminium). Merck silica gel (40-63 μm, 230-240 mesh) was used for flash chromatography. Melting points were determined with a Reichert melting point apparatus. Elemental analyses were performed using a Carlo Erba EA1106.

Materials and Methods. All glassware used to prepare monolayers was immersed in piraña solution (conc. H_2SO_4 and 33% H_2O_2 in a 3:1 ratio). **(Warning piraña should be handled with caution; it has detonated unexpectedly)**.[13] Subsequently, the glassware was rinsed with large amounts of Milli-Q water. All adsorbate solutions were prepared prior to use. 11-mercapto-1-undecanol was purchased by Aldrich and 1 mM adsorbate solution were prepared in EtOH. Synthesis of the β-cyclodextrin adsorbate and preparation of SAMs on Au(111) were reported previously.[7] Synthesis and characterization of **1** has been performed by A. Sartori. All solvents used in monolayer preparation were of p.a. grade.

Substrate preparation Round glass-supported gold substrates for SPR (2.54 cm diameter; 47.5 nm Au thickness) were obtained from SSENS bv (Hengelo, The Netherlands) as well as gold substrates for μCP and DPN (20 nm of gold on a 3" silicon wafer with a 2 nm titanium adhesion layer). Directly before use the substrates were cut to the desired shape and size. Substrates were cleaned by oxygen plasma treatment for 5 min and the resulting oxide layer was removed by leaving the substrates for 10 min in absolute EtOH.[14] The substrates were subsequently immersed in the adsorbate solution (0.1-1 mM) for ca. 16 hrs. The samples were removed from the solutions and rinsed thoroughly with dichloromethane or chloroform, ethanol, and Milli-Q water. Adsorption of **1** from solution for electrochemistry, contact angle, and XPS measurements was obtained by immersing a preformed β-CD SAM into a 0.5 mM aq. solution of **1** for 10 min, followed by rinsing with Milli-Q water.

Microcontact printed substrates. Microcontact printed substrates were prepared according to literature procedures.[2a,3a,15] Stamps were prepared by casting a 10:1 (v/v) mixture of poly(dimethylsiloxane) and curing agent (Sylgard 184, Dow Corning) against a patterned silicon master. After curing, the stamps were mildly oxidized in an ozone plasma reactor for 30 min and then inked by soaking them into the adsorbate solution (0.1 mM) for 30 min. Before printing, the stamps were blown dry in a stream of N_2. The stamps were applied by hand (no applied pressure control) for 60 s on preformed SAMs on gold and then carefully removed. After each printing step the inking procedure was repeated. Microcontact printed substrates were thoroughly rinsed with 200 ml of aqueous

solutions of either native β-CD (10 mM), or NaCl (50 mM) or Milli-Q water, respectively.

Surface Plasmon Resonance. SPR measurements were performed in a two-channel vibrating mirror angle scan set-up based on the Kretschmann configuration, described by Kooyman *et al.*[16] Light from a 2 mW HeNe laser is directed onto a prism surface by means of a vibrating mirror. The intensity of the light is measured by means of a large-area photodiode. This set-up allows determination of changes in plasmon angle with an accuracy of 0.002°. The gold substrates with the monolayer were optically matched to the prism using an index matching oil. A teflon cell was placed on the monolayer via an O-ring, to avoid leakage, and filled with 800 μl of β-CD solution at the same concentration as in the guest solution. After stabilization of the SPR signal, titrations were performed by removing an amount of solution from the cell and adding the same amount of stock solution (0.1 mM) of **1**. Between each addition the cell was thoroughly washed with native 10 mM β-CD solution (5 times 700 μl) and then water was added to a final volume of 800 μl to restore the proper buffer concentration. SPR measurements were repeated 3 times.

XPS. XPS measurements were performed with a Physical Electronics Quantum2000 equipped with a spherical sector analyzer and a multichannel plate detector (16 detector elements). Analyzer Mode was constant pass energy. For the survey scan the pass energy was 117 eV, the X-ray beam was set to High Powermode 100 Watt/100 μm, and the diameter beam scanned over a 1000 μm × 500 μm area; for element scans pass energy was 29.35 eV, the X -ray beam was set to 25 W/100 μm, and the diameter beam scanned over a 1000 μm × 500 μm area. The excitation source was Al K Alpha monochromatic radiation with a source energy = 1486.7 eV. The take-off angle (analyzer angle to sample surface) was set to 30 degrees. The surface potential was controlled by using both low energy electrons and ions. The temperature during analysis was 298 K, and the pressure was between 1 and 3 × 10^{-8} Torr (Argon pressure for charge control). For atomic concentration calculation the Shirley background subtraction was employed. The sensitivity factors were provided by Physical Electronics MultiPack software version 6.1A. The hydrocarbon C1s signal at 284.8 eV was used as a reference for surface charging.

Contact Angle Goniometry. The advancing contact angles were measured with Milli-Q water on a Krüss G10 Contact Angle Measuring Instrument, equipped with a CCD camera. Measurements with a drop of water, the volume of which was gradually increased (advancing CA) and then decreased (receding CA), were repeated on three different sites of each sample.

Electrochemistry. Electrochemical measurements were performed with an AUTOLAB PGSTAT10, in a custom built three-electrode setup equipped with a platinum counter electrode, a mercury sulfate reference electrode (V_{MSE} = +0.61 V_{NHE}) and a screw cap holding the gold working electrode (area exposed to the solution = 0.44 cm^2). Cyclic voltammograms were recorded in 0.1 M K_2SO_4, between –0.4 V and –0.1 V, at scan rates of 0.1, 0.2, and 0.5 V/s. Impedance spectroscopy measurements were performed in 1 mM $K_3Fe(CN)_6/K_4Fe(CN)_6$ and 0.1 M K_2SO_4 with a 5 mV amplitude using a frequency range from 50 kHz to 0.1 Hz. The charge-transfer resistance of the monolayer was obtained by fitting the experimental data to an equivalent circuit.[17]

AFM. The AFM experiments were carried out with a NanoScope III multimode AFM (Digital Instruments, Santa Barbara, CA, USA) in contact mode using V-shaped Si_3N_4 cantilevers (Nanoprobes, Digital Instruments) with a spring constant of 0.1 N/m. Images were captured in ambient atmosphere (ca. 40 - 50 % relative humidity, 25ºC temperature) unless stated otherwise. For measurements in liquid a standard AFM liquid cell (Digital Instruments) was used. To ensure maximum sensitivity for lateral forces in the friction force images, the sample was scanned in 90° with respect to the long axis of the cantilever.

DPN. For DPN, cleaned Si_3N_4 tips were coated with **1** by soaking them for 15 min in a 0.5 mM aqueous solution and drying, and then scanned twice across a 7 × 7 μm^2 area of a SAM on gold while the 290 ± 20 nm, 480 ± 30 nm, and 885 ± 50 nm lines were produced by scanning each line for a 10 min period (scan velocity ~ 21 μm/s, T = 25 °C, relative humidity 47 ± 3 %). The readout was performed increasing the scan size to 30 × 30 μm^2, the scan velocity to 100 - 300 μm/s and adjusting accordingly the relative scan angle. For each of the 50-nm and of the 60-nm thick lines arrays the scanning time was 1 min and 40 sec, respectively (scan velocity of ~ 2 μm/s, T = 25 °C and relative humidity 47 ± 3 %) and the readout was performed increasing the scan size to 4 × 4 μm^2 and the scan velocity to 30 μm/s. Prior to rinsing, the tip was withdrawn. The liquid cell was then flushed with 5 ml of Milli-Q water and new images were recorded. Eventually the cell was flushed with 5 ml 50 mM aq. NaCl, before new images were recorded.

7.7 References and notes

[1] a) Ito, T.; Okazaki, S. *Nature* **2000**, *406*, 1027-1031. b) Walraff, G. M.; Hinsberg, W. D. *Chem. Rev.* **1999**, *99*, 1801-1821. c) Okazaki, S. *J. Vac. Sci. Technol. B* **1991**, *9*, 2829-2833. d) Jeong, H. J.; Markle, D. A.; Owen, G.; Pease, F.; Grenville, A.; Von Bünau, R.

Solid State Technol. **1994**, *37*, 39-47. e) Levenson, M. D. *Solid State Technol*. **1995**, *38*, 57-66. f) Geppert, L. *IEEE Spectrum* **1996**, *33*(4), 33-38.

[2] a) Kumar, A.; Whitesides, G. M. *Appl. Phys. Lett.* **1993**, *63*, 2002-2004. b) Xia, Y.; Kim, E.; Zhao, X.-M.; Rogers, J. A.; Prentiss, M.; Whitesides, G. M. *Science* **1996**, *273*, 347-349. c) Zhao, X.-M.; Xia, Y.; Whitesides, G. M. *Adv. Mater.* **1996**, *8*, 837-840. d) Kim, E.; Xia, Y.; Whitesides, G. M. *Nature* **1995**, *376*, 581-584. e) Kim, E.; Xia, Y.; Zhao, X.-M.; Whitesides, G. M. *Adv. Mater.* **1997**, *9*, 651-654. f) Zhao, X.-M.; Xia, Y.; Whitesides, G. M. *J. Mater. Chem.* **1997**, *7*, 1069-1074. g) Qin, D.; Xia, Y.; Rogers, J. A.; Jackman, R. J.; Zhao, X.-M.; Whitesides, G. M. *Top. Curr. Chem.* **1998**, *194*, 1-20. h) Whitesides, G. M.; Xia, Y. *Annu. Rev. Mater. Sci.* **1998**, *28*, 153-184.

[3] a) Xia, Y.; Whitesides, G. M. *Angew. Chem. Int. Ed.* **1998**, *37*, 550-575. b) Biebuyck, H. A.; Larsen, N. B.; Delamarche, E.; Michel, B. *IBM J. Res. Dev.* **1997**, *41*, 159-170.

[4] a) Piner, R. D.; Zhu, J.; Xu, F.; Hong, S.; Mirkin, C. A. *Science* **1999**, *283*, 661-663. b) Mirkin, C. A.; Hong, S.; Levine, R. D. *ChemPhysChem* **2001**, *2*, 37-39.

[5] a) Fraenkel, Y.; Shalev, D. E.; Gershoni, J. M.; Navon, G. *Crit. Revs. Biochem Mol. Biol.* **1996,** *31*, 273-301. b) Wold, M. S. *Annu. Rev. Biochem.* **1997,** *66*, 61-92. C) Travers, A. A. *Annu. Rev. Biochem.* **1989,** *58*, 427-452. d) Stryer, L. *Biochemistry* 3rd ed.; W. H. Freeman and Company: New York, 1988.

[6] a) Steed, J. W.; Atwood, J. L. *Supramolecular Chemistry Ch. 7*; Wiley: Chichester, UK, 2000. b) Templating, Self-assembly, and Self-organization. *Comprehensive Supramolecular Chemistry*; Pergamon Press: Oxford, 1996, vol. 9. c) Philp, D.; Stoddart, J. F. *Angew. Chem. Int. Ed.* **1996**, *35*, 1154-1196.

[7] a) Beulen, M. W. J.; Bügler, J.; Lammerink, B.; Geurts, F. A. J.; Biemond, E. M. E. F.; Van Leerdam, K. G. C.; Van Veggel, F. C. J. M.; Engbersen, J. F. J.; Reinhoudt, D. N. *Langmuir* **1998**, *14*, 6424-6429. b) Beulen, M. W. J.; Bügler, J.; De Jong, M. R.; Lammerink, B.; Huskens, J.; Schönherr, H.; Vancso, G. J.; Boukamp, B. A.; Wieder, H.; Offenhäuser, A.; Knoll, W.; Van Veggel, F. C. J. M.; Reinhoudt D. N. *Chem. Eur. J.* **2000**, *6*, 1176-1183. c) Schönherr, H.; Beulen, M. W. J.; Bügler, J.; Huskens, J.; Van Veggel, F. C. J. M.; Reinhoudt D. N. Vancso, G. J. *J. Am. Chem. Soc.* **2000**, *122*, 4963-4967. d) De Jong, M. R.; Huskens, J.; Reinhoudt, D. N. *Chem. Eur. J.* **2001**, *7*, 4164-4170. e) Zapotoczny, S.; Auletta, T.; De Jong, M. R.; Schönherr, H.; Huskens, J.; Van Veggel, F. C. J. M.; Reinhoudt, D. N.; Vancso, G. J. *Langmuir* **2002**, *18*, 6988-6994.

[8] Raether, H. in *Physics of Thin Films*; Academic Press: New York, 1977, vol. 9, pp. 145-261.

[9] Matsubara, K.; Kawata, S.; Minami, S. *Appl. Opt.* **1988**, *27*, 1160-1163.

[10] An alternative approach considers two independent binding sites, each one interacting with a binding strength per cavity as given for native β-cyclodextrin, $K_i = 5.0 \times 10^4\ M^{-1}$. A β-CD "effective molarity" $[CD]_{eff}$, can be defined as the host concentration experienced by the second guest once the first complex is formed. The free CD concentration at the surface $[CD]_{surf}$, used in the equilibrium related to the first host-guest complex, is equal to the number of moles of CD divided by the sampled volume. For the second equilibrium it is instead calculated as the number of accessible binding sites divided by the sampled volume. On the basis of molecular modeling of the guest and of the AFM lattice constant of the SAM, 18 β-CD cavities are accessible on the surface and thus available to complex the second guest molecule, leading to a $[CD]_{eff}$ of 0.19 M. For a more detailed description *cfr*. Huskens, J.; Deij, M. A.; Reinhoudt, D. N. *Angew. Chem. Int. Ed.* **2002**, *41*, 4467-4471.

[11] Martin, B. D.; Brandow, S. L.; Dressick, W. J.; Schull, T. L.; *Langmuir*, **2000**, *16*, 9944-9946.

[12] a) Yan, L.; Huck, W. T. S.; Zhao, X.-M.; Whitesides, G. M. *Langmuir* **1999**, *15*, 1208-1214. b) Lahiri, J.; Ostuni, E.; Whitesides, G. M. *Langmuir* **1999**, *15*, 2055-2060.

[13] a) Dobbs, D. A.; Bergman, R. G.; Theopold, K. H. *Chem. Eng. News* **1990**, 68 (17), 2. b) Wnuk, T. *Chem. Eng. News* **1990**, 68 (26), 2. (c) Matlow, S. L. *Chem. Eng. News* **1990**, 68 (30), 2.

[14] Ron, H.; Rubinstein, I. *Langmuir* **1994**, *10*, 4566–4573.

[15] a) Lopez, G. P.; Biebuyck, H. A.; Whitesides, G. M. *Langmuir* **1993**, *9*, 1513-1516. b) Kumar, A.; Biebuyck, H. A.; Whitesides, G. M. *Langmuir* **1994**, *10*, 1498-1511. b) Wilbur, J. L.; Kim, E.; Xia, Y.; Whitesides, G. M. *Adv. Mater.* **1995**, *7*, 649-652. d Xia, Y.; Whitesides, G. M. *Adv. Mater.* **1995**, *7*, 471-473.

[16] Lenferink, A. T. M.; Kooyman, R. P. H.; Greve, J. *Sens. Act. B* **1991**, *3*, 261-265.

[17] a) Boukamp, B. A. *Solid State Ionics* **1986**, *18-19*, 136-140. b) Boukamp, B. A. *Solid State Ionics* **1986**, *20*, 31-44.

Summary

In this thesis, the use of self-assembled monolayers (SAMs) of sulfur-containing molecules on gold as platforms to perform single molecule chemistry is presented. Several systems have been employed, exploiting reactions in the supramolecular field, ranging from metallo-dendrimer coordination chemistry to β-cyclodextrin (β-CD) host-guest complexes. Central to this project are applications in the nanotechnology research field, and combinations of top-down and bottom-up approaches are presented to produce nanosize patterns.

In Chapter 2, an overview of unconventional nanofabrication techniques is given, with special focus on soft-lithographic techniques such as microcontact printing and dip pen nanolithography. At the end of the chapter, a brief section on single molecule detection and manipulation focusing on scanning probe techniques is included.

Chapters 3 and 4 describe the reactivity of surface-confined isolated single dendritic architectures in coordination chemistry. Chapter 3 reports thioether dendritic wedges with four pyridine moieties at the periphery that have been assembled into SAMs of decanethiol by insertion, yielding individually addressable entities. Reactions at the single molecule level on such platforms have been monitored by atomic force microscopy (AFM) as an increase in height of the nanosize features upon reaction with dendron moieties bearing a sulfur-carbon-sulfur (SCS) Pd^{II} pincer. In Chapter 4, it is described how a thioether adsorbate having a SCS Pd^{II} pincer as the terminal moiety has been isolated into SAMs of decanethiol and has been reacted with phosphine-derivatized gold colloids. This proves the applicability of the process on both organic materials as well as composite organic/inorganic systems. In addition, an approach to direct the insertion process towards predefined areas of the substrate has been developed by using SAMs of alkanethiols patterned by microcontact printing.

Chapter 5 describes the characterization of mixed SAMs of ferrocenylalkanethiols co-adsorbed with ω-hydroxyalkanethiols by means of electrochemistry. Cyclic voltammetry has been employed to quantify the amount of electroactive component adsorbed onto the layer, which has been related to the solution composition. The influence of the chain length of the adsorbates has been tested by changing the alkyl spacer of both the hydroxyalkanethiol and the ferrocenylalkanethiol. At low fractions of ferrocenyl-alkanethiol neither preferential adsorption nor phase segregation has been observed. However, such effects become significant upon increasing the percentage of the

electroactive component in solution, and are predominant for the longer chain components.

These substrates have been employed in the AFM experiments reported in Chapter 6. Gold-coated AFM tips have been modified with mixed SAMs of ferrocenylalkanethiols and hydroxyalkanethiols. Interactions between the surface-confined ferrocene guest and β-cyclodextrin heptathioether SAMs have been investigated using AFM force spectroscopy. Statistical analysis of the characteristic force displacement curves revealed a periodic distribution of forces, which arises exclusively from the presence of both the host and guest molecules. The observed force quantum is assigned to the rupture of a single host-guest complex. The force quantum has shown neither dependence on the alkyl spacer length of the guest nor on the unloading rate. Several thiol-modified guests have been synthesized and the force spectroscopy experiments showed once more periodic distributions of force, with force quanta related to the thermodynamics of the host-guest complex formation as investigated by isothermal titration calorimetry (ITC) and surface plasmon resonance (SPR) spectroscopy for model compounds. A theoretical model has been developed that correlates the force quanta and the ΔG^{o} values of the complexes. Chapter 7 deals with the use of β-cyclodextrin SAMs as molecular printboards on which guest molecules can be immobilized selectively and multiple host-guest interactions have been chosen to enhance the stability of the patterns on the surface. A novel water-soluble calix[4]arene bearing two adamantyl moieties on the lower rim has been used. SPR experiments have shown that the complexation constant with the β-CD SAMs is exceptionally high, which is attributed to preorganization and a high effective molarity of the CD cavities at the surface. Selective transfer of the guest molecules has been achieved by soft lithographic techniques such as microcontact printing and dip pen nanolithography. The patterns based on host-guest interactions have proven to resist several rinsing procedures, while the same experiments carried out on hydroxyl-terminated reference layers have led to complete removal of the adsorbed material. Sub-100 μm resolution has been obtained by applying the supramolecular dip pen nanolithography approach.

The results discussed in this thesis show that self-assembled monolayers can be used successfully as platforms for single molecule chemistry. Exploiting non-covalent reversible supramolecular interactions allows the formation of highly stable assemblies on SAMs, which can be applied in various patterning strategies. Combinations of top-down and bottom-up approaches are indeed a viable option in nanofabrication and may provide new options in nanotechnology and miniaturization of devices.

Samenvatting

Dit proefschrift beschrijft het gebruik van zelforganiserende monolagen (SAMs) van zwavelbevattende moleculen op goud als substraten voor het uitvoeren van chemie aan enkelvoudige moleculen. Een aantal verschillende systemen zijn hiervoor getest, waarbij gebruik is gemaakt van supramoleculaire reacties, variërend van de coördinatie-chemie van metallodendrimeren tot β-cyclodextrine-inclusiecomplexen. Toepassing en innovatie binnen de nanotechnologie staan centraal in dit onderzoek en er wordt aangetoond dat door de combinatie van top-down- en bottom-up-technieken structuren met nano-afmetingen gemaakt kunnen worden.

Hoofdstuk 2 geeft een overzicht van onconventionele nanofabricage-technieken, met de nadruk op soft-lithografische technieken als microcontact-printen en dip-pen-nanolithografie. Aan het eind van het hoofdstuk is een sectie gewijd aan het detecteren van enkelvoudige moleculen en het manipuleren daarvan, voornamelijk met behulp van scanning-probe-technieken.

Hoofdstuk 3 en 4 beschrijven de coördinatie-chemische reactiviteit van aan oppervlakken verankerde, geïsoleerde dendrimere structuren. In hoofdstuk 3 zijn thioether-dendrimeren met vier pyridine-eenheden aan de periferie ingebracht in SAMs van decaanthiol met behulp van de zogenaamde insertie-methode, met als resultaat afzonderlijk aanspreekbare moleculen. Reacties aan geïsoleerde moleculen op deze oppervlakken zijn gevolgd door de toename van de hoogte van de deeltjes na de reactie met de dendrimere deeltjes met een zwavel-koolstof-zwavel- (SCS) Pd^{II}-pincer te meten met behulp van atomaire-krachtmicroscopie (AFM). In hoofdstuk 4 zijn thioether-moleculen met een SCS-Pd^{II}-pincer als eindgroep geïnserteerd in SAMs van decaanthiol waarna ze zijn gereageerd met phosphine-gederivatiseerde goudcolloïden. Dit toont de bruikbaarheid van het insertie-proces voor de bereiding van zowel organische materialen als van organische/anorganische composiet-systemen. Daarnaast is een aanpak ontwikkeld voor het sturen van het insertieproces naar geselecteerde gebieden van het substraat door het gebruik van SAMs met patronen van verschillende thiolen verkregen met behulp van microcontact-printen.

Hoofdstuk 5 beschrijft de karakterisering van gemengde zelforganiserende monolagen van ferrocenylalkaanthiolen gecoadsorbeerd met hydroxyalkaanthiolen met behulp van elektrochemie. Cyclische voltammetrie is gebruikt om de hoeveelheid electroactieve component geadsorbeerd op de lagen te quantificeren, welke gerelateerd is aan de samenstelling in oplossing. De invloed van de ketenlengte van de absorbaten is

bestudeerd door variatie van de ketenlengte van zowel de alkylspacer van de ferrocenyl- als van de hydroxyalkaanthiol. Bij lage hoeveelheden van het ferrocenylalkaanthiol werd noch preferentiële adsorptie noch fasescheiding vastgesteld. Dergelijke effecten werden echter meer significant bij toename van het percentage van de electroactieve component in oplossing en werden met name waarneembaar voor het systeem met de langere alkylketens.

Deze substraten zijn gebruikt voor de atomaire-krachtmicroscopie-experimenten beschreven in Hoofdstuk 6. Met goud bedekte AFM tips zijn gemodificeerd met gemengde zelf-organiserende monolagen van ferrocenylalkaanthiolen en hydroxyalkaanthiolen. Interacties tussen de aan het oppervlakte verankerde ferroceen-gastmoleculen en SAMs van β-cyclodextrine-heptathioether zijn bestudeerd met behulp van AFM-kracht-spectroscopie. Statistische analyse van de karakteristieke kracht-verplaatsingscurves gaf een periodieke verdeling van krachten die enkel waarneembaar was voor de combinatie van zowel gast- als gastheer-moleculen. De resulterende gequantiseerde kracht wordt toegeschreven aan het verbreken van een enkel inclusiecomplex. Deze gequantiseerde kracht is onafhankelijk van de lengte van de alkylspacer van de gast en van de verplaatsingssnelheid. Verscheidene thiolgemodificeerde gasten zijn gesynthetiseerd en de kracht-spectroscopie-experimenten vertoonden ook voor deze gasten een periodieke verdeling met gequantiseerde krachten gerelateerd aan de thermodynamica van de inclusiecomplexen, die bepaald is met behulp van microcalorimetrie (ITC) en oppervlakte-plasmon-resonantie (SPR) voor modelverbindingen. Een theoretisch model is ontwikkeld voor de correlatie van de gequantiseerde krachten en de ΔG^{o}-waarden van de complexen.

Hoofdstuk 7 behandelt het gebruik van zelforganiserende monolagen van β-cyclodextrine als moleculaire printplaten waarop selectief gastmoleculen geïmmobiliseerd kunnen worden. Meervoudige gast-gastheer-interacties zijn gekozen voor het verhogen van de stabiliteit van de patronen op het oppervlak. Een nieuw wateroplosbaar calixareen met twee adamantyl-eenheden is voor dit doeleinde gebruikt. Met behulp van SPR werd aangetoond dat de stabiliteit van deze gastmoleculen op de β-CD-monolagen uitzonderlijk sterk was, hetgeen toegeschreven wordt aan preorganisatie en een hoge effectieve molariteit van de CD-holtes aan het oppervlak. Selectieve overdracht van de gastmoleculen is gerealiseerd door gebruik te maken van zacht-lithografische technieken zoals microcontact-printen en dip-pen-nanolithografie; ook is de stabiliteit van de patronen getest. De patronen gebaseerd op gast-gastheer-interacties zijn bestand tegen verschillende wasprocedures, terwijl dezelfde experimenten, uitgevoerd op een hydroxyalkaanthiol-monolaag, volledige verwijdering van het geadsorbeerde materiaal

gaven. Sub-100 μm resolutie werd verkregen door gebruik te maken van supramoleculaire dip-pen-nanolithografie.

De resultaten beschreven in dit proefschrift tonen aan dat zelforganiserende monolagen met succes toegepast kunnen worden als substraten voor chemie aan enkelvoudige moleculen. Door gebruik te maken van niet-covalente reversibele interacties is het mogelijk zeer stabiele patronen te creëren, die toegepast kunnen worden in diverse patroneringstechnieken. Het combineren van top-down- en bottom-up-technieken is zeker een praktisch toepasbare optie voor nanofabricage en biedt nieuwe mogelijkheden binnen de nanotechnologie en de miniaturisering van functionele systemen.

Acknowledgements

This thesis summarizes four years of work at the University of Twente. When I read the first time about Enschede I had no clue where it was and I had only a faint idea about the Netherlands. After four years I can not imagine a better choice than coming here, a place where I grew and learned very much both from a professional and personal perspective. And all these things would have not been possible without a number of people, excellent friends and brilliant scientists, whom I have been so fortunate to meet.

Allereerst wil ik mijn promotor David Reinhoudt bedanken voor de mogelijkheid om binnen zijn groep te promoveren. David, jij hebt mij laten zien dat het opbouwen, sturen en managen van een goede internationale groep minstens zo waardevol is als het verkrijgen van goede resultaten. Je hebt mij veel vrijheid gegeven voor mijn onderzoeksproject en dat heeft mij bijzonder geholpen in mijn professionele ontwikkeling. De mogelijkheid om op vele plekken in de wereld mijn onderzoek te presenteren heeft mijn zienswijze verbreed en heeft van mij een meer openstaand persoon gemaakt.

Frank en Jurriaan, een overstap van begeleider in het laatste jaar mag dan beangstigend lijken, maar ik heb het bijzonder getroffen, want dit gaf mij de mogelijkheid om met jullie beiden te werken. Jullie hebben een vergelijkbare aanpak en hebben me geholpen vele dingen te leren. Frank, altijd nauwgezet, maar ook openstaand voor discussie en klaarstaand om te luisteren naar een alternatieve zienswijze. Dankzij jou ben ik in staat om een klein aantal Nederlandse woorden te “knauwen”. Ik moet toegeven dat ik, wat taal betreft, nooit begrepen heb waarom het “andare in bicicletta” is, maar niet “andare in cavallo”! Jurriaan, ik heb nimmer meer angstaanjagende files gezien dan jouw Excel sheets en ik ben je zeer dankbaar dat jij de tijd hebt genomen om mij te laten zien hoe je deze sheets kunt ontcijferen en dat je mij de wereld van kinetiek en thermodynamica hebt laten ontdekken.

And then I had the chance to collaborate with a number of colleagues. Henk-Jan van Manen, from whose hands came out the molecular dendritic architectures presented in Chapter 3 and 4. For chapter 4 I also have to thank Xue-Mei Li and Romina Ramingo. The work described in Chapter 6 has been carried out in collaboration with Szczepan Zapotoczny (now I can confess that I had to “copy/paste” your name, when I wrote you an e-mail!!!) who has always been able to smile and has been an excellent co-worker. Thanks also to Kobus Kuipers, Menno de Jong, Holger Schönherr and Shan Zou. Chapter

7 has seen very many people working together from Alart, to Barbara, to Andrea, to Steffen, to Christiaan, to Christian, to Maria.
Andrea grazie anche per avermi offerto il tuo pavimento su cui stendere il mio sacco a pelo e per aver sopportato le mie irruzioni alle sette di mattina in camera tua!
And now come so many more friends that I have seen arriving and sometimes leaving the group, and every time it has been difficult to walk in the corridor and not find you where you used to work. Classification is impossible, thus I will just proceed via a random order. Maik, the German, who said once that: “In the Netherlands it never rains so heavily that you can’t bike!” and with whom I then spent a few hours in a bar because outside it was pouring water. Kjeld and Ari, the social engine of the group: how many colonist games did we play? Maik and Arianna also helped me very much at the beginning of my Ph.D. with all the monolayer stuff. And then Niels “il barbaro” and Mercedes, who by now is staff member and I can not take the liberty to make fun of her, thank you also for the experience of a Spanish-Dutch noisy and unforgettable wedding!!!
Richard, deus ex machina of our computer systems, always willing to help when you lost all your data the day before a presentation, unless he was busy running around in his orange suit.
Thanks also to Mark Brouwer and Marcel de Bruine for the technical support through these years and to Roel Fokkens, Tieme Stevens, and Hanny Visser for the help provided in the analytical field. Fundamental analytical support came as well from Rico Keim, Mark Smithers and Albert van den Berg from the Analytical Material Laboratory of MESA^{+}.
Carla and Izabel thank you very much for your administrative work, always welcoming everybody with a smile.
Alessio grazie per le mangiate e le bevute. Grazie per non esserti lamentato quando, passando la notte sul pavimento della mia stanza ti ho calpestato al buio. E grazie anche anche alla tua mamma che ha fatto a gara con la mia per chi spediva i pacchi dono più prelibati a noi emigranti.
And then Stefano e Petra, Jasper, Gerald, Leonard e Maria, Menno Deij, Juanjo, Francesca, Marta, Bianca, Marius, Monica and Emiel, Paolo, Becky, Mrinal, Olga, Eva, Fernando, Miguel and Jessica, Lourdes, Mario, Susanna. I just hope I didn’t forget anybody.
Very many thanks to my friends out of the group, Lisa, Dragana, Richard, Irene, Zoran, Caroline.
A special thank to Jeff and Becky who “volunteered” as proofreaders of my thesis to check out my English.

Grazie Roberto, paraninfo, compagno di casa e gastronomo eccezionale. Quando sei andato via mi sono sentito un poco orfano senza nessuno pronto a dispensare consigli utili su come ottenere il perfetto risotto o come tirar via il prodotto dalla colonna. Si dice che ogni buon chimico deve essere anche un buon cuoco e nessuno meglio di te ha saputo incarnare questa veritá.

Alart, paranimph as well. Always smiling and in a good mood, it has been a pleasure for me to work with you. Unfortunately no beer for you, but only some colorful fruit drinks. All these sugars are probably needed to catch your train in time on the way to Deventer; you rarely had more than 7 minutes to bike to the station in Hengelo.

Barbara, ingegnere, cosa scrivere a questo punto. Per tutte le parole che potrei mettere su carta, nessuna sará mai in grado di esprimere tutta la mia gratitudine, il mio affetto e la mia ammirazione. Lo stesso vale per quello che hai saputo dimostrare nel tuo lavoro e forse dovrei anche provare a ringraziarti per l'impegno, la dedizione e i risultati che abbiamo ottenuto dal punto di vista scientifico, ma non credo che ce ne sia bisogno.

Grazie ai miei genitori e a Francesco, il mio "fratellino", che hanno sempre creduto in me e non mi hanno mai fatto mancare il loro supporto e il loro incoraggiamento, a volte esplicito, a volte silenzioso ma sempre sostanziale. Ogni volta che ho avuto bisogno sapevo che voi eravate lí.

Jeanette, min lilla svenska flicka. Oväntat dök du upp i mitt liv och ställde hela min tillvaro på ända. När mina arbetskollegor såg mig med en fullpackad ryggsäck fredag eftermiddag visste de att jag skulle med kvällsplanet till Stockholm. När jag inte dök upp exakt klockan sju på måndag morgon, utan först ett par timmar senare, visste de att du var på besök här i Enschede. Du har alltid funnits där, visserligen diskret, men alltid redo att hjälpa och stödja mig, speciellt under slutet av mitt doktorsarbete. Jag kan inte finna ord på något språk för allt jag vill säga dig.

The author

Tommaso Auletta was born in Palermo (Italy) on October the 24th, 1972. In 1990 he received his diploma from the "Liceo Classico" N. Spedalieri (Catania). From 1990 to 1995 he attended the Laurea course in Chemistry at the University of Catania, and he graduated in July 1995, magna cum laude. During his undergraduate thesis he worked on the synthesis and characterization of β-cyclodextrins modified with nitrogen containing ligands, investigating the complexation properties towards copper atom as a function of pH.

After his military service and until September 1997 he worked as quality assurance manager in a chemical laboratory. From September 1997 until September 1999 he attended the School of Specialization in Synthesis "A. Quilico" at the Department of Chemistry of the Polytechnic of Milano (Italy). Here he obtained is specialization degree (100/100) in December 1999 with a thesis on reactivity of ketones and ketoesters, under the supervision of Prof. A. Citterio. In September 1999 he joined the supramolecular chemistry and technology group of Prof. Dr. Ir. David N. Reinhoudt at the University of Twente (The Netherlands). The research carried out in the period 1999-2003 has been described in this thesis, and focuses on the use of self-assembled monolayers on gold as platforms to perform single molecule chemistry, with a special aim toward nanotechnology issues.

Starting from 1st of October 2003 he will work as postdoc in the Surface Force Group of Prof. Per Claesson at the Kungl Tekniska Högskolan in Stockholm.